Article

Targeting G1–S-checkpoint-compromised cancers with cyclin A/B RxL inhibitors

https://doi.org/10.1038/s41586-025-09433-w

Received: 30 July 2024

Accepted: 18 July 2025

Published online: 20 August 2025

Open access

Check for updates

Shilpa Singh[1], Catherine E. Gleason[2], Min Fang[3], Yasmin N. Laimon[4], Vishal Khivansara[3], Shanhai Xie[3], Yavuz T. Durmaz[1], Aniruddha Sarkar[5], Kenneth Ngo[1,6], Varunika Savla[4], Yixiang Li[1], Muhannad Abu-Remaileh[1], Xinyue Li[1], Marie-Anais Locquet[1], Bishma Tuladhar[6], Ranya Odeh[2], Frances Hamkins-Indik[2], Daphne He[2], Miles W. Membreno[2], Meisam Nosrati[2], Nathan N. Gushwa[2], Siegfried S. F. Leung[2], Breena Fraga-Walton[2], Luis Hernandez[2], Miguel P. Baldomero[2], Bryan M. Lent[2], David Spellmeyer[2], Joshua F. Luna[2], Dalena Hoang[2], Yuliana Gritsenko[2], Manesh Chand[2], Megan K. DeMart[2], Sammy Metobo[2], Chinmay Bhatt[2], Justin A. Shapiro[2], Kai Yang[2], Nathan J. Dupper[2], Andrew T. Bockus[2], Jinshu Fang[2], Ramesh Bambal[2], Peadar Cremin[2], John G. Doench[7], James B. Aggen[2], Li-Fen Liu[2], Bernard Levin[2], Evelyn W. Wang[2], Iolanda Vendrell[8], Roman Fischer[8], Benedikt Kessler[8], Prafulla C. Gokhale[1,6], Sabina Signoretti[4,9], Alexander Spektor[5], Constantine Kreatsoulas[2], Marie Evangelista[2], Rajinder Singh[2], David J. Earp[2], Deepak Nijhawan[3], Pablo D. Garcia[2] & Matthew G. Oser[1,10] ✉

Small-cell lung cancers (SCLCs) contain near-universal loss-of-function mutations in *RB1* and *TP53*, compromising the G1–S checkpoint and leading to dysregulated E2F activity[1]. Other cancers similarly disrupt the G1–S checkpoint through loss of *CDKN2A* or amplification of cyclin D or cyclin E, also resulting in excessive E2F activity[2,3]. Although E2F activation is essential for cell cycle progression, hyperactivation promotes apoptosis[4–9], presenting a therapeutic vulnerability. Cyclin proteins use a conserved hydrophobic patch to bind to substrates bearing short linear RxL motifs[10–13]. Cyclin A represses E2F through an RxL-dependent interaction[10,14], which, when disrupted, hyperactivates E2F[15]. However, this substrate interface has remained difficult to target. Here we developed cell-permeable, orally bioavailable macrocyclic peptides that inhibit RxL-mediated interactions of cyclins with their substrates. Dual inhibitors of cyclin A and cyclin B RxL motifs (cyclin A/Bi) selectively kill SCLC cells and other cancer cells with high E2F activity. Genetic screens revealed that cyclin A/Bi induces apoptosis through cyclin B- and CDK2-dependent spindle assembly checkpoint activation. Mechanistically, cyclin A/Bi hyperactivates E2F and cyclin B by blocking cyclin A–E2F and cyclin B–MYT1 RxL interactions. Notably, cyclin A/Bi promoted the formation of neomorphic cyclin B–CDK2 complexes, which drive spindle assembly checkpoint activation and mitotic cell death. Finally, orally administered cyclin A/Bi showed robust anti-tumour activity in chemotherapy-resistant SCLC patient-derived xenografts. These findings reveal gain-of-function mechanisms through which cyclin A/Bi triggers apoptosis and support their development for E2F-driven cancers.

SCLC is an aggressive lung cancer subtype lacking effective targeted therapies[16]. It is genomically defined by near-universal loss-of-function (LOF) mutations in *RB1* and *TP53*, without recurrent druggable oncogenic drivers[1], making new therapeutic strategies particularly challenging. One approach is to identify synthetic lethal vulnerabilities associated with *RB1* and/or *TP53* LOF.

In G1, unphosphorylated pRB represses activating E2Fs (E2F1–E2F3)[17,18]. Phosphorylation by CDK4 and CDK6 (CDK4/6)–cyclin D and CDK2–cyclin A/E inhibits this repression, allowing E2F-driven S-phase entry[18]. Various cancers deregulate the G1–S checkpoint through genomic alterations of different components of the pRB–E2F pathway including inactivation of *RB1* or *CDKN2A*, or amplifications of cyclin D or cyclin E[2,3]. Although activating E2Fs are necessary for cellular proliferation, too much E2F activity paradoxically induces apoptosis[4–9], suggesting a Goldilocks phenomenon. E2F1 is further negatively regulated by phosphorylation during S phase through cyclin A–CDK2, which limits its DNA binding[14,19–21].

Studies from budding yeast to mammalian cells demonstrated that cyclin substrate specificity is determined by a hydrophobic patchon

[1]Department of Medical Oncology, Dana-Farber Cancer Institute, Harvard Medical School, Boston, MA, USA. [2]Circle Pharma, San Francisco, CA, USA. [3]Department of Radiation Oncology, University of Texas Southwestern Medical Center, Dallas, TX, USA. [4]Department of Pathology, Brigham and Women's Hospital, Harvard Medical School, Boston, MA, USA. [5]Department of Radiation Oncology, Dana-Farber Cancer Institute, Brigham & Women's Hospital, Harvard Medical School, Boston, MA, USA. [6]Belfer Center for Applied Cancer Science, Experimental Therapeutics Core, Dana-Farber Cancer Institute, Boston, MA, USA. [7]Broad Institute of MIT and Harvard, Cambridge, MA, USA. [8]Target Discovery Institute, Centre for Medicines Discovery, Nuffield Department of Medicine, University of Oxford, Oxford, UK. [9]Department of Oncologic Pathology, Dana-Farber Cancer Institute, Boston, MA, USA. [10]Department of Medicine, Brigham and Women's Hospital, Harvard Medical School, Boston, MA, USA. ✉e-mail: matthew_oser@dfci.harvard.edu

cyclins recognizing short linear motifs on cyclin target proteins[10–13]. The most well-studied linear motif is the RxL motif[10–13], but additional motifs include the LxF, NLxxxL and PxF motifs[22–24]. The hydrophobic patch of cyclin A recognizes and binds to an RxL motif on E2F1 to initiate cyclin A–CDK2-mediated E2F phosphorylation[10,14]. Disrupting this interaction using tool peptides induces apoptosis selectively in cells with deregulated pRB and increased E2F activity[15].

Despite efforts, small-molecule inhibitors of cyclin A–RxL interactions have not progressed beyond early stages[25], reflecting the challenges of targeting intracellular protein–protein interactions. Macrocyclic peptides can overcome these challenges[26–29] but often lack drug-like properties[30]. Here we report the development of orally bioavailable macrocyclic peptide inhibitors of cyclin A/B–RxL interactions, elucidate their mechanism of inducing apoptosis in SCLCs with high E2F activity and demonstrate their efficacy in SCLC models.

Development of cyclin RxL macrocycles

To design passively permeable macrocyclic inhibitors targeting RxL-motif interactions with the hydrophobic patch of cyclins (Fig. 1a), we built a structural model using macrocycle-bound (Protein Data Bank (PDB): 1URC) and $p27^{Kip1}$-bound (PDB: 1JSU) cyclin A2–CDK2 complexes (Extended Data Fig. 1a). A composite molecule combining the lariat macrocycle (magenta) and the RxL motif of $p27^{Kip1}$ (yellow) occupying the larger hydrophobic patch and the smaller adjacent hydrophobic pocket (Fig. 1a and Extended Data Fig. 1b) was used as the starting scaffold.

Structure-based design and synthesis focused on optimizing cyclin binding affinity, engineering differential selectivity across cyclins A, B and E (guided by PDB: 1JSU, 2B9R and 1W98), and improving cell permeability for oral bioavailability. Scaffold optimization used peptidic and peptidomimetic features, with permeability-enhancing modifications guided by Circle Pharma's synthetic and computational platforms (Methods). This iterative approach yielded a series of passively permeable macrocycles with high affinity and diverse cyclin selectivity profiles (Fig. 1b, Extended Data Fig. 1c,e and Supplementary Methods). CIRc-004 bound to both the hydrophobic patch and smaller adjacent hydrophobic pockets on cyclin A2–CDK2, as shown by space-filling and stick representations (Fig. 1c and Extended Data Fig. 1d); additional compound properties are shown in Extended Data Fig. 1e,f. The medicinal chemistry effort to identify passively permeable cyclin RxL inhibitors has been described elsewhere[31].

Given previous work[15] and the near-universal loss of RB1 and E2F dysregulation in SCLC[1,32] (Extended Data Fig. 1g), we first tested these compounds for anti-proliferative activity in a limited panel of SCLC cell lines. Although we initially hypothesized that cyclin A RxL inhibition alone would be sufficient, cytotoxicity unexpectedly required inhibition of both cyclin A and B RxL interactions. Dual inhibitors, including CIRc-004, showed the strongest anti-proliferative activity, whereas a cyclin-A-selective RxL inhibitor had little effect (Fig. 1b and Extended Data Fig. 1h). The inactive enantiomer CIRc-005 lacked activity. Non-transformed WI-38 fibroblasts were insensitive to cyclin A/B inhibition.

High E2F activity correlates with sensitivity

We next screened 46 SCLC cell lines with the dual cyclin A/B RxL inhibitor CIRc-004 in anti-proliferation assays (Fig. 1d and Supplementary Table 1). Nearly all lines were highly sensitive to CIRc-004 at low nanomolar concentrations. Gene set enrichment (GSEA) and variation (GSVA) analyses[33] using MSigDb Hallmark gene sets[34] showed strong correlation between CIRc-004 sensitivity and expression of E2F targets and G2/M checkpoint pathway genes, independent of the SCLC subtype (Fig. 1d,e).

To determine broader applicability and ensure that cyclin A/B RxL inhibitors were not generally toxic, we screened the Horizon OncoSignature panel of 302 cancer cell lines using CIRc-001, a broader cyclin A/B/E RxL inhibitor (Fig. 1b and Extended Data Fig. 1h). Approximately 180 cell lines, including lung, breast and ovarian models, showed selective sensitivity to CIRc-001 (half-maximum effective concentration (EC_{50}) < 1 μM) (Extended Data Fig. 2a and Supplementary Table 2). E2F target gene signatures were enriched in sensitive lines across cancer types, whereas epithelial–mesenchymal transition -associated signatures were enriched in resistant lines (Extended Data Fig. 2b). Thus, low E2F activity and high expression of genes associated with epithelial–mesenchymal transition may predict resistance to cyclin A/B RxL inhibition, regardless of the tumour type.

We further compared responses to CIRc-004 in CIRc-004-sensitive SCLC (NCI-H1048, H446 and H69) and CIRc-004-resistant NSCLC (A549, HCC4006 and H1299) lines (Fig. 1f). CIRc-004 sensitivity was not due to differences in proliferation rates (Extended Data Fig. 2c) and all lines were resistant to the inactive enantiomer CIRc-005 even at high micromolar concentrations (Extended Data Fig. 2d). In sensitive SCLCs, CIRc-004 induced apoptosis (Fig. 1g,h) and mitotic arrest (Fig. 1i and Extended Data Fig. 2e). These effects required inhibition of both cyclin A and B, as selective inhibitors CIRc-018 (cyclin A) and CIRc-019 (cyclin B) lacked activity in proliferation, apoptosis and cell cycle assays (Extended Data Fig. 2f–h).

Normal cells, including RPE1 and $CD34^+$ haematopoietic stem and progenitor cells, were insensitive to CIRc-004, showing no mitotic arrest or apoptosis, even at high doses, consistent with a potentially large therapeutic window (Fig. 1f,h,i and Extended Data Fig. 2i,j). Instead, CIRc-004 induced p53 expression and G1 arrest at micromolar levels (Extended Data Fig. 2k–m). Lastly, NCI-H82, an SCLC line with lower E2F signatures, was also resistant to CIRc-004, with an EC_{50} comparable to resistant NSCLCs and RPE1 cells (Fig. 1f,h,i).

Genetic screens identify SAC-dependent killing

To elucidate the downstream mechanisms by which cyclin A/B RxL inhibitors induce apoptosis, we conducted a genome-wide CRISPR–Cas9 resistance screen in the highly sensitive NCI-H1048 SCLC cell line. Cells were transduced with the Brunello sgRNA library and, on day 10 (early timepoint, ETP), were pooled into four treatment arms: (1) dual cyclin A/B RxL inhibitor (CIRc-004); (2) broader cyclin A/B/E RxL inhibitor (CIRc-001); (3) selective orthosteric CDK2 inhibitor (CDK2i; PF-07104091); and (4) the inactive enantiomer CIRc-005 as a control (Fig. 2a). Compounds were dosed at EC_{90} concentrations (Extended Data Fig. 3a–c). The CDK2i was included to identify similarities and differences between CDK2i and cyclin A/B RxL inhibition. After 16 days of drug exposure (day 26, late timepoint, LTP), resistant populations emerged and were collected for deep sequencing. sgRNA enrichment analysis across replicates showed consistent enrichment of specific sgRNAs (Extended Data Fig. 3d–g). Comparing the LTP drug arms to the inactive enantiomer control and the ETP identified highly enriched hits of which the loss conferred resistance. Notably, hits from CIRc-004 and CIRc-001 were largely distinct from those enriched under CDK2i, suggesting a distinct mechanism of action (Fig. 2b,c and Extended Data Fig. 3h–l). Among the top enriched hits for CIRc-004 was cyclin B itself (encoded by *CCNB1*), providing evidence for cyclin B as a likely target of CIRc-004, but also indicating that cyclin B is required for cell death, and may therefore act through a gain-of-function mechanism. CDK2 was the only shared hit across all three treatments, supporting its central role but again suggesting that cell killing may involve a gain of CDK2 function.

Notably, many hits enriched under CIRc-004 and CIRc-001 mapped to the spindle assembly checkpoint (SAC), including *KNTC1*, *ESPL1*, *ZWINT*, *ZWILCH*, *ZW10* and *MAD1L1* (Fig. 2b,c, Extended Data Fig. 3h,j,k and Supplementary Table 3), indicating that SAC integrity is required for cell killing by cyclin A/B RxL inhibition. By contrast, these were not enriched under CDK2i (Extended Data

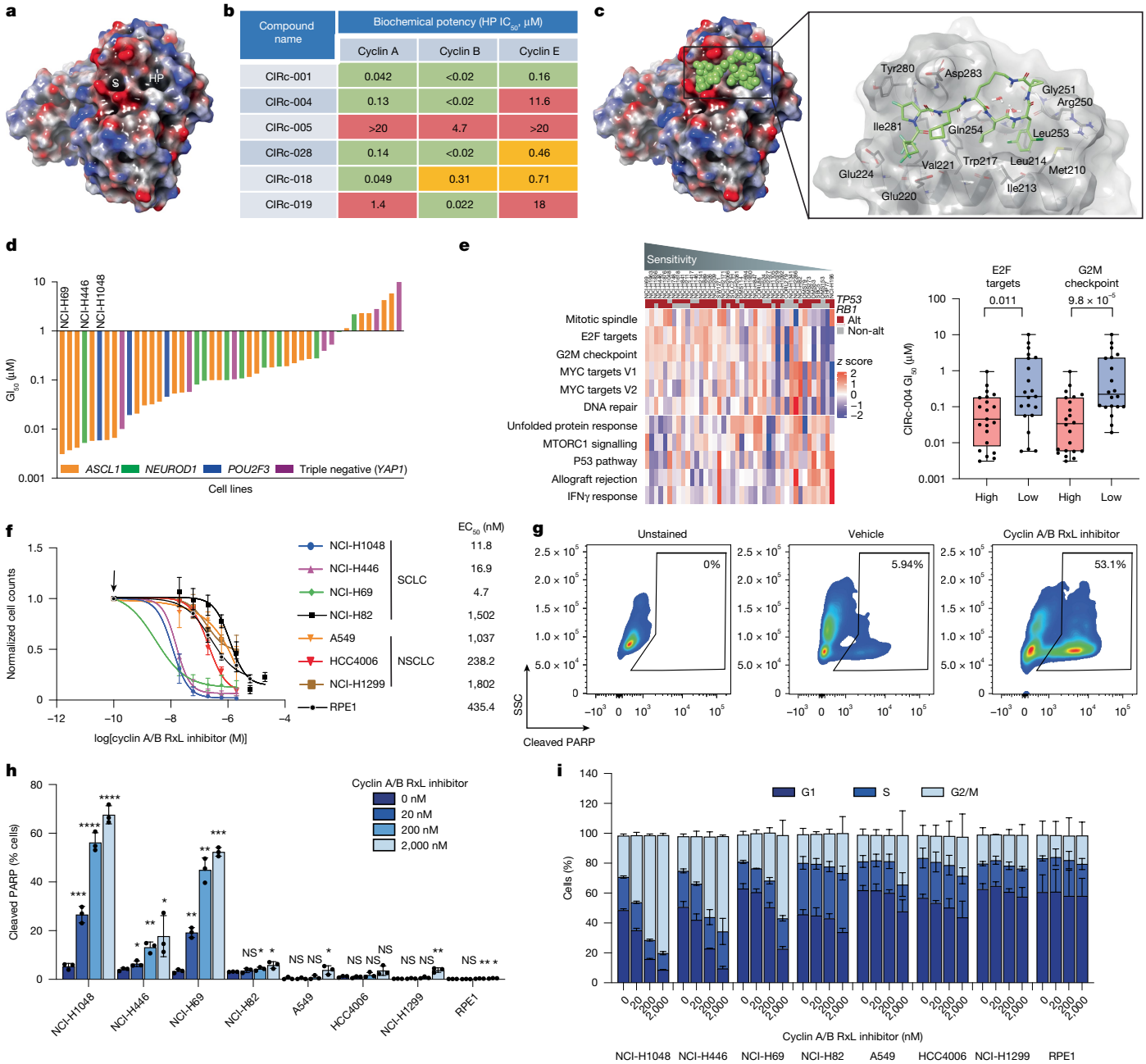

Fig. 1 | Cyclin A/B RxL inhibitors induce apoptosis in cancer cells with high E2F activity. a, The structure of cyclin A (PDB: 1JSU), coloured by surface charge (blue, basic; red, acidic; white, neutral). HP, hydrophobic patch; S, the smaller adjacent hydrophobic pocket. **b**, The biochemical activity of cyclin RxL macrocycles against cyclin A1–CDK2, cyclin E1–CDK2 and cyclin B–CDK1 complexes was measured using fluorescence polarization. **c**, Docked model of CIRc-004 (green) bound to cyclin A and a detailed stick representation. **d**, GI_{50} (concentrations resulting in 50% growth inhibition) waterfall plot of CIRc-004 in 46 human SCLC cell lines. **e**, Hallmark pathways associated with CIRc-004 sensitivity (false discovery rate (FDR) < 0.05) in 42 SCLC cell lines, calculated by GSVA using MSigDb Hallmark RNA-seq data (left). Cell lines were ranked by GI_{50}. Each column represents a distinct SCLC cell line, ranked from most to least sensitive. Right, comparison of CIRc-004 GI_{50} values between high versus low E2F targets or G2M pathway groups (threshold, median pathway score; Mann–Whitney *t*-test). Alt., altered; non-alt, non-altered. **f**, Dose–response curves of the indicated SCLC (NCI-H1048, NCI-H446, NCI-H69, NCI-H82), NSCLC (A549, HCC4006, NCI-H1299) and human non-transformed RPE1 cell lines treated with CIRc-004 for 6 days. The average EC_{50} values are shown. The arrows indicate DMSO controls (used for normalization). **g**, Representative flow cytometry plots of cleaved PARP in NCI-H1048 cells treated with CIRc-004 (200 nM) or DMSO for 3 days. **h**, Flow cytometry quantification of cleaved-PARP-positive cells after 3 days of CIRc-004 treatment. **i**, The cell cycle distribution after 24 h treatment with CIRc-004 or DMSO followed by propidium iodide staining. For **f**, **h** and **i**, $n = 3$ biological replicates. Data are mean ± s.d. Statistical significance in **h** was determined using unpaired two-tailed Student's *t*-tests; $^{*}P < 0.05$, $^{**}P < 0.01$, $^{***}P < 0.001$, $^{****}P < 0.0001$.

Fig. 3i,l). Conversely, depleted hits—whose inactivation sensitized cells—included *E2F7* and *E2F8*, repressive E2Fs that oppose E2F1 activity[35] and *STMN1*[36], a mitotic phosphoprotein (Fig. 2b, Extended Data Fig. 3h,j–k and Supplementary Table 3). In contrast to the cyclin A/B RxL inhibitor screen, *CCNB1* was depleted in the CDK2i screen, consistent with cyclin B suppression enhancing CDK2i-induced death.

To validate the CRISPR screen, we performed knockouts of *CCNB1*, *CDK2*, *KNTC1*, *LIN54*, *MAD1L1* and *ZWINT* in NCI-H1048 cells, all of which conferred robust resistance to CIRc-004 (Fig. 2d–g and Extended Data

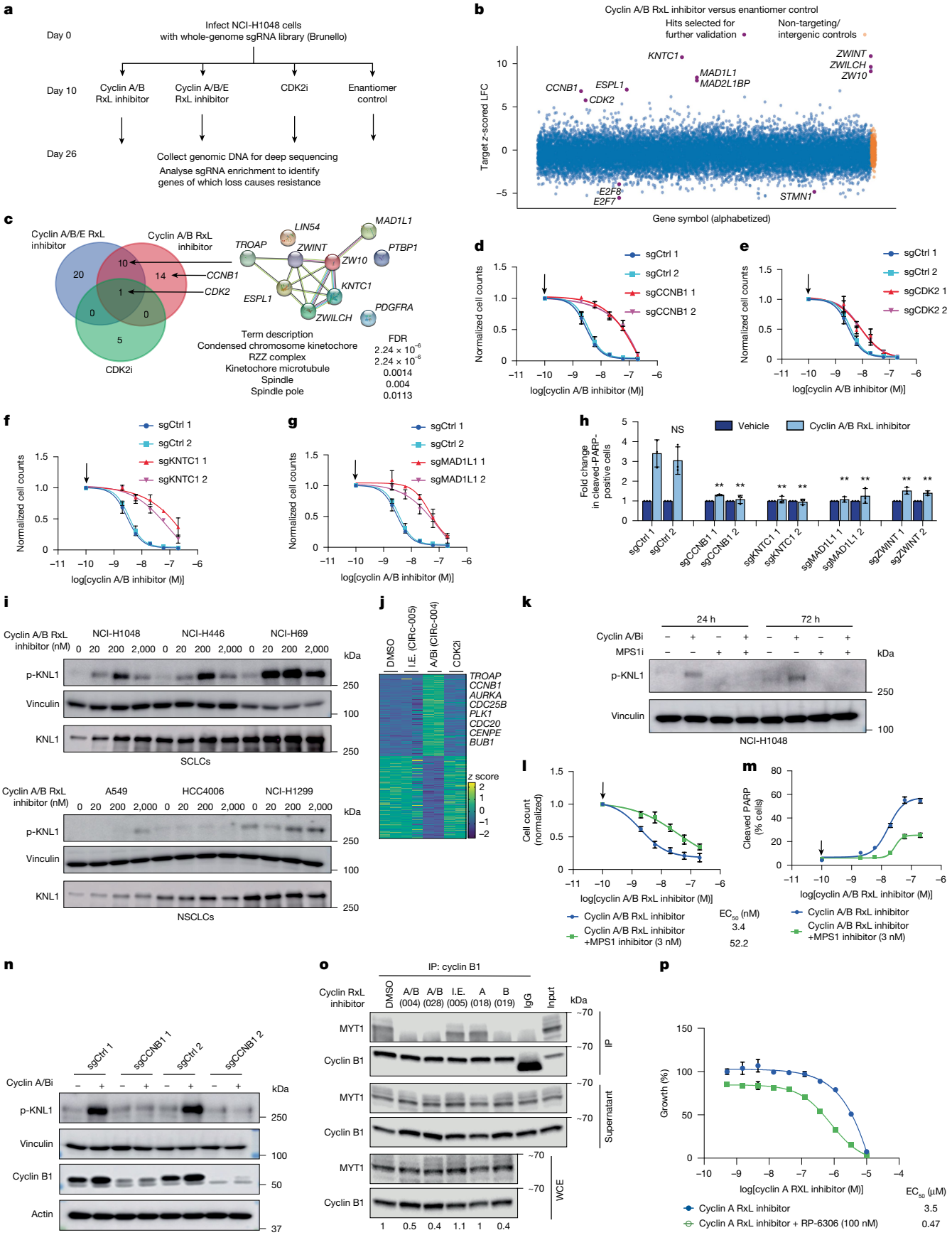

Fig. 2 | See next page for caption.

Fig. 2 | Genetic screens reveal SAC-dependent mechanisms of cyclin A/B RxL inhibitor killing. a, Schematic of the genome-wide CRISPR–Cas9 knockout resistance screen in NCI-H1048 cells transduced with the Brunello sgRNA library. After selection (day 10), cells were treated with CIRc-004 (200 nM), CIRc-001 (200 nM), PF-07104091 (CDK2i, 500 nM) or inactive enantiomer (I.E.) CIRc-005 (200 nM) and collected at day 26 (LTP). **b**, The top enriched and depleted hits from Apron analysis of CIRc-004 LTP versus CIRc-005 LTP. $n = 2$ biological replicates. **c**, The top enriched hits ($q < 0.25$) across treatments. Right, STRING network (https://string-db.org; CC BY 4.0)[66] of shared hits highlights SAC proteins. **d**–**g**, Dose–response curves of NCI-H1048 cells expressing two non-targeting sgRNAs (sgCtrl) or two sgRNAs targeting *CCNB1* (**d**), *CDK2* (**e**), *KNTC1* (**f**) or *MAD1L1* (**g**), treated with CIRc-004 for 6 days. **h**, Flow cytometry quantification of cleaved PARP in cells from **d**–**g** treated with CIRc-004 (20 nM). Data are the fold change relative to vehicle. **i**, Immunoblot of the indicated SCLC and NSCLC cell lines treated for 24 h with increasing doses of CIRc-004. In **d**–**h**, data are mean ± s.d. In **d**–**i**, $n = 3$ biological replicates. **j**, RNA-seq analysis of NCI-H1048 cells treated for 24 h with CIRc-004 (200 nM), CIRc-005 (200 nM) or PF-07104091 (500 nM); the top 150 differentially expressed genes are shown (adjusted P (P_{adj}) < 0.05). **k**, Immunoblot analysis of p-KNL1 in NCI-H1048 cells treated with CIRc-004 (20 nM), BAY-1217389 (MPS1i, 3 nM) or both for 24 h. **l**,**m**, CIRc-004 dose–response for proliferation (**l**) and cleaved PARP FACS assays (**m**) in the presence or absence of 3 nM BAY-1217389 for 3 days in NCI-H1048 cells. Data are mean ± s.d. $n = 3$ biological replicates. **n**, Immunoblot analysis of NCI-H1048 cells expressing sgCtrl or *CCNB1* sgRNAs treated with CIRc-004 (20 nM) or DMSO for 24 h ($n = 3$ biological replicates). **o**, Cyclin B1 immunoprecipitations from NCI-H1048 cells treated for 2 h with CIRc-004 (004), CIRc-028 (028), CIRc-005 (005), CIRc-018 (018) or CIRc-019 (019) (300 nM); MYT1 binding normalized to cyclin B1 is shown. $n = 3$ biological replicates for all except for CIRc-028, for which $n = 2$. **p**, Dose–response analysis of NCI-H1048 cells treated with CIRc-018 with or without RP-6306 (100 nM) for 5 days. Data are mean ± s.d. from two technical replicates; $n = 3$ biological replicates. In **d**–**g**, **l** and **m**, the arrows indicate the DMSO-treated normalization controls. Statistical significance in **h** was calculated using unpaired two-tailed Student's *t*-tests.

Fig. 4a, b). Similar resistance was confirmed in NCI-H446 SCLC cells for a subset of hits (Extended Data Fig. 4c–f). Furthermore, *CCNB1* inactivation increased sensitivity to the CDK2i, while CDK2 inactivation conferred partial resistance (Extended Data Fig. 4g,h), validating the mechanistic divergence. Lastly, knockout of *CCNB1*, *KNTC1*, *MAD1L1* or *ZWINT* rescued mitotic arrest and apoptosis induced by CIRc-004 (Fig. 2h and Extended Data Fig. 4i–l).

To orthogonally validate these findings, we used a forward genetic screen in iHCT116 cells, a colorectal cancer model engineered with inducible degradation of MLH1 using indole acetic acid (IAA), enabling high (mut-high, +IAA) or low (mut-low, −IAA) mutation rates depending on IAA treatment[37]. CIRc-004 suppressed proliferation in iHCT116 cells (Extended Data Fig. 5a). After barcoded iHCT116 cells were cultured for an extended period with CIRc-004, resistant clones were isolated from both mut-low and mut-high populations (Extended Data Fig. 5b,c). These clones were over 100-fold more resistant than parental cells and remained sensitive to an unrelated toxin (MLN4924), ruling out non-specific resistance (Extended Data Fig. 5d). Exome sequencing of eight resistant clones revealed CDC20 mutations in five (Extended Data Fig. 5e,f). Notably, two mutations affected Arg445, and all four unique mutations mapped to the same surface of CDC20 in the crystal structure where CDC20 interacts with the mitotic checkpoint complex to promote SAC activation[38–41] (Extended Data Fig. 5g). These heterozygous mutations are probably dominant negatives, allowing SAC bypass and anaphase progression in the presence of CIRc-004. Ectopic expression of CDC20(R445Q), but not wild-type CDC20, in both iHCT116 and NCI-H1048 cells conferred resistance to CIRc-004 (Extended Data Fig. 5h–m). Together, these complementary CRISPR knockout and forward genetic screens converge on the spindle assembly checkpoint as the critical mechanism through which cyclin A/B RxL inhibitors induce mitotic arrest and apoptosis in SCLC and other cancer models.

To further determine how CIRc-004 induces mitotic arrest and apoptosis, we performed live-cell imaging of NCI-H1048 cells expressing GFP–H2B. CIRc-004 blocked anaphase initiation, consistent with SAC activation causing mitotic cell death (Extended Data Fig. 6a,b and Supplementary Videos 1 and 2). SAC components assemble on the scaffold protein KNL1, which is phosphorylated by MPS1 in early mitosis[42]. As KNL1 is dephosphorylated after satisfaction of SAC, persistent phosphorylated KNL1 (p-KNL1) serves as a SAC activation marker. CIRc-004 robustly increased p-KNL1 levels in sensitive, but not resistant, cell lines at apoptosis-inducing concentrations (Figs. 1h and 2i and Extended Data Fig. 6c–h). RNA-sequencing (RNA-seq) analysis of NCI-H1048 cells acutely treated with CIRc-004 revealed upregulation of SAC-related genes (such as *CCNB1* and *CDC20*) and mitotic signatures, while the inactive enantiomer CIRc-005 had minimal transcriptional impact (Fig. 2j, Extended Data Fig. 6i,j and Supplementary Table 4). In RPE1 cells, CIRc-004 induced mitotic arrest and p-KNL1 only after CRISPR inactivation of *RB1* and *TP53*, and only at high concentrations (Extended Data Fig. 6k,l), consistent with their relative resistance (Fig. 1f,h,i and Extended Data Fig. 2k–m), demonstrating that disruption of G1–S checkpoint control is necessary for induction of SAC. In contrast to cyclin A/B RxL inhibitors, CDK2 inhibition using PF-07104091 did not activate the SAC in NCI-H1048 cells (Extended Data Fig. 7a), but instead reduced S-phase progression and led to accumulation of 4N cells undergoing DNA replication, consistent with a late S-phase/early G2 arrest (Extended Data Fig. 7b,c). Consistent with this, PF-07104091 treatment upregulated S-phase-associated genes, including *CDC6* and *CCNE1* (Extended Data Fig. 7d,e and Supplementary Table 4).

We hypothesized that chemical inhibition of MPS1 would phenocopy genetic SAC disruption. Using a sublethal dose of MPS1 inhibitor BAY-1217389 (3 nM), which blocked KNL1 phosphorylation without affecting proliferation (Fig. 2k and Extended Data Fig. 8a,b), we found that MPS1 inhibition blocked SAC activation and rescued SCLC (NCI-H1048, NCI-H69 and NCI-H446) cells from CIRc-004-induced growth arrest and apoptosis (Fig. 2k–m and Extended Data Fig. 8c–f). Similarly, expression of CDC20(R445Q), but not wild-type CDC20, abolished CIRc-004-induced SAC activation in iHCT116 and NCI-H1048 cells (Extended Data Fig. 8g,h). These findings confirm that SAC activation is essential for the apoptotic activity of cyclin A/B RxL inhibitors.

Cyclin B–MYT1 blockade activates SAC

Cyclin B emerged as a top enriched hit in the CIRc-004 resistance screen, suggesting its activity is essential for the apoptotic effect of cyclin A/B RxL inhibitors (Fig. 2). This is paradoxical if CIRc-004 merely blocks cyclin B function, instead indicating a gain of cyclin B activity. Supporting this, increased cyclin B–CDK1 activity can drive SAC activation[40,43], and CIRc-004 increased cyclin B activity as measured by phosphorylation at Ser126[44,45] (Extended Data Fig. 8i). Furthermore, *CCNB1*-knockout NCI-H1048 cells failed to activate the SAC in response to CIRc-004 (Fig. 2n), demonstrating that cyclin B activity is necessary for SAC activation. We therefore hypothesized that CIRc-004 disrupts an interaction between cyclin B and an RxL-containing substrate that normally functions as a negative regulator of cyclin B–CDK1 activity. One such substrate is MYT1 (encoded by *PKMYT1*), a kinase that inhibits cyclin B–CDK1 activity by phosphorylating CDK1 at Thr14[46]. Co-immunoprecipitation experiments showed that dual cyclin A/B RxL inhibitors and the cyclin B-selective inhibitor CIRc-019 disrupted the cyclin B–MYT1 interaction, whereas the cyclin-A-selective inhibitor CIRc-018 and inactive enantiomer CIRc-005 did not (Fig. 2o). Moreover, the MYT1 inhibitor RP-6306[47] potentiated cell killing by CIRc-018 in multiple SCLC cell lines (Fig. 2p and Extended Data Fig. 8j–n). This was selective for CIRc-018 as CIRc-004 and CIRc-019 did not (Extended Data Fig. 8o–t). WEE1 is another kinase that negatively

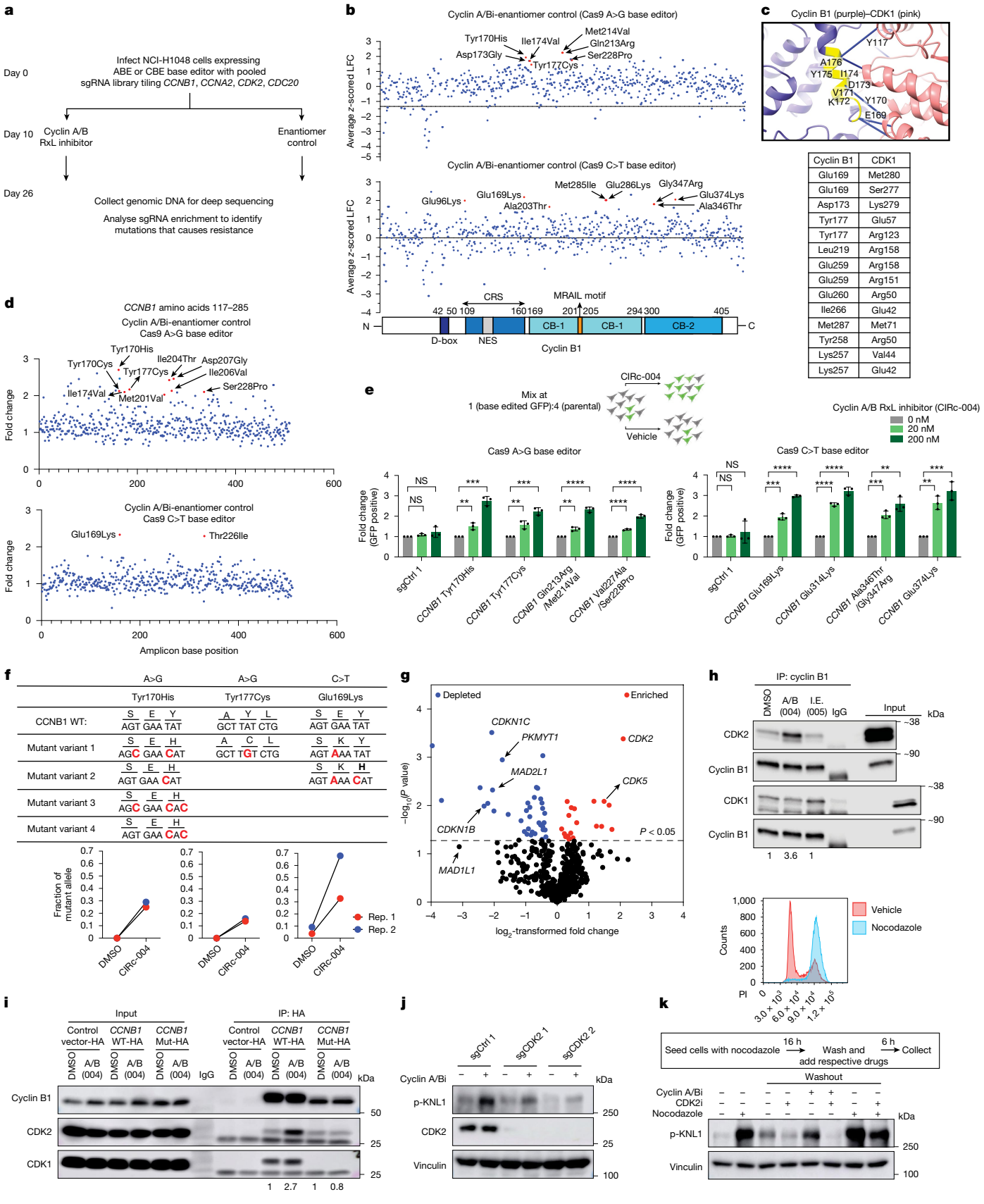

Fig. 3 | See next page for caption.

regulates CDK1 activity[48]. Although a smaller fraction of WEE1 appears to co-immunoprecipitate with cyclin B, CIRc-004 and CIRc-019 also disrupted this interaction (Extended Data Fig. 8u). However, the selective WEE1 inhibitor MK1775 did not hypersensitize NCI-H1048 cells to CIRc-018 (Extended Data Fig. 8v–x). Together, these data show that cyclin B RxL inhibition can disrupt either a MYT1 or WEE1 interaction with

Fig. 3 | Cyclin A/B RxL inhibitors promote cyclin B–CDK2 complex formation for SAC-induced cell death. a, Schematic of the base-editor (BE) CRISPR resistance screen in NCI-H1048 cells transduced with an sgRNA library tiling *CCNB1*, *CCNA2*, *CDK2*, *CDC20* and controls. After selection (day 10), cells were treated with CIRc-004 (200 nM) or inactive enantiomer CIRc-005 (200 nM) and collected at day 26. **b**, The average *z*-scored log-transformed fold change (LFC) of sgRNAs tiling *CCNB1* in CIRc-004 versus CIRc-005 in A>G (top) and C>T (bottom) base-editor screens. Mutations are labelled by predicted amino acid changes. $n = 4$ biological replicates. **c**, Predicted AlphaFold 2 model of the cyclin B1–CDK1 interaction, showing cyclin B residues 169–177. **d**, The fold change in variant reads at each *CCNB1* base in CIRc-004 versus CIRc-005. Mutations of interest are labelled. $n = 2$ biological replicates. **e**, FACS-based competition assays for the indicated *CCNB1* sgRNA variants in GFP$^+$ NCI-H1048 base-editor cells mixed with parental base-editor counterparts at 1:4 and treated with CIRc-004 for 13 days; the fold change enrichment over DMSO is shown. Data are mean ± s.d. $n = 3$ biological replicates. Statistical significance was calculated using unpaired two-tailed Student's *t*-tests. **f**, The fraction of variant alleles in *CCNB1*-mutant lines from **e** after CIRc-004 (200 nM) or DMSO treatment for 13 days was analysed using deep amplicon sequencing. $n = 2$ biological replicates. **g**, Volcano plot of cyclin B Immunoprecipitation–mass spectrometry in NCI-H1048 cells treated for 2 h with CIRc-004 (50 nM) relative to CIRc-005. $n = 3$ biological replicates. Statistical significance was calculated using two-sample Student's t-tests corrected for multiple hypothesis testing using permutation-based FDR (5%). **h**,**i**, Immunoblots after cyclin B1 immunoprecipitation (IP) from NCI-H1048 cells (**h**) or HA-tagged wild-type (WT) *CCNB1* versus *CCNB1* triple-mutant expressed in HEK293T cells (**i**) treated with CIRc-004 (300 nM) or DMSO. CDK2 band intensities were normalized to cyclin B1. $n = 2$ (**h**) or $n = 3$ (**i**) biological replicates. For **h** and **i**, the fold increase in CDK2 relative to DMSO is shown. **j**, Immunoblot of NCI-H1048 cells infected with *CDK2* sgRNAs or sgCtrl and treated with CIRc-004 (20 nM) or DMSO for 24 h. **k**, Immunoblot of NCI-H69 cells synchronized in mitosis with nocodazole (60 ng ml^{-1}) and released into CIRc-004 (20 nM), PF-07104091 (500 nM) or both. Top, propidium iodide (PI) histogram showing 16 h post-nocodazole synchronization. For **j** and **k**, $n = 3$ biological replicates.

cyclin B and that disruption of the cyclin B–MYT1 interaction is functionally important for cell killing by cyclin A/B RxL inhibitors leading to CDK activation on the cyclin B complex to promote SAC activation and mitotic cell death.

Cyclin B–CDK2 complex drives cell death

To further investigate how CIRc-004 induces mitotic cell death, we performed a CRISPR–Cas9 base editor screen in NCI-H1048 cells using A>G and C>T base editors[49] and a custom sgRNA library tiling *CCNB1*, *CCNA2*, *CDK2* and *CDC20* (Fig. 3a). Cells were treated with CIRc-004 or the inactive control CIRc-005 from day 10 (ETP) to day 26 (LTP). Sequencing confirmed strong replicate correlation and robust depletion of essential gene controls (Supplementary Fig. 2a,b), validating screen performance. Consistent with our forward genetic screen (Extended Data Fig. 5f–m), sgRNAs predicted to mutate *CDC20* at Arg445 were enriched (Supplementary Fig. 2c). Notably, sgRNAs targeting *CCNB1* residues 169–177—where cyclin B canonically binds CDK1[50]—were also enriched (Fig. 3b,c). We then repeated the screen and performed focused amplicon sequencing on *CCNB1* amino acid residues 117–285. Amplicon sequencing directly validated several *CCNB1* mutants (Glu169Lys, Tyr170His and Tyr177Cys) that conferred CIRc-004 resistance, all located within the region where cyclin B interacts with CDK1 (Fig. 3c,d). Additional enriched mutations were located in the hydrophobic patch of cyclin B where CIRc-004 binds (Fig. 3b,d and Extended Data Fig. 9a), suggesting on-target effects. Fluorescence-associated cell sorting (FACS)-based competition assays confirmed that mutations disrupting either the cyclin B–CDK interface or the hydrophobic patch conferred resistance (Fig. 3e). Amplicon sequencing of mixed cell populations from these assays identified the precise base editor-induced *CCNB1* mutations, with the fraction of cells carrying Glu169Lys, Tyr170His or Tyr177Cys substantially enriched after CIRc-004 treatment (Fig. 3f).

To examine protein-level effects, we performed cyclin B immunoprecipitation followed by mass spectrometry. Consistent with our experiments above (Fig. 2o), one of the top depleted proteins after treatment with CIRc-004 was MYT1 (encoded by *PKMYT1*) and known cyclin–CDK RxL-dependent inhibitors including p27^{Kip1} and p57^{Kip2} (encoded by *CDKN1B* and *CDKN1C*, respectively)[14] (Fig. 3g and Extended Data Fig. 9b). Notably, a top enriched protein after CIRc-004 treatment was CDK2 (Fig. 3g and Extended Data Fig. 9b). Although cyclin B binds to CDK2 in vitro[51], cyclin B canonically binds to CDK1[52] and not to CDK2 in cells[50]. An AlphaFold model supported binding between cyclin B residues 169–177 and CDK2 (Extended Data Fig. 9c). Immunoprecipitation experiments for cyclin B in NCI-H1048, NCI-H446 and RPE1 cells confirmed that CIRc-004 increased the co-immunoprecipitation of CDK2 without affecting CDK1 (Fig. 3h and Extended Data Fig. 9d–g). CIRc-004 did not alter the immunoprecipitation/co-immunoprecipitation interaction between cyclin A and CDK2 (Extended Data Fig. 9h). CIRc-004 also induced phosphorylation of the CDK mitotic RxL-independent substrate stathmin (STMN1)[53], which was blocked by a CDK2i, but not by a CDK1i (Extended Data Fig. 9i,j). Stathmin phosphorylation inactivates stathmin disabling its ability to depolymerize microtubules, which activates SAC[54]. Supporting this, *STMN1* depletion sensitized cells to CIRc-004 in our CRISPR knockout screen (Fig. 2b and Extended Data Fig. 3h,j,k), suggesting that CIRc-004-induced CDK2-dependent stathmin phosphorylation promotes sensitivity to cyclin A/B RxL inhibitors.

We next tested whether the cyclin B triple mutant (Glu169Lys/Tyr170His/Tyr177Cys) blocked CDK2 binding. Co-immunoprecipitation experiments showed that CIRc-004 induced an interaction between CDK2 and wild-type cyclin B that was abrogated in cells expressing the cyclin B triple mutant (Fig. 3i and Extended Data Fig. 9k). Moreover, CDK2 inactivation in NCI-H1048 cells partially abrogated CIRc-004-induced SAC activation (Fig. 3j). Lastly, acute CDK2i also abrogated SAC activation by CIRc-004 after release from mitotic arrest with nocodazole further validating that CDK2 activity is necessary for SAC activation by CIRc-004 (Fig. 3k). These data, together with CDK2 being a top enriched hit in our CRISPR knockout screen, demonstrate that cyclin A/B RxL inhibitors promote the redirection of CDK2 to cyclin B to form cyclin B–CDK2 complexes to promote SAC activation and mitotic cell death.

E2F hyperactivation sensitizes cells

Having established the role of cyclin B RxL inhibition in the CIRc-004 mechanism of action, we next explored the contribution of cyclin A RxL inhibition. Cyclin A is expressed and canonically associates with CDK2 in S phase[55]. SAC is normally activated during mitosis when there is improper attachment of kinetochores to the mitotic spindles, which can be caused by DNA damage and replication stress that occurs during S phase[40]. Consistent with this, pulse-labelling with EdU showed a large fraction of G2 cells undergoing active DNA synthesis after treatment with CIRc-004 (Fig. 4a). Moreover, CIRc-004 also induced replication stress markers, including γH2AX, p-RPA2 and p-KAP1, specifically in sensitive SCLC lines (Fig. 4b and Extended Data Fig. 10a–c). CIRc-004 induced γH2AX irrespective of whether cells had the ability to form SAC complex and this required both cyclin A and cyclin B RxL inhibition (Extended Data Fig. 10d,e).

High E2F activity strongly correlated with sensitivity to CIRc-004 in SCLC lines (Fig. 1e), and repressive E2Fs (*E2F7* and *E2F8*) were top depleted hits in our CRISPR screen (Fig. 2b), suggesting that heightened E2F activity could enhance cyclin A/B RxL inhibitor sensitivity. Cyclin A binds to E2F1 through an RxL motif, enabling cyclin A–CDK2-mediated phosphorylation to repress E2F1 activity[14,19–21]. Blocking this interaction

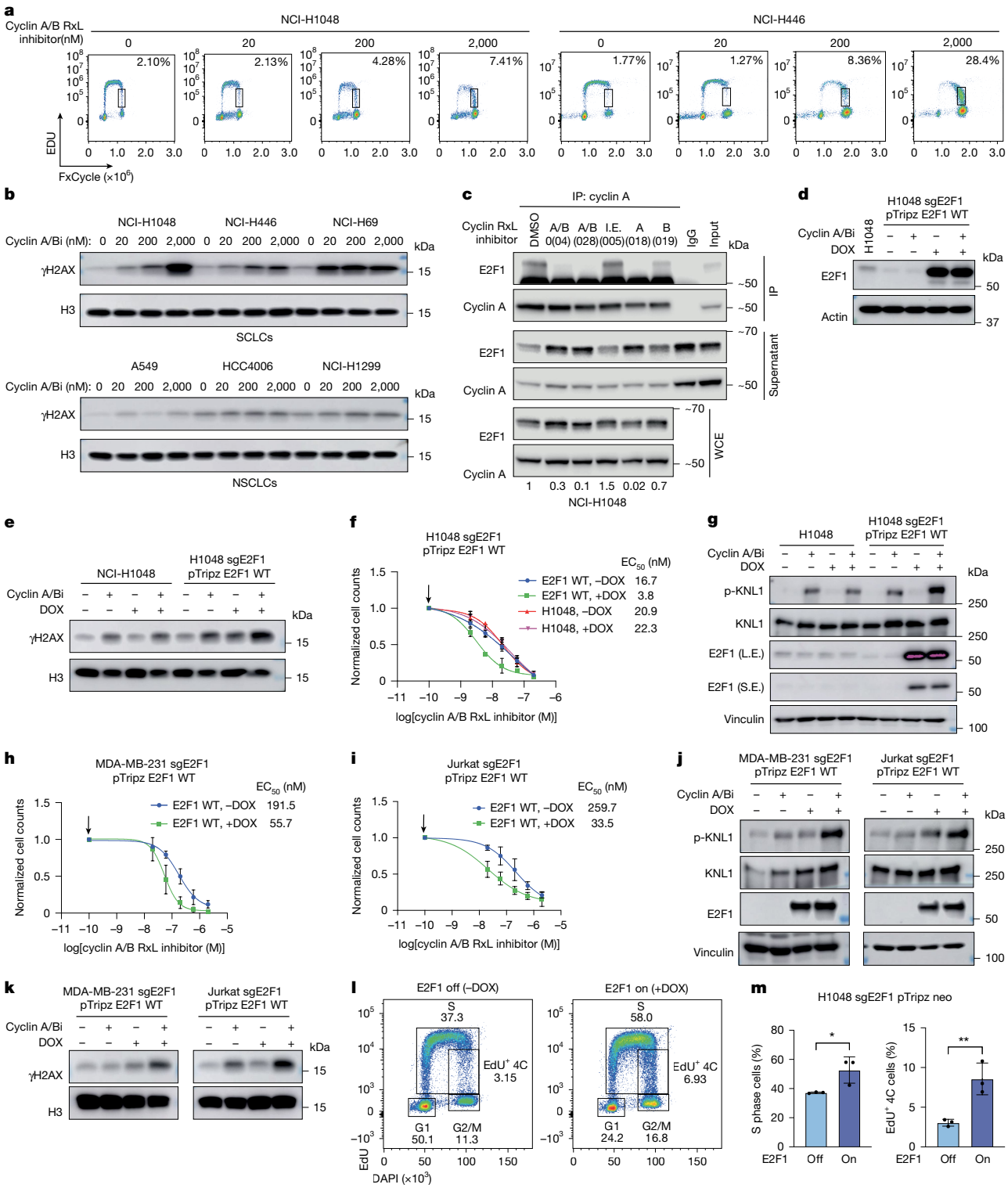

Fig. 4 | Cyclin A RxL inhibition induces E2F1 hyperactivation and sensitizes cells to cyclin A/B RxL inhibitors. a, FACS analysis of EdU and FxCycle staining in NCI-H1048 and NCI-H446 cells treated for 24 h with increasing CIRc-004 doses; the EdU$^+$ 4C population is indicated. **b**, Immunoblot of the indicated SCLC and NSCLC lines treated for 3 days with CIRc-004. **c**, Immunoblot after cyclin A immunoprecipitation in NCI-H1048 cells treated for 2 h with CIRc-004, CIRc-028, CIRc-005, CIRc-018, CIRc-019 or DMSO (300 nM each). The E2F1 band intensity was normalized to cyclin A; the fold change relative to DMSO shown. WCE, whole-cell extract. **d**–**e**,**g**, Immunoblots of NCI-H1048 cells expressing doxycycline (DOX)-inducible *E2F1*-sgRNA-resistant cDNA and endogenous *E2F1*-targeting sgRNA, treated with or without DOX and then with CIRc-004 (20 nM) for 24 h (**d**,**g**) or 72 h (**e**). **f**,**h**,**i**, Dose–response assays of NCI-H1048 (**f**), MDA-MB-231 (**h**) and Jurkat (**i**) cells with or without DOX for 24 h, followed by CIRc-004 treatment for 3 or 6 days. Data are mean ± s.d. The arrows indicate the DMSO controls. **j**,**k**, Immunoblots of MDA-MB-231 and Jurkat cells from the experiments in **h** and **i**. **l**, FACS analysis of EdU and 4′,6′-diamidino-2-phenylindole (DAPI) staining in DOX-induced E2F1-expressing NCI-H1048 cells; the indicated populations are shown with the gates. **m**, Quantification of S-phase and EdU$^+$ 4C populations from **l**. Data are mean ± s.d. Statistical significance was calculated using unpaired two-tailed Student's *t*-tests. For **a**, **b** and **d**–**m**, $n = 3$ biological replicates. For **c**, $n = 2$ biological replicates. For histone blots in **e** and **k**, total histone H3 was run as a sample-processing control on a separate gel.

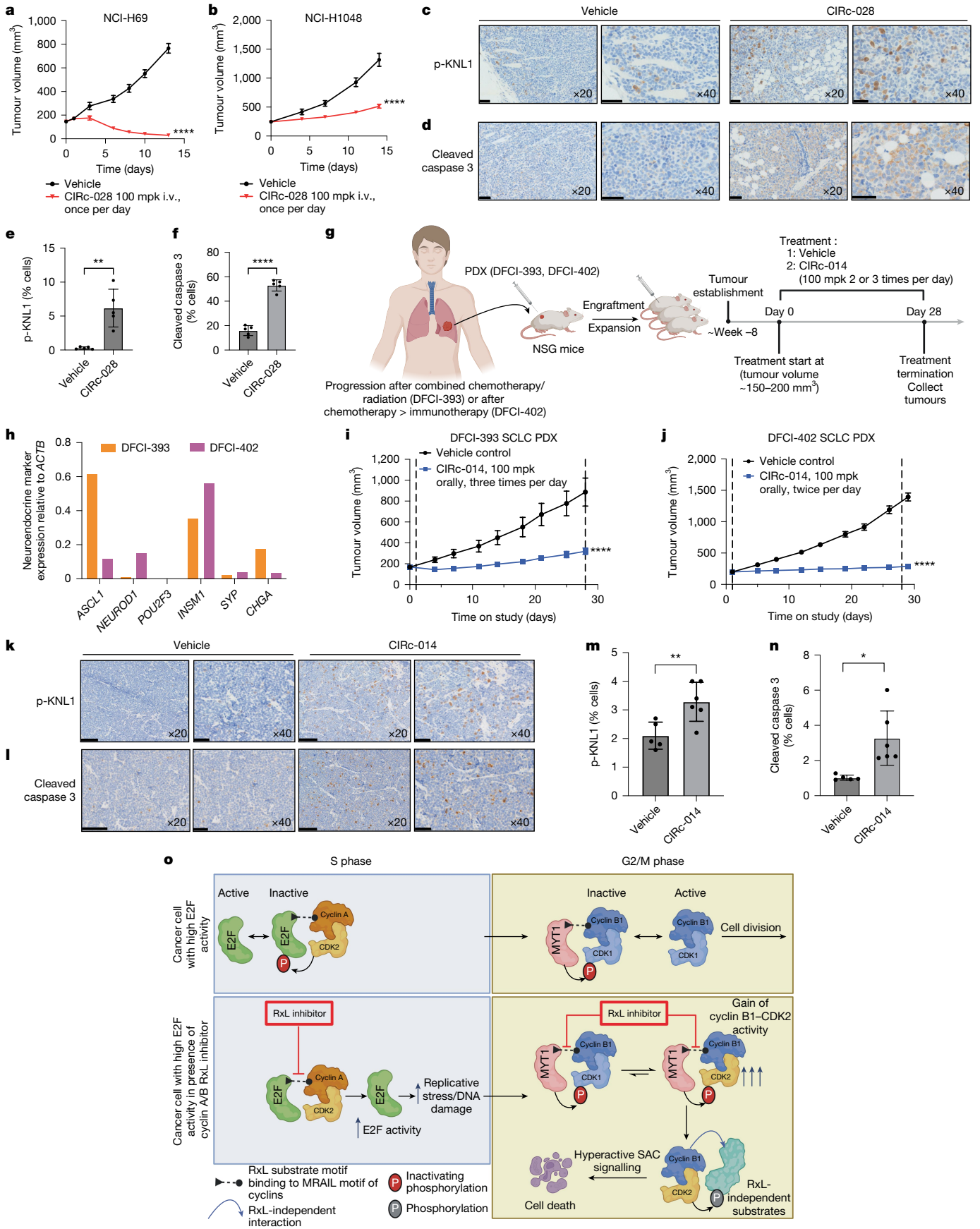

Fig. 5 | See next page for caption.

Fig. 5 | Cyclin A/B RxL inhibitors exhibit on-target anti-tumour activity in SCLC mouse models in vivo. a,**b**, Tumour volume curves of NCI-H69 (**a**) and NCI-H1048 (**b**) xenografts in athymic nude mice treated with vehicle or cyclin A/B RxL inhibitor (CIRc-028) dosed at 100 mg per kg (mpk) intravenously (i.v.) once per day for 14 days. $n = 10$ mice per arm (**a**), and $n = 10$ (vehicle) and $n = 8$ (CIRc-028) mice (**b**). Data are mean ± s.e.m. Statistical analysis was performed using two-way analysis of variance (ANOVA); $P < 0.0001$. **c**,**d**, Representative IHC analysis of p-KNL1 (**c**) and cleaved caspase-3 (**d**) in NCI-H69 tumours 18 h after treatment. **e**,**f**, Quantification of **c** (**e**) and **d** (**f**). $n = 5$ tumours from independent mice per group. Data are mean ± s.d. Statistical significance calculated using unpaired two-tailed Student's *t*-tests. **g**, Schematic for DFCI-393 and DFCI-402 PDX studies with oral cyclin A/B RxL inhibitor CIRc-014. **h**, mRNA expression of SCLC transcription factors and neuroendocrine markers by RNA-seq. **i**,**j**, Tumour volume curves of DFCI-393 (**i**) and DFCI-402 (**j**) PDXs treated with CIRc-014 (100 mg per kg orally three times per day (**i**) or twice per day (**j**)) or vehicle for 28 days. The dashed lines indicate the start and end of treatment. For **i**, $n = 10$ (vehicle) and $n = 9$ (CIRc-014) mice. For **j**, $n = 10$ mice per arm. Data are mean ± s.e.m. Statistical analysis was performed using two-way ANOVA; $P < 0.0001$. **k**,**l**, Representative IHC analysis of p-KNL1 (**k**) and cleaved caspase-3 (**l**) in DFCI-393 tumours treated with CIRc-014 (100 mg per kg orally three times per day) for 4 days. **m**,**n**, Quantification of **k** (**m**) and **l** (**n**). For **m** and **n**, $n = 5$ (vehicle) and 6 (CIRc-014) tumours from independent mice. Data are mean ± s.d. Statistical significance was calculated using unpaired two-tailed students *t*-tests. **o**, The proposed mechanism: in cancers with compromised G1–S checkpoint (for example, *RB1* and *TP53* loss) and consequently high E2F activity, cyclin A binds to activating E2Fs through RxL motifs to dampen E2F activity, and cyclin B binds to MYT1 to restrain CDK1 activity during G2. Cyclin A/B RxL inhibitors disrupt both interactions: (1) blocking cyclin A–E2F1 repression increases replication stress; (2) blocking cyclin B–MYT1 binding allows cyclin B to form a neomorphic complex with CDK2, driving RxL-independent phosphorylation (of, for example, stathmin), SAC activation and mitotic death. The diagrams in **g** and **o** were created with BioRender. Scale bars, 50 μm (**c**,**d**), and 100 μm (×20) and 50 μm (×40) (**k**,**l**).

can promote apoptosis[15]. We therefore hypothesized that cyclin A RxL inhibition blocks the RxL-dependent interactions of cyclin A with activating E2Fs (E2F1, E2F2 and E2F3), leading to heightened E2F activity. Co-immunoprecipitatoin experiments confirmed that only dual cyclin A/B and cyclin A-selective RxL inhibitors disrupted interactions between cyclin A and E2F1 or E2F3 (Fig. 4c and Extended Data Fig. 10f). E2F2 was undetected, probably due to low abundance in NCI-H1048 cells. Overexpression of E2F1 in NCI-H1048, MDA-MB-231, NCI-H82 and Jurkat cells enhanced sensitivity to cyclin A/B RxL inhibitors with a corresponding increase in γH2AX and SAC activation after drug treatment in the cell lines examined (Fig. 4d–k and Extended Data Fig. 10g,h). Similarly, E2F2 or E2F3 overexpression also sensitized cells to the cyclin A/B RxL inhibitor (Extended Data Fig. 10i–l).

Consistent with this mechanism, both E2F1 overexpression and CDK2 inhibition led to persistent DNA replication during late S phase/early G2 (Fig. 4l,m and Extended Data Fig. 7b,c). As shown above, CIRc-004 induced this phenotype but also induced a profound mitotic arrest (Fig. 4a). However, in contrast to CIRc-004, neither E2F1 overexpression nor CDK2 inhibition triggered mitotic arrest, highlighting the unique contribution of cyclin B RxL inhibition to cell killing. Together, these results support a model in which the cyclin A–E2F RxL interaction is selectively disrupted by cyclin A RxL inhibition causing E2F hyperactivation leading to S-phase dysregulation and replication stress, which is necessary for cell killing by cyclin A/B RxL inhibitors.

Anti-tumour activity of cyclin A/B RxL inhibitors

We next performed in vivo studies first with a cyclin A/B RxL inhibitor tool compound, CIRc-028, with improved pharmacokinetic properties capable of being dosed intravenously (Fig. 1b and Extended Data Fig. 1c,e,f,h). Administered daily at 100 mg per kg for 14 days, CIRc-028 induced tumour regressions in NCI-H69 xenografts (Fig. 5a), substantially inhibited growth in NCI-H1048 xenografts (Fig. 5b) and was well tolerated without weight loss (Extended Data Fig. 11a,b). Tumour analyses confirmed that CIRc-028 induced SAC activation and apoptosis in vivo (Fig. 5c–f and Extended Data Fig. 11c).

We next developed a cyclin A/B RxL inhibitor, CIRc-014 (Extended Data Figs. 1c,e,f,h and 11d–f), with improved physicochemical properties and capable of being dosed orally. Orally dosed CIRc-014 was tested in two patient-derived xenograft (PDX) models—DFCI-393 and DFCI-402—each derived from a patient with chemotherapy-resistant SCLC (Fig. 5g). RNA-seq analysis classified DFCI-393 as *ASCL1*$^+$ and DFCI-402 as *ASCL1*$^+$*NEUROD1*$^+$, with both models clustering with neuroendocrine-high SCLC tumours[1] (Fig. 5h, Extended Data Fig. 11g and Supplementary Table 7). Notably, CIRc-014 caused near complete tumour growth inhibition in both chemoresistant SCLC PDX models (Fig. 5i,j) without weight loss relative to vehicle (Extended Data Fig. 11h,i).

Pharmacokinetic analysis in mice dosed with CIRc-014 for 4 days in an independent pharmacokinetic/pharmacodynamic study showed that peak concentrations of unbound CIRc-014 (C_{max}) were 141.6 nM, aligned with efficacious in vitro levels (Extended Data Fig. 11j). In contrast to CIRc-014—but as expected for an intravenously administered compound—the peak unbound concentration of CIRc-028 was higher, with a C_0 of 4.9 μM for NCI-H69 and a C_0 of 8.3 μM for NCI-H1048 xenografts studies (Extended Data Fig. 11k,l). Four days of CIRc-014 treatment induced SAC activation and apoptosis in DFCI-393 PDX tumours (Fig. 5k–n). RNA-seq analysis of these tumours showed upregulation of G2/M checkpoint and mitotic spindle gene sets, consistent with our in vitro findings and confirming on-target activity (Extended Data Fig. 11m,n and Supplementary Tables 4 and 7). Together, these studies demonstrate that orally dosed CIRc-014 achieves potent, on-target anti-tumour efficacy in chemoresistant SCLC PDX models without overt toxicity.

Discussion

Here we describe the development of cell-permeable and orally bioavailable macrocycles that bind to cyclins to block their RxL-dependent interactions with RxL-containing substrates. We find that SCLCs with high E2F activity due to a compromised G1–S checkpoint from *RB1* and *TP53* loss are highly sensitive to macrocycles that inhibit the ability of both cyclin A and cyclin B to interact with their corresponding RxL-binding proteins, leading to SAC activation and mitotic cell death. Two unbiased orthogonal genome-wide genetic screens in cell lines from different cancer types both show that cell killing by cyclin A/B RxL inhibitors is achieved through activation of SAC, which is distinct from the mechanism of cell killing by an orthosteric CDK2i. Our data show that the efficacy of cyclin A/B RxL inhibitors is achieved by blocking the ability of cyclins to interact with at least two RxL-containing substrates including: (1) disruption of a cyclin A–E2F1 inhibitory interaction, leading to increased E2F activity, priming cells for SAC-induced apoptosis; and (2) disruption of a cyclin B–MYT1 RxL inhibitory interaction, which hyperactivates cyclin B–CDK activity, thereby increasing downstream SAC activation and mitotic cell death (the proposed mechanism is shown in Fig. 5o). While disruption of these two RxL interactions is necessary for cell killing by cyclin A/B RxL inhibitors, there are almost certainly other cyclin–RxL–substrate interactions[10,14,56–58] disrupted by these macrocycles that contribute to their ability to induce apoptosis.

We found that cyclin A/B RxL inhibitors promote a neomorphic interaction between cyclin B and CDK2, forming complexes that phosphorylate RxL-independent substrates such as stathmin[54], leading to SAC activation and apoptosis (Fig. 5o). This finding explains why *CCNB1*

and *CDK2* were among the top enriched hits in our CRISPR knockout screen. Canonically, cyclin A[50,59] binds to and activates CDK2 during S phase, while cyclin B binds to and activates CDK1 during mitosis[50]. Although cyclin B–CDK2 binding has been observed in vitro[51], to our knowledge, this is the first demonstration that such an interaction occurs in cells achieved through a cyclin A/B RxL macrocycle. Future studies will investigate how RxL macrocycles promote this complex and whether CDK2 activity in this setting is regulated by MYT1, which is likely given the high sequence homology between CDK1 and CDK2 at their N termini and the central role of cyclin–substrate interactions in determining specificity[12,51,60].

Despite cyclin A and cyclin B being essential for proliferation[61,62], RxL macrocycles are well tolerated in vivo and selectively toxic to E2F^{high} cancer cells with 1,000-fold lower concentrations required to kill sensitive cancer cells relative to normal cell lines that were inherently resistant indicating a therapeutic window.

We focused this study on SCLC as SCLCs have near-universal LOF mutations in *RB1* and *TP53*, compromising cell cycle checkpoints leading to high and dysregulated E2F activity[1]. However, our findings probably extend beyond SCLC. Genomic alterations that disrupt the G1–S checkpoint—such as *RB1* mutation[1], *CDKN2A* deletion, or cyclin D or E amplifications[2,3]—are common across many cancer types and lead to E2F hyperactivation. Our data show that high E2F activity sensitizes diverse cancer cell lines to cyclin A/B RxL inhibition, suggesting that E2F expression signatures may serve as predictive biomarkers for therapeutic response. Moreover, this work aligns with previous studies showing SCLCs and other cancers with genomic alterations that compromise the G1–S checkpoint can be therapeutically exploited by disrupting mitotic checkpoint control[47,63–65].

In summary, we present cyclin A/B RxL macrocycles as a promising class of anti-cancer agents with a distinct mechanism from orthosteric CDK inhibitors. The orally bioavailable inhibitor CIRc-014 shows potent, on-target activity in chemoresistant SCLC PDX models without overt toxicity. Circle Pharma is advancing CID-078, a related compound, as a first-in-class cyclin A/B RxL inhibitor into phase 1 clinical evaluation (NCT06577987) to test the therapeutic potential of targeting cyclin–substrate interactions in SCLC and other cancers.

Online content

Any methods, additional references, Nature Portfolio reporting summaries, source data, extended data, supplementary information, acknowledgements, peer review information; details of author contributions and competing interests; and statements of data and code availability are available at https://doi.org/10.1038/s41586-025-09433-w.

1. George, J. et al. Comprehensive genomic profiles of small cell lung cancer. *Nature* **524**, 47–53 (2015).
2. Kent, L. N. & Leone, G. The broken cycle: E2F dysfunction in cancer. *Nat. Rev. Cancer* **19**, 326–338 (2019).
3. Suski, J. M., Braun, M., Strmiska, V. & Sicinski, P. Targeting cell-cycle machinery in cancer. *Cancer Cell* **39**, 759–778 (2021).
4. Wu, X. & Levine, A. J. p53 and E2F-1 cooperate to mediate apoptosis. *Proc. Natl Acad. Sci. USA* **91**, 3602–3606 (1994).
5. Qin, X. Q., Livingston, D. M., Kaelin, W. G. Jr & Adams, P. D. Deregulated transcription factor E2F-1 expression leads to S-phase entry and p53-mediated apoptosis. *Proc. Natl Acad. Sci. USA* **91**, 10918–10922 (1994).
6. Kowalik, T. F., DeGregori, J., Schwarz, J. K. & Nevins, J. R. E2F1 overexpression in quiescent fibroblasts leads to induction of cellular DNA synthesis and apoptosis. *J. Virol.* **69**, 2491–2500 (1995).
7. Stiewe, T. & Putzer, B. M. Role of the p53-homologue p73 in E2F1-induced apoptosis. *Nat. Genet.* **26**, 464–469 (2000).
8. Lissy, N. A., Davis, P. K., Irwin, M., Kaelin, W. G. & Dowdy, S. F. A common E2F-1 and p73 pathway mediates cell death induced by TCR activation. *Nature* **407**, 642–645 (2000).
9. Irwin, M. et al. Role for the p53 homologue p73 in E2F-1-induced apoptosis. *Nature* **407**, 645–648 (2000).
10. Schulman, B. A., Lindstrom, D. L. & Harlow, E. Substrate recruitment to cyclin-dependent kinase 2 by a multipurpose docking site on cyclin A. *Proc. Natl Acad. Sci. USA* **95**, 10453–10458 (1998).
11. Russo, A. A., Jeffrey, P. D., Patten, A. K., Massague, J. & Pavletich, N. P. Crystal structure of the p27Kip1 cyclin-dependent-kinase inhibitor bound to the cyclin A-Cdk2 complex. *Nature* **382**, 325–331 (1996).
12. Loog, M. & Morgan, D. O. Cyclin specificity in the phosphorylation of cyclin-dependent kinase substrates. *Nature* **434**, 104–108 (2005).
13. Ord, M. et al. Multisite phosphorylation code of CDK. *Nat. Struct. Mol. Biol.* **26**, 649–658 (2019).
14. Adams, P. D. et al. Identification of a cyclin-cdk2 recognition motif present in substrates and p21-like cyclin-dependent kinase inhibitors. *Mol. Cell. Biol.* **16**, 6623–6633 (1996).
15. Chen, Y. N. et al. Selective killing of transformed cells by cyclin/cyclin-dependent kinase 2 antagonists. *Proc. Natl Acad. Sci. USA* **96**, 4325–4329 (1999).
16. Rudin, C. M., Brambilla, E., Faivre-Finn, C. & Sage, J. Small-cell lung cancer. *Nat. Rev. Dis. Primers* **7**, 3 (2021).
17. Burkhart, D. L. & Sage, J. Cellular mechanisms of tumour suppression by the retinoblastoma gene. *Nat. Rev. Cancer* **8**, 671–682 (2008).
18. Dick, F. A. & Rubin, S. M. Molecular mechanisms underlying RB protein function. *Nat. Rev. Mol. Cell Biol.* **14**, 297–306 (2013).
19. Dynlacht, B. D., Flores, O., Lees, J. A. & Harlow, E. Differential regulation of E2F transactivation by cyclin/cdk2 complexes. *Genes Dev.* **8**, 1772–1786 (1994).
20. Xu, M., Sheppard, K. A., Peng, C. Y., Yee, A. S. & Piwnica-Worms, H. Cyclin A/CDK2 binds directly to E2F-1 and inhibits the DNA-binding activity of E2F-1/DP-1 by phosphorylation. *Mol. Cell. Biol.* **14**, 8420–8431 (1994).
21. Krek, W. et al. Negative regulation of the growth-promoting transcription factor E2F-1 by a stably bound cyclin A-dependent protein kinase. *Cell* **78**, 161–172 (1994).
22. Ord, M., Venta, R., Moll, K., Valk, E. & Loog, M. Cyclin-specific docking mechanisms reveal the complexity of M-CDk function in the cell cycle. *Mol. Cell* **75**, 76–89 (2019).
23. Faustova, I. et al. A new linear cyclin docking motif that mediates exclusively S-phase CDK-specific signaling. *EMBO J.* **40**, e105839 (2021).
24. Ord, M. et al. Proline-rich motifs control G2-CDK target phosphorylation and priming an anchoring protein for polo kinase localization. *Cell Rep.* **31**, 107757 (2020).
25. Nandha Premnath, P., Craig, S. & McInnes, C. Development of inhibitors of protein-protein Interactions through REPLACE: application to the design and development non-ATP competitive CDK inhibitors. *J. Vis. Exp.* https://doi.org/10.3791/52441 (2015).
26. Boehm, M. et al. Discovery of potent and orally bioavailable macrocyclic peptide-peptoid hybrid CXCR7 modulators. *J. Med. Chem.* **60**, 9653–9663 (2017).
27. Buyanova, M. & Pei, D. Targeting intracellular protein-protein interactions with macrocyclic peptides. *Trends Pharmacol. Sci.* **43**, 234–248 (2022).
28. Merz, M. L. et al. De novo development of small cyclic peptides that are orally bioavailable. *Nat. Chem. Biol.* https://doi.org/10.1038/s41589-023-01496-y (2023).
29. Rafi, S. B., Hearn, B. R., Vedantham, P., Jacobson, M. P. & Renslo, A. R. Predicting and improving the membrane permeability of peptidic small molecules. *J. Med. Chem.* **55**, 3163–3169 (2012).
30. Giordanetto, F. & Kihlberg, J. Macrocyclic drugs and clinical candidates: what can medicinal chemists learn from their properties? *J. Med. Chem.* **57**, 278–295 (2014).
31. Bockus, A. T. et al. Discovery of cell-permeable macrocyclic cyclin A/B RxL inhibitors that demonstrate anti-tumor activity in vivo. *J. Med. Chem.* https://doi.org/10.1021/acs.jmedchem.5c00253 (2025).
32. Febres-Aldana, C. A. et al. Rb tumor suppressor in small cell lung cancer: combined genomic and IHC analysis with a description of a distinct Rb-proficient subset. *Clin. Cancer Res.* **28**, 4702–4713 (2022).
33. Hanzelmann, S., Castelo, R. & Guinney, J. GSVA: gene set variation analysis for microarray and RNA-seq data. *BMC Bioinform.* **14**, 7 (2013).
34. Liberzon, A. et al. The Molecular Signatures Database (MSigDB) hallmark gene set collection. *Cell Syst.* **1**, 417–425 (2015).
35. Li, J. et al. Synergistic function of E2F7 and E2F8 is essential for cell survival and embryonic development. *Dev. Cell* **14**, 62–75 (2008).
36. Rubin, C. I. & Atweh, G. F. The role of stathmin in the regulation of the cell cycle. *J. Cell. Biochem.* **93**, 242–250 (2004).
37. Nguyen, T. P. et al. Inducible mismatch repair streamlines forward genetic approaches to target identification of cytotoxic small molecules. *Cell Chem. Biol.* **30**, 1453–1467 (2023).
38. Izawa, D. & Pines, J. How APC/C-Cdc20 changes its substrate specificity in mitosis. *Nat. Cell Biol.* **13**, 223–233 (2011).
39. Kapanidou, M., Curtis, N. L. & Bolanos-Garcia, V. M. Cdc20: at the crossroads between chromosome segregation and mitotic exit. *Trends Biochem. Sci.* **42**, 193–205 (2017).
40. Lara-Gonzalez, P., Pines, J. & Desai, A. Spindle assembly checkpoint activation and silencing at kinetochores. *Semin. Cell Dev. Biol.* **117**, 86–98 (2021).
41. Corbett, K. D. Molecular mechanisms of spindle assembly checkpoint activation and silencing. *Prog. Mol. Subcell. Biol.* **56**, 429–455 (2017).
42. Yamagishi, Y., Yang, C. H., Tanno, Y. & Watanabe, Y. MPS1/Mph1 phosphorylates the kinetochore protein KNL1/Spc7 to recruit SAC components. *Nat. Cell Biol.* **14**, 746–752 (2012).
43. Hayward, D., Alfonso-Perez, T. & Gruneberg, U. Orchestration of the spindle assembly checkpoint by CDK1-cyclin B1. *FEBS Lett.* **593**, 2889–2907 (2019).
44. Jackman, M., Lindon, C., Nigg, E. A. & Pines, J. Active cyclin B1-Cdk1 first appears on centrosomes in prophase. *Nat. Cell Biol.* **5**, 143–148 (2003).
45. Hagting, A., Jackman, M., Simpson, K. & Pines, J. Translocation of cyclin B1 to the nucleus at prophase requires a phosphorylation-dependent nuclear import signal. *Curr. Biol.* **9**, 680–689 (1999).
46. Liu, F., Rothblum-Oviatt, C., Ryan, C. E. & Piwnica-Worms, H. Overproduction of human Myt1 kinase induces a G2 cell cycle delay by interfering with the intracellular trafficking of Cdc2-cyclin B1 complexes. *Mol. Cell. Biol.* **19**, 5113–5123 (1999).
47. Gallo, D. et al. CCNE1 amplification is synthetic lethal with PKMYT1 kinase inhibition. *Nature* **604**, 749–756 (2022).
48. McGowan, C. H. & Russell, P. Human Wee1 kinase inhibits cell division by phosphorylating p34cdc2 exclusively on Tyr15. *EMBO J.* **12**, 75–85 (1993).
49. Sangree, A. K. et al. Benchmarking of SpCas9 variants enables deeper base editor screens of BRCA1 and BCL2. *Nat. Commun.* **13**, 1318 (2022).

50. Malumbres, M. & Barbacid, M. Cell cycle, CDKs and cancer: a changing paradigm. *Nat. Rev. Cancer* **9**, 153–166 (2009).
51. Brown, N. R. et al. Cyclin B and cyclin A confer different substrate recognition properties on CDK2. *Cell Cycle* **6**, 1350–1359 (2007).
52. Petri, E. T., Errico, A., Escobedo, L., Hunt, T. & Basavappa, R. The crystal structure of human cyclin B. *Cell Cycle* **6**, 1342–1349 (2007).
53. Larsson, N., Melander, H., Marklund, U., Osterman, O. & Gullberg, M. G2/M transition requires multisite phosphorylation of oncoprotein 18 by two distinct protein kinase systems. *J. Biol. Chem.* **270**, 14175–14183 (1995).
54. Cassimeris, L. The oncoprotein 18/stathmin family of microtubule destabilizers. *Curr. Opin. Cell Biol.* **14**, 18–24 (2002).
55. Rosenblatt, J., Gu, Y. & Morgan, D. O. Human cyclin-dependent kinase 2 is activated during the S and G2 phases of the cell cycle and associates with cyclin A. *Proc. Natl Acad. Sci. USA* **89**, 2824–2828 (1992).
56. Chen, J., Saha, P., Kornbluth, S., Dynlacht, B. D. & Dutta, A. Cyclin-binding motifs are essential for the function of p21CIP1. *Mol. Cell. Biol.* **16**, 4673–4682 (1996).
57. Zhu, L., Harlow, E. & Dynlacht, B. D. p107 uses a p21CIP1-related domain to bind cyclin/cdk2 and regulate interactions with E2F. *Genes Dev.* **9**, 1740–1752 (1995).
58. Dynlacht, B. D., Moberg, K., Lees, J. A., Harlow, E. & Zhu, L. Specific regulation of E2F family members by cyclin-dependent kinases. *Mol. Cell. Biol.* **17**, 3867–3875 (1997).
59. Jeffrey, P. D. et al. Mechanism of CDK activation revealed by the structure of a cyclinA-CDK2 complex. *Nature* **376**, 313–320 (1995).
60. Ord, M. et al. High-throughput discovery and deep characterization of cyclin-CDK docking motifs. Preprint at *bioRxiv* https://doi.org/10.1101/2024.12.03.625240 (2024).
61. Santamaria, D. et al. Cdk1 is sufficient to drive the mammalian cell cycle. *Nature* **448**, 811–815 (2007).
62. Kalaszczynska, I. et al. Cyclin A is redundant in fibroblasts but essential in hematopoietic and embryonic stem cells. *Cell* **138**, 352–365 (2009).
63. Gong, X. et al. Aurora A kinase inhibition is synthetic lethal with loss of the RB1 tumor suppressor gene. *Cancer Discov.* **9**, 248–263 (2019).
64. Oser, M. G. et al. Cells lacking the RB1 tumor suppressor gene are hyperdependent on aurora B kinase for survival. *Cancer Discov.* **9**, 230–247 (2019).
65. Witkiewicz, A. K. et al. Targeting the vulnerability of RB tumor suppressor loss in triple-negative breast cancer. *Cell Rep.* **22**, 1185–1199 (2018).
66. Szklarczyk, D. et al. The STRING database in 2025: protein networks with directionality of regulation. *Nucleic Acids Res.* **53**, D730–D737 (2025).

Methods

Cell lines and cell culture

NCI-H446, NCI-H69 cells, NCI-H1048, NCI-H526, NCI-H82, WI-38, RPE1 and HEK293T cells were originally obtained from American Type Culture Collection (ATCC) and authenticated by ATCC. A549, HCC4006 and NCI-H1299 cells were a gift from P. Janne's laboratory at DFCI and originally obtained and validated by ATCC. NCI-H1048, Jurkat, NCI-H82 and MDA-MB-231 cells with DOX-on inducible E2F1 expression were a gift from W. G. Kaelin's laboratory at DFCI and were originally obtained and authenticated by ATCC prior to genetically manipulation. G-CSF mobilized human peripheral blood $CD34^+$ cells were obtained from StemCell Technologies (700060.1, 230472503C) and validated by flow cytometry. No commonly misidentified cell lines were used in this study.

NCI-H69, NCI-H446, HCC4006, NCI-H1299, NCI-H526, A549, NCI-H82 and Jurkat cells were maintained in RPMI-1640 medium supplemented with 10% fetal bovine serum (FBS) (Gemini), 100 U ml^{-1} penicillin and 100 μg ml^{-1} streptomycin. NCI-H1048 cells were cultured in RPMI-1640 medium supplemented with 10% fetal bovine serum (FBS), penicillin–streptomycin and insulin–transferrin–selenium (Gemini). WI-38 cells were maintained in DMEM supplemented with 10% FBS. HEK293T cells were maintained in DMEM medium with 10% FBS and penicillin–streptomycin. MDA-MB-231 and RPE1 cells were maintained in DMEM/F12 with 10% FBS and penicillin–streptomycin. G-CSF mobilized human peripheral blood $CD34^+$ cells were thawed into StepSpan Serum Free Expansion Medium (SFEM II) Hematopoietic Stem Cell Medium (StemCell Technologies, 09655) supplemented with StemSpan $CD34^+$ Expansion Supplement (StemCell Technologies, 02691). Early-passage cells of all of the cell lines listed above were tested for mycoplasma (Lonza, LT07-218) and then were frozen using Bambanker's freezing medium (Bulldog Bio) and maintained in culture no more than 4 months in cases in which early-passage vials were thawed. iHCT116 cells were previously described[37] and cultured in 10% fetal bovine serum in DMEM medium (Sigma-Aldrich) supplemented with 2 mM L-glutamine (Sigma-Aldrich).

Pharmacological inhibitors

Macrocycle peptides offer a feasible strategy to block broad and shallow protein-protein interaction surfaces that until recently have been considered undruggable. Over the past decade, a growing body of research has demonstrated that peptidic macrocycles can be engineered to be both passively cell permeable[67–70] and orally bioavailable[26,28,71,72], therefore offering promise for this modality to access previously undruggable intracellular targets[27]. Our approach to identify passively permeable cyclin RxL inhibitors included the incorporation of peptidomimetic features based on our previous research[67,68,73,74]. Detailed descriptions of our medical chemistry efforts to achieve passive permeability, cyclin binding affinity and selectivity of an earlier series of distinct tool cyclin RxL macrocycles not included in this manuscript are reported in ref. 31. A detailed description of the synthesis of the cyclin RxL inhibitors in this manuscript is provided in the Supplementary Methods.

Where indicated, the following chemicals (stored at −20 °C or −80 °C) were also added to the medium: CIRc-004 (cyclin A/B RxL inhibitor, stock 10 mM in DMSO, obtained from Circle Pharma), CIRc-005 (inactive enantiomer of CIRc-004, stock 10 mM in DMSO, obtained from Circle Pharma), CIRc-001 (cyclin A/B RxL inhibitor, stock 10 mM in DMSO, obtained from Circle Pharma), CDK2i (PF-07104091, stock 10 mM in DMSO, chemically synthesized and validated to be the same PF-07104091 in the published patent), CIRc-018 (cyclin-A-selective RxL inhibitor, stock 10 mM in DMSO, obtained from Circle Pharma), CIRc-019 (cyclin-B-selective RxL inhibitor, stock 10 mM in DMSO, obtained from Circle Pharma), MPS1 inhibitor (BAY-1217389, Selleck chemicals, S8215, stock 10 mM), doxycycline hydrochloride (Sigma-Aldrich, 3447, stock 1 mg ml^{-1}), RP-6306 (MedChemExpress, HY-145817A, stock 20 mM), roscovitine (Selleck Chemical, S115350MG, stock 10 mM), staurosporine (MedChemExpress, HY-15141, stock 20 mM), nocodazole (Sigma-Aldrich, M1404, stock 2 mg ml^{-1}), RO-3306 (ENZO, ALX-270-463-M001, stock 10 mM) and MK-1775 (Selleck Chemical, NC1097015, stock 10 mM).

Biochemical activity assays

The binding potency of macrocycles for cyclin–CDK complexes was determined by a fluorescence polarization competitive assay based on previously established protocols[25,75] with the following modifications: (1) a higher-affinity fluorescent-labelled probe was identified referred to as CIR7-2706 (Supplementary Methods); (2) cyclin–CDK protein complexes were sourced as follows: cyclin A2–CDK2 (CRELUX Protein Services; www.crelux.com), cyclin B1–CDK1 (Eurofins, Discovery, 14-450) and cyclin E1–CDK2 (Eurofins, Discovery, 14-475). Fluorescence polarization binding assays were performed in 25 mM HEPES pH 7.5, 100 mM NaCl, 1 mM DTT, 0.01% NP-40 and 1 mg ml^{-1} BSA for all 3 protein complexes in black 96-well plates (Costar, 3356). After experimental plates were set, they were equilibrated by gentle mixing by placing them on an orbital shaker at 100 rpm for 2 h at room temperature and then read on the SpectraMax i3X Multi-Mode Microplate Detection platform. The 50% inhibitory concentration (IC_{50}) of binding of a fluorescence labelled probe CIR7-2706 at 2 nM to the cyclin–CDK complex was determined from an eight-point threefold serial dilution curve of CID-078. The protein concentrations used were 8 nM for cyclin A2–CDK2, and 10 nM for cyclin B1–CDK1 and cyclin E1–CDK2. Under these conditions, the assay dynamic range was about 120 mP units between 100% binding of CIR7-2706 to the proteins and its complete displacement by an unlabelled competitor compound. All experiments showed a Z' factor of >0.80. The reported IC_{50} values are the average of all experiments described in Fig. 1b.

RxL inhibitor affinity determinations were performed in a WaveDelta instrument (Malvern Panalytical). Each of the cyclin–CDK complexes were immobilized to the chip surface by amine coupling on one of four channels of a 4PCP chip (9060001, Malvern Panalytical) in 10 mM MES pH 6.5 buffer for cyclin A2–CDK2 and cyclin E1–CDK2 and 10 mM MOPS pH 7.0 for cyclin B1–CDK1. For coupling, the proteins were diluted at 25 mg ml^{-1} and applied to the corresponding chip channel for 600 s at a flow rate of 10 ml min^{-1}, followed by quenching by injecting 1 M ethanolamine-HCl pH 8.5 for 420 s at a flow rate of 10 ml min^{-1}. Compounds were dissolved at 300 nM in 20 mM HEPES pH 7.5, 300 mM NaCl, 0.5 mM TCEP, 0.05% Tween-20 and 3% DMSO. An eight-point 1:3 serial dilution of the compounds was sequentially injected into the chip at flow rate of 100 ml min^{-1} for 120 s to measure the association rates, followed by injection for 600 s of buffer alone to measure the dissociation rates. Background readings were subtracted using an empty channel on the chip on which no protein was immobilized. The data were analysed using a 1:1 binding kinetic model using the instrument software (Wave Control, v.4.5.17). The reported K_d, k_a and k_d are the average of two or more experiments as indicated. ClogP values were calculated using the calculator in ChemDraw. MDCK monolayer cell permeability, kinetic solubility (K_{sol}), and logD experimental values were generated by Quintara Discovery using standard experimental conditions.

sgRNA cloning to make lentiviruses

sgRNA sequences were designed using the Broad Institutes sgRNA designer tool (http://portals.broadinstitute.org/gpp/public/analysis-tools/sgrna-design) and chosen from the Brunello CP0043 sgRNA library and synthesized by IDT technologies. The sense and antisense oligonucleotides were mixed at equimolar ratios (0.25 nmol of each sense and antisense oligonucleotide) and annealed by heating to 100 °C in annealing buffer (1× annealing buffer: 100 mM NaCl, 10 mM Tris-HCl, pH 7.4) followed by slow cooling to 30 °C for 3 h. The annealed oligonucleotides were then diluted at 1:400 in 0.5× annealing buffer. For CRISPR–Cas9 knockout experiments in cells, the annealed oligos were

ligated into pLentiCRISPR Puro V2 (Addgene, 52961). Ligations were done with T4 DNA ligase for 2 h at 25 °C. The ligation mixture was transformed into HB101 competent cells. Ampicillin-resistant colonies were screened by restriction digestion of miniprep DNAs and subsequently validated by DNA sequencing.

The following sgRNA oligos were used for LentiCRISPRV2 Puro vector for CRISPR knockout experiments: non-targeting 1 sense (5′-CCGTCTCC GCATCGTCTTTT-3′); non-targeting 1 antisense (5′-AAAAGACGATGCGGA GACGG-3′); non-targeting 2 sense (5′-TATTTTGACTTGACGCAGGC-3′); non-targeting 2 antisense (5′-GCCTGCGTCAAGTCAAAATA-3′); human *CCNB1* 1 sense (5′-CATCAGAGAAAGCCTGACAC-3′); human *CCNB1* 1 antisense (5′-GTGTCAGGCTTTCTCTGATG-3′); human *CCNB1* 2 sense (5′-GAGGCCAAGAACAGCTCTTG-3′); human *CCNB1* 2 antisense (5′-CA AGAGCTGTTCTTGGCCTC-3′); human *CDK2* 1 sense (5′-CAAATA TTATTCCACAGCTG-3′); human *CDK2* 1 antisense (5′-CAGCTGTGG AATAATATTTG-3′); human *CDK2* 2 sense (5′-CATGGGTGTAAGTAC GAACA-3′); human *CDK2* 2 antisense (5′-TGTTCGTACTTACACCCATG-3′); human *KNTC1* 1 sense (5′-AAACATTCGGAACACTATGG-3′); human *KNTC1* 1 antisense (5′-CCATAGTGTTCCGAATGTTT-3′); human *KNTC1* 2 sense (5′-AAGCTAACGATGAAAATCGG-3′); human *KNTC1* 2 antisense (5′-CCGA TTTTCATCGTTAGCTT-3′); human *LIN54* 1 sense (5′-GTTCTTTCAC AGTCTACTCC-3′); human *LIN54* 1 antisense (5′-GGAGTAGACTGTG AAAGAAC-3′); human *LIN54* 2 sense (5′-AAGTAGTTACCATTGGAGGG-3′); human *LIN54* 2 antisense (5′-CCCTCCAATGGTAACTACTT-3′); human *MAD1L1* 1 sense (5′-GAAGAAGCGCGAGACCCACG-3′); human *MAD1L1* 1 antisense (5′-CGTGGGTCTCGCGCTTCTTC-3′); human *MAD1L1* 2 sense (5′-GAGAGACTGGACCAGACCAT-3′); human *MAD1L1* 2 antisense (5′-AT GGTCTGGTCCAGTCTCTC-3′); human *ZWINT* 1 sense (5′-CACCTA CAGGGAGCACGTAG-3′); human *ZWINT* 1 antisense (5′-CTACGTGC TCCCTGTAGGTG-3′); human *ZWINT* 2 sense (5′-CAGTGGCAGCTA CAACAGGT-3′); human *ZWINT* 2 antisense (5′-ACCTGTTGTAGCTG CCACTG-3′); human *RB1* 2 sense (5′-CGGTGGCGGCCGTTTTTCGG-3′); human *RB1* 2 antisense (5′-CCGAAAAACGGCCGCCACCG-3′); human *TP53* 1 sense (5′-CCATTGTTCAATATCGTCCG-3′); and human *TP53* 1 antisense (5′-CGGACGATATTGAACAATGG-3′).

cDNA expression plasmids

CDC20 (NM_001255.3) or CDC20 with an N-terminal 3×Flag tag was cloned into the pLVX IRES Hygro vector (Clontech). The *CDC20* R445Q mutation was generated using site-directed mutagenesis (Pfu polymerase). pTwist Lenti SFFV Puro WPRE lentiviral vectors encoding: (1) *CCNB1* wild-type-HA, (2) *CCNB1* triple mutant-HA (E169K/Y170H/Y177C) or a (3) negative control that encodes a functionally inactivated EED mutant-HA with mutations to inactivate EED (F97A/Y148A/Y365A) were codon optimized and synthesized by Twist Biosciences. All plasmids were sequence verified by sanger sequencing. To make the DOX-on pTripz neo E2F1, E2F2 or E2F3 construct, pDONR223 E2F1 (W. G. Kaelin's laboratory), pCMVHA E2F2 (Addgene, 24226) and pCMV Tag2B E2F3 (Addgene, 202522) were used as templates for overhang PCR to introduce the attB1 and attB2 sites onto the 5′ and 3′ ends of E2F1 (sense primer, 5′-GGGGACAAGTTTGTACAAAAAAGCAGGCTTCACCATGGCCTTGGCC GGGGCCCCTGCG; and antisense primer, 5′-GGGGACCACTTTGTACA AGAAAGCTGGGTTGAAATCCAGGGGGGTGAGGTCCCC-3′), E2F2 (sense primer, 5′-GGGGACAAGTTTGTACAAAAAAGCAGGCTTCACCA TGCTGCAAGGGCCCCGGGCCTTG-3′; and antisense primer, 5′-GGGG ACCACTTTGTACAAGAAAGCTGGGTTATTAATCAACAGGTCCCCAAGG TC-3′) and E2F3 (sense primer, 5′-GGGGACAAGTTTGTACAAAAAAG CAGGCTTCACCATGAGAAAGGGAATCCAGCCCGCT; and antisense primer, 5′-GGGGACCACTTTGTACAAGAAAGCTGGGTTACTACACATGA AGTCTTCCACCAG-3′). The PCR product was then gel extracted according to the manufacturer's instructions (Qiagen). Purified E2F1, E2F2 and E2F3 double-stranded DNA fragments containing attB1 and attB2 sites were introduced into the pDONR223 vector by homologous recombination using BP clonase (Life Technologies, 11789020) for 1 h at 25 °C according to the manufacturer's instructions. The reaction mixture was then transformed at a ratio of 1:10 (reaction volume/volume competent cells) into HB101 competent cells (Promega). Spectinomycin-resistant colonies were screened by restriction digestion of miniprep DNA and subsequently validated by DNA sequencing. A homologous recombination reaction was then performed using LR Clonase II (Life Technologies, 11791100) with the pDONR223-E2F1, pDONR223-E2F2 or pDONR223-E2F3 plasmids and DOX-on pTripz-NEO DEST vector that was modified to be used as destination vectors for Gateway recombination cloning. The LR reaction was transformed into HB101 competent cells (Promega). Kanamycin-resistant (pTripz-NEO) colonies were screened by restriction digestion of miniprep DNA and subsequently validated by DNA sequencing. Lentivirus was then generated and then transduced into cells to make stable DOX-on cell lines for inducible E2F1, E2F2 or E2F3 expression.

Lentivirus production

Lentiviruses were made by Lipofectamine-2000-based co-transfection of HEK293FT cells with the respective lentiviral expression vectors and the packaging plasmids psPAX2 (Addgene, 12260) and pMD2.G (Addgene, 12259) at a ratio of 4:3:1. Virus-containing supernatant was collected at 48 and 72 h after transfection, pooled together (7 ml total per 6 cm tissue culture dish), passed through a 0.45-μm filter, aliquoted and frozen at −80 °C until use.

Lentiviral infection

The cells were counted using a Vi-Cell XR Cell Counter (Beckman Coulter) and 2×10^6 cells were resuspended in 1 ml lentivirus with 8 μg ml^{-1} polybrene in individual wells of a 12-well plate. The plates were then centrifuged at 931*g* (Allegra X-15R Centrifuge (Beckman Coulter), rotor SX4750A, 2,000 rpm) for 2 h at 30 °C. Then, 16 h later, the virus was removed and cells were grown for 72 h before being placed under drug selection. Cells were selected in puromycin (0.5 μg ml^{-1}) or G418 (500 μg ml^{-1}).

RB1 TP53 CRISPR–Cas9 double-knockout experiments in RPE1 cells

RPE1 cells were first infected with lentivirus encoding an sgRNA targeting *RB1* (sgRB1) or a non-targeting sgRNA (sgC0111, sgControl) in LentiCRISPR-V2 Puro vector. RPE1 sgRB1 or sgControl cells were superinfected with lentiviruses encoding an sgRNA targeting *TP53* (sgTP53) or a non-targeting sgRNA (sgC0111, sgControl) and a G418 resistance gene in the pLentiCRISPR-V2 vector. Cells were selected in G418 (500 μg ml^{-1}) until all mock-infected cells were killed and immunoblot analysis was performed for RB1 and p53 in the presence or absence of CIRc-004 at the concentrations indicated.

Cyclin A/B RxL inhibitor, CDK2i and MPS1 inhibitor dose–response assays

For dose–response assays with cyclin A/B RxL inhibitor (CIRc-004), inactive enantiomer of CIRc-004 (CIRc-005) and CDK2i (PF-07104091), the cells were counted on day 0 using a Vi-Cell XR Cell Counter and plated in a tissue-culture-treated six-well plate at 50,000 cells per ml in 2 ml of complete medium. Cells were treated with the compounds (CIRc-004, CIRc-005, PF-07104091) at the indicated concentrations for 6 days. Normalized cell counts were calculated as (day 6 count for treated samples)/(day 6 count for DMSO treated sample). The EC_{50} was calculated using GraphPad Prism v.10.0.0.

For DOX-inducible (DOX-on) E2F1-, E2F2- or E2F3-overexpressing cell lines, cells were counted on day 0 and plated in tissue-culture-treated six-well plates at 250,000 cells per ml for 3-day assays or 50,000 cells per ml in 2 ml of complete medium for 6-day assays. For 3-day cyclin A/B RxL inhibitor assays, E2F1 expression was induced with DOX (1 μg ml^{-1}) for 24 h followed by drug treatment for 3 days. For 6-day cyclin A/B RxL inhibitor assays, E2F1 expression was induced with DOX for 24 h followed by drug treatment for 6 days, with replacement with fresh DOX every 3 days.

MTT proliferation assays

NCI-H1048, NCI-H446 and WI-38 cells were counted using a Countess II FL (Invitrogen) and plated at 5,000 cells per well in 96-well plates. NCI-H69 cells were grown to confluency in a T150 flask. Cells were collected by centrifugation at 283*g* (Thermo Fisher Scientific X4R Pro-MD centrifuge, Sorvall TX1000 rotor, 1,100 rpm) and resuspended in 30 ml medium of which 10 ml was used to seed six 96-well plates. NCI-H526 cells were grown to confluency in a T75 flask, collected by centrifugation at 283*g* and resuspended in 10 ml medium of which 2.5 ml was used to seed six 96-well plates. The next day, cells were dosed with cyclin A/B/E RxL inhibitor (CIRc-001), cyclin A/B RxL inhibitors (CIRc-004; CIRc-028), cyclin-A-selective RxL inhibitor (CIRc-018), cyclin-B-selective RxL inhibitor (CIRc-019) or inactive enantiomer of CIRc-004 (CIRc-005). Roscovitine and staurosporine were used as plate controls to define the top and bottom of the growth inhibition curves, respectively. Inhibitors were dosed in duplicate in either an 8-point (WI-38) or 10-point (SCLC cell lines) 1:3 serial dilution with 10 µM maximum concentration. Roscovitine was dosed in singlet in an 8- or 10-point 1:2 serial dilution with 100 µM maximum concentration. Staurosporine was dosed in singlet in an 8- or 10-point 1:2 serial dilution with 1 µM maximum concentration. After dosing, plates were maintained in tissue culture incubators (37 °C, 5% CO_2) for 3 days (WI-38) or 5 days (SCLC cell lines) to allow for at least two cell doublings before processing in an MTT proliferation assay (R&D systems, 4890-050-K) performed according to the manufacturer's instructions. The average absorbance value obtained with the highest two concentrations dosed for roscovitine and staurosporine was used for background subtraction. The top of the assay (100% growth) was determined by normalization with the top of the roscovitine curve. The GI_{50} was determined by nonlinear regression analysis using log(inhibitor) versus response-variable slope (four parameters) using GraphPad Prism (v.10.1.0).

For MTT proliferation assays with the MYT1 inhibitor RP-6306, NCI-H1048, NCI-H446 and NCI-H69 cells were seeded in 96-well plates as described above. The next day, cells were dosed in duplicate in a 10-point 1:3 serial dilution with CIRc-018, CIRc-019, or CIRc-004 alone or in combination with RP-6306 at 100 nM for NCI-H1048 cells or 500 or 1,000 nM for NCI-H446 and 1,000 nM for NCI-H69 cells. After 5 days, cells were processed in an MTT proliferation assay and GI_{50} values were determined using GraphPad Prism (v.10.1.0) as described above.

Dose–response studies in iHCT-116 cells

Viability of cells were quantified using Cell Titer Glo according to the manufacturer's instructions (Promega) and the IC_{50} values were determined using GraphPad Prism (log inhibitor versus response four parameters).

FACS-based cleaved PARP apoptosis assays

Cells were plated at 250,000 cells per ml density and grown in cyclin A/B RxL inhibitor (CIRc-004), MPS1 inhibitor (BAY-1217389) or DMSO at the indicated concentrations for 72 h. Cells were then collected and fixed in 4% paraformaldehyde followed by a PBS wash, and then permeabilized in ice-cold 90% methanol (added dropwise) for 30 min on ice. The cells were then centrifuged at 206*g* (Eppendorf centrifuge 5804R, A-4-44 rotor, 2,000 rpm) washed once in PBS, centrifuged again at 206*g* and then incubated with Pacific blue conjugated cleaved PARP antibody (Cell Signaling, Asp214, D64E10, 60068) at a dilution of 1:100 for 1 h at room temperature protected from light. Cells were then washed again in PBS containing 0.5% BSA, resuspended in PBS containing 0.5% BSA and analysed on the LSR Fortessa flow cytometer (Becton Dickinson). Analysis for cleaved-PARP-positive cells was carried out using FlowJo v.10.8.1. The FACS gating strategy is provided in Supplementary Fig. 3.

FACS-based p-histone H3 (Ser10) analysis

Cells were plated at 500,000 cells per ml and grown in cyclin A/B RxL inhibitor (CIRc-004) or DMSO at the indicated concentrations for 24 h. The cells were then washed once in room temperature PBS and then fixed in 4% paraformaldehyde for 15 min at room temperature. The cells were then centrifuged at 206*g* (Eppendorf centrifuge, 5804R, A-4-44 rotor, 2,000 rpm) for 5 min at room temperature, washed once in PBS, centrifuged again at 206*g* and then permeabilized with ice-cold methanol at 4 °C for 30 min. The cells were then washed again in PBS and then incubated with Alexa-647-conjugated phospho-histone H3 (Ser10) antibody (Cell Signaling, 3458) at a dilution of 1:100 for 1 h at room temperature, then washed once in PBS containing 0.5% BSA, centrifuged at 400*g* and then counterstained with DAPI) (Cell Signaling, 4083) for 15 min at room temperature. FACS analysis was then performed to determine the percentage of positive p-histone H3 (Ser10) cells using FlowJo v.10.8.1. The FACS gating strategy is provided in Supplementary Fig. 3.

FACS-based PI cell cycle analysis

Cells were plated at 500,000 cells per ml and grown in cyclin A/B RxL inhibitor (CIRc-004) or DMSO at the indicated concentrations for 24 h. After incubation, cells were washed once in ice-cold PBS and then fixed in ice-cold 80% ethanol (added dropwise) for at least 2 h at −20 °C. The cells were then centrifuged at 206*g* (Eppendorf centrifuge 5804R, A-4-44 rotor, 2,000 rpm) for 5 min, washed once in PBS, centrifuged again at 206*g* and then washed again in PBS containing 0.5% BSA. Finally, cells were stained with propidium iodide (BD, 550825) for 15 min at room temperature. FACS analysis for PI was then performed on the LSR Fortessa flow cytometer (Becton Dickinson) and analysis was performed using FlowJo v.10.8.1. The FACS gating strategy is provided in Supplementary Fig. 3.

FACS-based EdU incorporation and DNA content analysis

NCI-H1048 cells were plated at 500,000 cells per ml in a 12-well (Fig. 4a) or 6-well (Fig. 4l and Extended Data Fig. 7b) plate and allowed to adhere overnight. Cells were dosed with cyclin A/B RxL inhibitor (CIRc-004) or DMSO for 24 h. Cells were pulsed for 1 h with 10 µM EdU (Click-It Plus EdU Flow Cytometry Assay kit, Invitrogen, C10632) before collection. After incubation, cells were washed once with ice-cold PBS and fixed by incubation in ice-cold 80% ethanol for at least 2 h at −20 °C. EdU was fluorescently tagged with Alexa Fluor 488 by click reaction (Click-it Plus EdU flow cytometry assay kit, Invitrogen, C10632). DNA content was monitored by FxCycle Violet stain (Invitrogen, F10347) or 1 µg ml^{-1} DAPI (4,6-diamidino-2-phenylindole, Cell Signaling) for 5 min. For Fig. 4a, flow cytometry analysis for EdU and DNA content was performed by full spectral flow cytometry on the Northern Lights cytometer (Cytek Biosciences) and analysis was carried out using FlowJo v.10.9.0. For Fig. 4l and Extended Data Fig. 7b, flow cytometry analysis for EdU and DNA content was performed using the LSR Fortessa flow cytometer (Becton Dickinson) and analysis was carried out using FlowJo v.10.8.1. FACS gating strategy is given in Supplementary Fig. 3.

FACS-based EdU cell cycle and apoptosis analysis in haematopoietic stem and progenitor cells

G-CSF mobilized human peripheral blood $CD34^+$ cells were plated in a 24-well plate at 25,000 cells per ml after counting with a VI-Cell BLU (Beckman Coulter). Cells were then allowed to recover for 48 h before dosing cells with CIRc-004, staurosporine (100 nM) or DMSO for 24 h. Cells were pulsed for 1 h with 10 µM EdU (Click-It Plus EdU Flow Cytometry Assay kit, Invitrogen, C10634) before collection. After incubation, cells were collected, washed once with PBS and resuspended in 1% BSA-PBS before staining with CD34 (8G12) Per-CP (BD, 340666) for 30 min at a 1:10 dilution protected from light. The cells were centrifuged for 200*g* (Eppendorf centrifuge, 5424R) for 5 min at all wash steps. Cells were then washed in 1% BSA-PBS. Cells were then fixed by resuspending cells in 50 µl of Click-it Fixitive (4% PFA) and incubated for 15 min. Cells were then washed with 1% BSA-PBS and resuspended in permeabilization and wash buffer prepared as directed from Click-It Plus kit

(Click-It Plus EdU Flow Cytometry Assay kit, Invitrogen, C10634) for 15 min. EdU was fluorescently tagged with Alexa Fluor 647 by click reaction (Click-It Plus EdU Flow Cytometry Assay kit, Invitrogen, C10634). Cells were then resuspended in permeabilization buffer and stained with FITC mouse anti-cleaved PARP (Asp214) (BD, 558576) for 1 h at a 1:5 dilution protected from light. DNA content was monitored by FxCycle Violet stain (Invitrogen, F10347). Flow cytometry analysis for EdU and DNA content was performed by full spectral flow cytometry on a Northern Lights cytometer (Cytek Biosciences) and analysis was carried out using FlowJo v.10.9.0. The FACS gating strategy is given in Supplementary Fig. 3.

Immunoblotting

Cell pellets were lysed in a modified EBC lysis buffer (50 mM Tris-Cl pH 8.0, 250 mM NaCl, 0.5% NP-40, 5 mM EDTA) supplemented with a protease inhibitor cocktail (Complete, Roche Applied Science, 11836153001) and phosphatase inhibitors (PhosSTOP, Sigma-Aldrich, 04906837001). Soluble cell extracts were quantified using the Bradford protein assay. Then, 20 µg of protein per sample was boiled after adding 3× sample buffer (6.7% SDS, 33% glycerol, 300 mM DTT and Bromophenol Blue) to a final concentration of 1×, resolved by SDS–PAGE using either 10% or 6% SDS–PAGE, semi-dry transferred onto nitrocellulose membranes, blocked in 5% milk in Tris-buffered saline with 0.1% Tween-20 (TBS-T) for 1 h, and probed with the indicated primary antibodies overnight at 4 °C. The membranes were then washed three times in TBS-T, probed with the indicated horseradish peroxidase (HRP)-conjugated secondary antibodies for 1 h at room temperature, and washed three times in TBS-T. Bound antibodies were detected with enhanced chemiluminescence (ECL) western blotting detection reagents (Immobilon, Thermo Fisher Scientific, WBKLS0500) or Supersignal West Pico (Thermo Fisher Scientific, PI34078). The primary antibodies and dilutions used were as follows: mouse anti-β-actin AC-15 (Sigma-Aldrich, A3854, 1:25,000), mouse anti-vinculin hVIN-1 (Sigma-Aldrich, V9131, 1:10,000), rabbit anti-p-CASC5/KNL1 Thr943/Thr1155 D8D4N (Cell Signaling, 40758, 1:1,000), rabbit anti-CASC5/KNL1 E4A5L (Cell Signaling, 26687, 1:1,000), rabbit anti-cyclin B1 D5C10 (Cell Signaling, 12231, 1:1,000), rabbit anti-E2F1 (Cell Signaling, 3742, 1:1,000), CDC20 (Cell Signaling, 4823S, 1:1,000), rabbit anti-p-KAP1 Ser824 (Cell Signaling, 4127, 1:1,000) and Flag (Sigma-Aldrich, A8592). The secondary antibodies and dilutions were as follows: goat anti-mouse (Jackson ImmunoResearch, 115-035-003, 1:5,0000) and goat anti-rabbit (Jackson ImmunoResearch, 111-035-003, 1:5,000).

To detect p-stathmin S38, total stathmin, p-cyclin B1 (Ser126), p-nucleolin (Thr84), p-RPA2 (Ser33) and p-FOXM1 (Thr600), after incubation with the indicated cyclin RxL inhibitors or DMSO control, NCI-H1048 cells were washed once in ice-cold PBS and lysed in 1% Triton X-100 buffer (40 mM HEPES pH 7.5, 1 mM EDTA pH 8.0, 10 mM sodium pyrophosphate, 10 mM β-glycerophosphate, 50 mM sodium fluoride, 120 mM sodium chloride and 1% Triton X-100) supplemented with a protease inhibitor cocktail (cOmplete, Sigma-Aldrich, 5892970001) and phosphatase inhibitors (PhosSTOP, Sigma-Aldrich, 4906837001). Cell lysates were centrifuged at 9,391*g* (Eppendorf centrifuge 5424R, FA-45-24-11 rotor, 10,000 rpm) for 10 min. The supernatant (cell extract) was removed and the protein content was estimated by performing a Bradford assay. Cell extracts (30 µg of protein) were boiled after adding 4× Laemmli buffer and separated by SDS–PAGE and transferred to PVDF membranes. Membranes were blocked in TBS plus 0.2% Tween-20 (TBS-T) containing 5% skimmed milk and incubated with relevant primary antibodies overnight at 4 °C in blocking buffer containing 5% BSA. After incubation with primary antibodies, the membranes were washed in TBS-T and then incubated with HRP-labelled secondary antibodies for 1–-2 h at room temperature. Membranes were washed again in TBS-T, incubated with ECL reagent (LI-COR, WesternSure, 92695000) and scanned on the Odyssey Fc Analyzer (LI-COR Biosciences). The primary antibodies and dilutions used were as follows: rabbit anti-p-stathmin (Ser38) (Cell Signaling, 3426S, 1:1,000), rabbit anti-total stathmin (Abcam, ab52630), rabbit anti-p-cyclin B (Ser126) (Abcam, ab3488, 1:1,000), rabbit anti-p-nucleolin (Thr84) (Abcam, ab155977, 1:1,000), rabbit anti-p-FOXM1 (Thr600) (Cell Signaling, 14655S, 1:500), rabbit anti-p-RPA2 (Ser33) (Fortis Life Sciences, A300-246A, 1:2,000), rabbit anti-tubulin-HRP (Cell Signaling, 9099S, 1:5,000). The secondary antibodies used and dilutions were as follows: goat anti-rabbit-IgG-HRP (Cell Signaling, 7074S, 1:5,000).

Immunoblots were quantified using Fiji (Image J2, v.2.9.0) or LICOR Odyssey built-in Image Studio Software (v.5.2). Quantified values from immunoblots are provided in Supplementary Tables 8 and 9. Raw immunoblots are included as Supplementary Fig. 1.

Immunoprecipitation analysis

For immunoprecipitation of endogenous cyclin A and cyclin B in Figs. 2o, 3h and 4c and Extended Data Figs. 8u and 9d–f,h, NCI-H1048 cells were seeded at 2.5×10^7 cells per 15 cm plate and were allowed to adhere overnight. The next day, cells were incubated with the indicated cyclin RxL inhibitors at 300 nM or DMSO for 2 h before rinsing once in ice-cold PBS and lysing in 1% NP-40 buffer (40 mM HEPES pH 7.5, 1 mM EDTA pH 8.0, 10 mM sodium pyrophosphate, 10 mM β-glycerophosphate, 50 mM sodium fluoride, 120 mM sodium chloride and 1% NP-40) supplemented with a protease inhibitor cocktail (cOmplete, Sigma-Aldrich, 5892970001) and phosphatase inhibitors (PhosSTOP, Sigma-Aldrich, 4906837001). The cell lysates were centrifuged at 9,391*g* for 10 min. The supernatant (cell extract) was removed and the protein content was estimated by performing a Bradford assay. Then, 2 mg cell extract was rotated overnight at 4 °C with 2 µg anti-cyclin A (Santa Cruz Biotechnology (SCBT) sc-271682) or 2 µg anti-cyclin B (SCBT sc-245) antibodies. The next day, 20 µl packed protein-A- and protein-G-coated magnetic beads (Dynabeads Protein A and Dynabeads Protein G, Invitrogen, 10002D and 10003D, respectively) were added and lysates were rotated for an additional 1 h at 4 °C. The protein A/G beads were collected using a magnet, washed three times with 1% NP-40 cell lysis buffer, boiled and denatured in 1× Laemmli sample buffer, separated by SDS–PAGE and immunoblotting was performed as described above. The primary antibodies and dilutions used were as follows: anti-MYT1 (Fortis Life Sciences, A302-424A, 1:1,000), rabbit anti-WEE1 (Cell Signaling, 4936, 1:1,000), mouse anti-cyclin B (Cell Signaling, 4135 1:1,000), mouse anti-E2F1 (SCBT, sc-251, 1:1,000), mouse anti-cyclin A (Cell Signaling, 4656, 1:1,000), mouse anti-CDK2 (Origene, TA502935), rabbit anti-CDC2 (Cell Signaling 28439). The secondary antibodies used and dilutions were: mouse anti-rabbit (confirmation specific)-IgG HRP (Cell Signaling, 5127, 1:2,000), goat anti-rabbit IgG-HRP (Cell Signaling, 7074S, 1:5,000), horse anti-mouse IgG-HRP (Cell Signaling, 7076S, 1:5,000), goat anti-mouse-IgE-HRP (Southern Biotech, 1110-05, 1:5,000).

For immunoprecipitations of cyclin B–HA and CDK2 in Fig. 3i and Extended Data Fig. 9k, HEK293T cells were stably infected with pTwist Lenti SFFV Puro WPRE lentiviral vectors (SYNTHESIZED by Twist Biosciences) encoding (1) *CCNB1* wild-type-HA, (2) *CCNB1* triple mutant-HA (E169K/Y170H/Y177C) or a (3) negative control encoding a functionally inactivated EED mutant-HA with mutations to inactivate EED (F97A/Y148A/Y365A). In total, 2.0×10^7 cells were seeded at 1×10^6 cells per ml density and, the next day, were treated with the cyclin A/B RxL inhibitor (CIRc-004) at 300 nM or DMSO for 2 h before cell collection. Cells were lysed in 700 µl lysis buffer (Cell Signaling, 9803) supplemented with protease inhibitor cocktail (Complete, Roche Applied Science, 11836153001) and phosphatase inhibitors (PhosSTOP, Sigma-Aldrich, 04906837001). Samples were sonicated (Branson Digital Sonifier) three times for 5 s each to ensure homogenization and centrifuged at 14,000*g* for 10 min at 4 °C (Eppendorf centrifuge 5424R, FA-45-24-11 rotor). The supernatant was precleared by rotating 20 µl protein A agarose beads (Cell Signaling, 9863) for 1 h at 4 °C. The samples were then briefly centrifuged to remove the beads and protein concentration was determined. Then, 60 µl of lysate was removed as input (~10% total

for ~2.5% input per immunoblot) and boiled after adding 3× sample buffer (6.7% SDS, 33% glycerol, 300 mM DTT and Bromophenol Blue) to a final concentration of 1×. Then 300 µl of lysate was immunoprecipitated by rotating overnight at 4 °C with rabbit anti-HA epitope (Cell Signaling, 3724, 1:100) for exogenous cyclin B, rabbit anti-CDK2 E8J9T (Cell Signaling, 18048, 1:100) or equivalent amount of rabbit (DA1E) monoclonal antibody IgG XP isotype control (Cell Signaling, 3900). The next day, 20 µl protein A agarose beads was added to each sample tube and incubated for 1 h at 4 °C with rotation. The beads were collected by centrifugation and washed five times with cold lysis buffer followed by boiling in 3× sample buffer. The samples were run on SDS–PAGE and immunoblotting was performed as described above. Primary antibodies used for immunoblotting were as follows: rabbit anti-cyclin B1 D5C10 (Cell Signaling, 12231, 1:1,000), rabbit anti-CDK2 E8J9T (Cell Signaling, 18048, 1:1,000) and mouse anti-HA.11 epitope tag (BioLegend, 901501, 1:1,000).

For immunoprecipitation of endogenous cyclin A with E2F3 in Extended Data Fig. 10f, NCI-H1048 cells were seeded at 2.5×10^7 cells per 15 cm plate and allowed to adhere overnight. The next day, cells were incubated with the indicated cyclin RxL inhibitors at 300 nM or DMSO for 2 h before rinsing once in ice-cold PBS and lysing in 1% Triton buffer (40 mM HEPES pH 7.5, 1 mM EDTA pH 8.0, 10 mM sodium pyrophosphate, 10 mM β-glycerophosphate, 50 mM sodium fluoride, 120 mM sodium chloride and 1% Triton X-100) supplemented with a protease inhibitor cocktail (cOmplete, Sigma-Aldrich, 5892970001) and phosphatase inhibitors (PhosSTOP, Sigma-Aldrich, 4906837001). Cell lysates were centrifuged at 9,391*g* for 10 min. The supernatant (cell extract) was removed and the protein content estimated by performing a Bradford assay. Anti-cyclin A antibody (SCBT, sc-271682) was covalently coupled to M-270 Expoxy dynabeads (Dynabeads Antibody Coupling Kit, Invitrogen 14311D) at a ratio of 10 µg antibody per mg of beads and rotated overnight at 37 °C. Next, 2 mg cell extract was then rotated overnight at 4 °C with 1 mg coupled dynabeads. The dynabeads beads were collected using a magnet, washed three times with 1% Triton cell lysis buffer, boiled and denatured in 1× Laemmli sample buffer, separated by SDS–PAGE, and immunoblotting was performed as described above. The primary antibodies were mouse anti-E2F3 (SCBT, sc-56665, 1:1,000), and mouse anti-cyclin A (Cell Signaling, 4656, 1:1,000). The secondary antibodies were horse anti-mouse IgG-HRP (Cell Signaling, 7076S, 1:5,000) and goat anti-mouse-IgE-HRP (Southern Biotech, 1110-05, 1:5,000).

Nocodazole cell synchronization experiments

To synchronize cells in mitosis, as depicted in Fig. 3k, a preliminary evaluation was conducted to determine the minimal nocodazole concentration required to induce mitotic arrest and the optimal time post-washout for facilitating the re-entry of the majority of cells into the cell cycle. In brief, 500,000 cells per ml of NCI-H69 cells were seeded in six-well plates and treated with increasing concentrations of nocodazole (60, 120, 240 ng ml^{-1}) or DMSO as a control. After overnight incubation, cells were collected, fixed and subjected to propidium iodide-based FACS to assess mitotic arrest. A nocodazole concentration of 60 ng ml^{-1} was sufficient to induce mitotic arrest in around 90% of cells. To determine the optimal wash-out time for mitotic exit, cells were plated at 500,000 cells per ml density and treated with 60 ng ml^{-1} nocodazole. After overnight incubation, nocodazole-containing media was removed, and cells were washed three times with DPBS (Life Technologies, 14190250). Fresh warm medium was then added, and cells were collected at 0, 3, 6 and 12 h after washout. A 6 h incubation period was optimal to allow the majority of cells to complete mitosis and re-enter the subsequent cell cycle. For the immunoblot analysis shown in Fig. 3k, cells were seeded in 6 cm tissue culture dish at a density of 500,000 cells per ml and incubated overnight with nocodazole (60 ng ml^{-1}). The next day, cells were washed three times with PBS and incubated with CDK2i (PF-07104091, 500 nM), cyclin A/B RxL inhibitor (CIRc-004, 20 nM), nocodazole (60 ng ml^{-1}) or the combinations as indicated using DMSO as control. At 6 h after incubation, cells were collected for immunoblot analysis.

Histone extractions and histone immunoblot analysis

For histone extractions in Fig. 4, cells were counted on day 0 using the Vi-Cell XR Cell Counter and plated in 6 cm plates at 250,000 cells per ml in 4 ml of medium per plate for all cell lines along with indicated concentration of cyclin A/B RxL inhibitor. Then, 3 days later, cells were pelleted by centrifugation at 400*g* for 3 min at 4 °C in a 15 ml conical tube. The cell pellets were then washed once in 1 ml of ice-cold PBS, transferred to a 1.5 ml Eppendorf tube and pelleted by centrifugation at 400*g* for 3 min at 4 °C. The PBS was removed by gentle aspiration and the soluble proteins from the cell pellets were extracted by incubation in nucleus lysis buffer (250 mM sucrose, 60 mM KCL, 15 nM NaCl, 15 mM Tris pH 7.5, 5 mM $MgCl_2$, 1 mM $CaCl_2$, 1 mM DTT, 0.3% NP-40 supplemented with a cocktail of protease inhibitor cocktail and phosphatase inhibitors) for 10 min at 4 °C. The extracts were then centrifuged at 10,000*g* for 1 min at 4 °C and the supernatant was removed by aspiration. The cell pellets were again resuspended in nucleus lysis buffer and incubated for 10 min at 4 °C and then centrifuged at 10,000*g* for 1 min at 4 °C. The supernatant was removed by aspiration and the histones in the insoluble pellet were extracted by overnight incubation in 60 µl of 0.2 N HCl followed by centrifugation at 16,800*g* for 15 min at 4 °C. The supernatant was transferred to a fresh 1.5 ml Eppendorf tube and quantified using the Bradford protein assay. The pH was neutralized by adding 1/5 volume of 1 N NaOH, as confirmed by the colour of the samples after the addition of sample buffer containing Bromophenol Blue. Then, 1 µg of protein in sample buffer was boiled and resolved by SDS–PAGE on a 15% SDS–PAGE gel. Immunoblot analysis was performed as described above. The primary antibodies were as follows: rabbit anti-histone-3 DH12 (Cell Signaling, 4499, 1:5,000) and rabbit anti-p-histone H2A.X Ser 139 (Cell Signaling, 2577, 1:1,000). For all experiments, total histone H3 protein was run as a sample processing control on a separate gel owing to the low amount of protein lysate loaded onto the gel (1 µg) for histone blots.

Cancer cell line sensitivity screening with cyclin A/B RxL inhibitors

A panel of 46 SCLC cell lines was tested for their sensitivity to cyclin A/B RxL inhibition in a Cell Titer Glo (CTG) proliferation assay performed at Shanghai ChemPartner (Fig. 1d). Cells were plated in 384-well format and dosed in duplicate with CIRc-004 in a 10-point, 1:3 serial dilution dose–response assay with a 10 µM starting concentration. Staurosporine was used as an assay control per cell line and was dosed in duplicate from 2 µM maximum concentration in a 10-point 1:3 serial dilution. Cells were exposed to inhibitor for 4–8 days depending on the length of time required for at least two cell doublings to occur. A time 0 h read and an end-point DMSO control read were obtained per cell line for calculation of GI_{50} values. SCLC panel GI_{50} values are included in Supplementary Table 1.

CIRc-001 was profiled in Horizon Discovery's High Throughput OncoSignature screening platform containing 302 cell lines across 18 indications (Extended Data Fig. 2a). Cells were seeded in 384-well tissue culture plates at 250–1,500 cells per well. Assay plates were dosed in triplicate with inhibitor in a 9-point, 1:3 serial dilution dose–response assay with 10 µM maximum concentration. Cells were incubated for 3 days and then analysed using CellTiter-Glo 2.0 (Promega). At the time of treatment, a set of assay plates that did not receive treatment were collected and ATP levels measured by adding CellTiter-Glo 2.0 (Promega). All datapoints were collected by automated processes and were subject to quality control. Potency and efficacy metrics were derived from logistics curves fitted to growth inhibition using Horizon's Chalice software. Horizon Discovery OncoSignature panel cell line GI_{50} values are provided in Supplementary Table 2.

GSEA

To identify differentially expressed gene sets associated with sensitivity and resistance to CIRc-001 across the Horizon Discovery OncoSignature cell line panel, and to CIRc-004 across the SCLC panel (Fig. 1e), GSEA was first performed between sensitive and resistant cell lines using the MSigDB hallmark pathways using mRNA expression data obtained from the Broad Institute's Cancer Cell Line Encyclopaedia (CCLE) database (2019 release: DepMap 2019q3). Sensitive and resistant are defined as the top and bottom quartile of the area over the curve to identify hallmark pathways that were differentially enriched in sensitive versus resistant lines based on FDR < 0.05 For the Horizon Discovery OncoSignature cell line panel, 42 out of 46 SCLC lines and 288 out of 302 cell lines across Horizon Discovery OncoSignature cell line panel had mRNA expression that was available for the analysis.

The GSVA method[33], using the MSigDb Hallmark collection of RNA-seq data, was then used to calculate GSVA scores for E2F targets and G2/M checkpoint pathway using the GSVA Bioconductor package (v.1.50.5). To visualize the top selected pathways from GSEA analysis, gene expression data were first aggregated as GSVA scores based on gene set annotations obtained from MSigDB. For each pathway, pathway scores were transformed to *z* scores across samples to standardize the data. The heat map was constructed using the ComplexHeatmaps package (v.2.18.0) in R (v.4.3.2), where rows represented Hallmark pathways, columns represented samples and the colour intensity reflected the mean *z* score of each pathway for each sample and was hierarchically clustered by pathway to reveal patterns of enrichment. For Fig. 1e (right), the median E2F target or G2M pathway score across the SCLC panel was used as the threshold to define low versus high groups and *P* values were calculated using Mann–Whitney *t*-tests.

CRISPR–Cas9 resistance screen with cyclin A/B RxL inhibitor, cyclin A/B/E RxL inhibitor and CDK2i

On day 0, NCI-H1048 cells were counted using the Vi-Cell Counter. In total, 1.50×10^8 cells (which would yield representation of at least 500 cells per sgRNA if multiplicity of infection (MOI) = 0.3) were pelleted and resuspended at 2×10^6 cells per ml in complete medium containing 50 µl ml^{-1} of human genome-wide Brunello sgRNA library (CP0043) (purchased from the Broad Institute) lentivirus, which contains both the sgRNA and Cas9, and 8 µg ml^{-1} polybrene. The lentiviral titre was determined empirically in pilot experiments with a goal MOI of 0.3–0.5. CP0043 contains 77,441 sgRNAs targeting 4 sgRNAs per gene with 1,000 non-targeting sgRNAs controls. The cells mixed with polybrene and lentivirus were then plated in 1 ml aliquots onto 12-well plates and centrifuged at 931*g* (Allegra X-15R Centrifuge (Beckman Coulter), rotor SX4750A, 2,000 rpm), for 2 h at 30 °C. In parallel, 2×10^6 cells were also centrifuged under the same conditions but without lentivirus as a control for puromycin selection (Mock). Around 16 h later (day 1), the cells were collected, pooled and centrifuged again at 448*g* to remove the lentivirus and polybrene, and the cell pellet was resuspended in complete medium and plated into twenty-three 15 cm tissue-culture-treated plates at 0.3×10^6 cells per ml or in 6-well plates at the same density for the control (mock) cells. The cells were then cultured for 72 h at which time (day 4) the cells were counted and plated at 0.4×10^6 cells per ml in 15 cm tissue-culture-treated plates with fresh medium containing puromycin (0.25 µg ml^{-1}) to select for puromycin-transduced cells. A parallel experiment was performed on day 4 to determine the MOI of the screen. To do this, cells infected with the sgRNA library or mock-infected cells were plated at 0.4×10^6 cells per ml in 6-well plates in the presence or absence of puromycin (0.25 µg ml^{-1}). After 72 h (day 7), cells were counted using the Vi-Cell XR Cell Counter and the MOI was calculated using the following equation: (number of puromycin-resistant cells infected with the sgRNA library/total number of cells surviving without puromycin after infection with the sgRNA library) − (number of puromycin-resistant mock-infected cells/total number of mock-infected cells). The calculated MOI was 0.33. On the same day (day 7), the puromycin-containing medium was exchanged with fresh complete medium not containing puromycin.

On day 10, cells were pooled, counted and split into two replicates. Each replicate was split into four arms: (1) CIRc-004 (cyclin A/B RxL inhibitor, 200 nM); (2) CIRc-001 (cyclin A/B/E RxL inhibitor, 200 nM); (3) CDK2i (PF-07104091, 500 nM); or (4) CIRc-005 (inactive enantiomer of CIRc-004, 200 nM). CIRc-005 had no effect on cellular proliferation (Extended Data Fig. 2d) and therefore was used as a negative control comparison for all drug treated arms. A total of 4×10^7 cells were plated at 0.2×10^6 cells per ml in 15 cm tissue culture plates in complete medium containing the respective drugs maintaining 500 cells per sgRNA. At the same time, the remaining cells were collected and divided in aliquots of 4×10^7 (again to maintain representation of 500 cells per sgRNA), washed in PBS and cell pellets were frozen for genomic DNA isolation for the ETP before drug selection. Mock-infected cells were maintained at the same density for all drug conditions and carried out in parallel for the entire screen described below.

The medium on the plates under drug selection was exchanged every 3 days with complete medium containing fresh drug. Treatment arms were counted and passaged when cells were about 80% confluent and split back to a representation of 4×10^7 cells at a density of 0.2×10^6 cells per ml onto 15 cm tissue culture plates. This was done for the CIRc-005 inactive enantiomer every 3 days as CIRc-005 had no effect on cellular proliferation, and it happened only once or twice during the screen for all of the other drug treatment conditions as the drugs exhibited strong cytotoxicity. When cells were passaged, all cells were pooled, counted and replated maintaining 500 cells per sgRNA. The remaining cells were divided into aliquots of 4×10^7 cells, washed in PBS and cells pellets were frozen for genomic DNA isolation. The screen was terminated on day 26 (LTP) when there was an obvious growth advantage in the CIRc-004, CIRc-001, CDK2i arms infected with the sgRNA library relative to the mock infected cells treated with the same compounds.

After completion of the screen, genomic DNA was isolated using the Qiagen Genomic DNA maxi prep kit (51194) according to the manufacturer's protocol. Raw Illumina reads were normalized between samples using: $\log_2[(\text{sgRNA reads/total reads for sample}) \times 1 \times 10^6) + 1]$. The initial common ETP (day 10) was then subtracted from the LTP after drug treatment (day 26) to determine the relative enrichment of sgRNAs in the CIRc-004, CIRc-001 and CDK2i arms relative to the CIRc-005 inactive enantiomer control arm for each replicate. Apron analysis, hypergeometric analysis and STARS analysis (GPP web portal, https://portals.broadinstitute.org/gpp/screener/) were performed using the normalized counts of the drug-treated arms LTP−ETP (Apron) or the log-normalized counts of the drug-treated arms LTP−ETP (hypergeometric, STARS) comparing the drug-treated condition to the CIRc-005 enantiomer control at the matched LTP or compared to the ETP. The averaged data from the two replicates were used for all analyses shown in the manuscript. All raw data and outputs of each analysis listed above are provided in Supplementary Table 3.

Dose–response assays for screen hit validation with CRISPR–Cas9 sgRNA knockout

For validation studies, we focused on the cyclin A/B RxL inhibitor (CIRc-004) and not CIRc-001, as CIRc-004 spared cyclin E and, perhaps as a result, demonstrated modestly increased cellular potency. NCI-H1048 and NCI-H446 cells were first infected with pLentiCRISPR V2-Puro lentiviruses encoding sgRNAs targeting the selected screen hits and selected with puromycin. Stably infected cells were counted on day 0 using a Vi-Cell XR Cell Counter and plated onto tissue-culture-treated 6-well plates at 50,000 cells per ml in 2 ml of complete medium. For dose–response assays with CIRc-004 and the CDK2i (PF-07104091), the cells were treated with the compounds at the indicated concentrations for 6 days and counted using the Vi-Cell system. Normalized

cell counts were calculated as day 6 counts for treated samples/day 6 counts for DMSO sample. Analysis was performed using GraphPad Prism v.10.0.0.

Forward genetic screen with cyclin A/B RxL inhibitor in iHCT-116 cells

The Nijhawan laboratory developed a forward genetic screening system using an engineered colorectal cancer cell line, termed iHCT116, that identifies mutations that confer compound resistance using HCT116 cells engineered for inducible protein degradation (with the addition of IAA) of mismatch repair protein, MLH1[37]. As a result, cells cultured without IAA have a lower mutation rate (mut-low) than cells cultured with IAA (mut-high). These cells are diploid and, therefore, resistance mutations are more likely to be the result of a gain of function. For the forward genetic screen, 5 million iHCT116 cells that had previously been treated with vehicle or indole acetic acid were cultured in 10 μM of CIRc-004 for 17 days, with the medium replenished every 3 days. Six and twelve clones from the mut-low and mut-high conditions, respectively, were isolated. The surviving clones were analysed for resistance to CIRc-004 in a 3-day proliferation assay in which CIRc-004 was added in dose–response with a final concentration of DMSO of 0.5%. The EC_{50} for all clones were at least 100-fold higher than parental cells. All clones tested were resistant to an unrelated toxin, MLN4924, suggesting that non-specific mechanisms of CIRc-004 resistance were unlikely (Extended Data Fig. 5d). After evaluating the barcode sequence in all 18 clones, 5 and 12 founder clones were identified in the mut-low and mut-high condition, respectively (Extended Data Fig. 5e). Eight distinct clones were selected for exome sequencing. Barcode sequences were PCR amplified and sequenced as described previously[37]. Genomic DNA was collected from select clones (Qiagen) and processed for whole-exome sequencing. Mutations unique to individual clones were identified using the previously described analysis[37]. Only four genes were mutated in more than 1 of 8 clones and heterozygous *CDC20* mutations were found in 5 of 8 clones.

Rescue experiments with MPS1 inhibitor

For dose–response assays with MPS1 inhibitor (BAY-1217389) to empirically identify concentrations of the MPS1 inhibitor that effectively blocked MPS1 activity (measured by immunoblotting for p-KNL1) without gross effects on cellular proliferation, the cells were counted on day 0 using the Vi-Cell XR Cell Counter and plated in a tissue-culture-treated 6-well plate at 250,000 cells per ml in 2 ml of complete medium. Cells were treated with the drug (BAY-1217389) at the indicated concentrations for 3 days. The normalized cell count was calculated as (day 3 count for treated samples)/(day 3 count for DMSO treated sample). Analysis was performed using GraphPad Prism v.10.0.0. These experiments identified 3 nM of BAY-1217389 blocks p-KNL1 without grossly affecting proliferation.

For rescue experiments with the MPS1 inhibitor, cells were counted using the Vi-Cell XR Cell and plated at 250,000 cells per ml for NCI-H1048 cells or at 50,000 cells per ml for NCI-H69 and NCI-H446 cells and then treated with cyclin A/B RxL inhibitor (CIRc-004) at the indicated concentrations with or without MPS1 inhibitor (BAY-1217389 at 3 nM) and collected after 3 days for dose–response assays using the Vi-Cell system. For FACS-based cleaved PARP apoptosis assay, cells were counted and plated at 250,000 cells per ml and then treated with CIRc-004 at the indicated concentrations with or without MPS1 inhibitor (BAY-1217389 at 3 nM) and, 3 days later, were collected, stained and analysed as described above.

For immunoblot analysis of p-KNL1 levels after BAY-1217389 treatment, about 2 million cells were counted using the Vi-Cell XR Cell and plated at 500,000 cells per ml and then treated with CIRc-004 at the indicated concentrations with or without BAY-1217389 at 3 nM, and collected 24 h later for immunoblot analysis.

Immunofluorescence

Cells were seeded onto glass coverslips at 250,000 cells per ml and treated with CIRc-004 as indicated. Coverslips were fixed with ice-cold 100% methanol for 15 min on ice. Cells were washed with PBS and incubated in blocking buffer (5% BSA in PBS) for 1 h. Coverslips were then incubated with the following primary antibodies diluted in fresh blocking buffer: rabbit anti-p-histone H2A.X Ser139 (Cell Signaling, 2577, 1:400), rabbit anti-p-CASC5/KNL1 Thr943/Thr1155 D8D4N (Cell Signaling 40758, 1:400), ACA (Antibodies, 15-235, 1:500) and incubated overnight at 4 °C. Cells were rinsed three times with PBS + 0.05% Triton X-100 and then incubated with secondary antibodies: Alexa Fluor 568 goat anti-rabbit (Thermo Fisher Scientific, A11011, 1:300) and Alexa Fluor 647 goat anti-human (Thermo Fisher Scientific, A21445, 1:300) for 1 h at room temperature. The coverslips were then washed three times in PBS containing 0.05% Triton X-100. Cells were then incubated with 1 μg ml^{-1} DAPI (Cell Signaling) for 5 min. After rinsing with PBS coverslips, the coverslips were mounted onto glass slides with ProLong Glass mounting reagent (Invitrogen, P36930). Images were acquired using the Zeiss LSM980 laser-scanning microscope (Oberkochen) with ZEN 2.3 SP1 software. Image analysis was performed using Image J2 v.2.9.0.

Fluorescence quantification of p-KNL1 confocal images

Image quantification was performed using Fiji (Image J2 v.2.9.0). In brief, regions of interest were defined by identifying mitotic cells and drawing an area centred on the DAPI stain. Background values measured in an adjacent region were subtracted and the resulting corrected total cell fluorescence (CTCF) was calculated using the formula CTCF = (integrated density) − (area of selected cell × mean fluorescence of background). Each individual mitotic cell CTCF was plotted in a dot plot and CIRc-004-treated cells were compared with vehicle-treated cells.

Live-cell imaging

Live-cell imaging was performed on a Ti2 inverted microscope fitted with a CSU-W1 spinning-disk system (Nikon). To perform live-cell imaging, NCI-H1048 cells were transduced to stably express both mCherry-PCNA and PGK-H2B-eGFP (Addgene, 21210). Two rounds of FACS sorting were performed to obtain a pure population of eGFP and mCherry double-positive cells. To capture mitotic events for these experiments, we focused our live-cell imaging experiments on H2B–eGFP. Cells were seeded onto 35 mm μ-Dish (iBiDi, 80137) at 500,000 cells per ml and allowed to attach and grow for 48 h. CIRc-004 (20 nM) was added 2 h before live-cell imaging. *z* stacks (+6 (above) and −4 (below) planes at 0.5 μm spacing) were captured every 5 min for 10 h, using a Zyla 4.2 sCMOS camera (Andor), and a ×20/0.95 NA Plan Apochromat Lambda objective with the correction collar set to 0.17. An environmental enclosure was used to maintain cell culture conditions (37 °C and humidified 5% CO_2) for all live-cell confocal imaging. Images were analysed on NIS Elements Viewer v.4.2 (Nikon). The timing of mitosis was measured from DNA condensation (beginning timepoint) to cytokinesis completion (end timepoint).

For FUCCI reporter LIC, RPE1 cells were stably transduced with Incucyte cell cycle green/red construct (47741, Sartorius). After selection with puromycin (2 μg ml^{-1}), cells were seeded in a 96-well plate at 1,000 cells per well. CIRc-004 (2,000 nM) was added before initiating live-cell imaging. Plates were imaged every 20 min for 24 h. Imaging and analysis was performed using Incucyte Zoom/S3 live-cell imagers (Essen Biosciences) and quantified using the Incucyte analysis software.

CRISPR–Cas9 base editor screens with the cyclin A/B RxL inhibitor

To establish the adenosine or cytosine base editor Cas9-expressing cell line for the screen with the tiling library, NCI-H1048 cells were transduced with pRDA_867 (A>G base editor Cas9) and pRDB_092 (C>T base editor Cas9), respectively. Successfully transduced cells were selected

with blasticidin (5 μg ml^{-1}) to make stable adenosine or cytosine base editor cell lines.

The base editor library (CP1985) was custom designed using the Broad Institute's CRISPR base editor library designer Beagle (https://portals.broadinstitute.org/gppx/beagle/screener) to include a total of 2,802 sgRNAs tiling *CCNB1*, NM_031966.4 (572 sgRNAs), *CCNA2* NM_001237.5 (577 sgRNAs), *CDK2* NM_001798.5 (476 sgRNAs) and *CDC20* NM_001255.3 (897 sgRNAs). As controls the library contained 56 guides against essential genes (*EEF2*, *DBR1*, *PLK1*, *KIF11*, *GAPDH*, *PCNA*, *RPA3*, *RPL3*, *POLR2B* and *PSMB1*), 112 guides against intergenic sites and 112 guides as non-targeting controls.

First a pilot experiment was performed to empirically determine the lentiviral titre needed for a goal MOI of 0.3–0.6. Cells were mixed with polybrene and increasing amounts of the lentiviral CP1985 sgRNA library and plated in 1 ml aliquots onto 12-well plates and centrifuged at 931*g* (Allegra X-15R Centrifuge (Beckman Coulter), rotor SX4750A, 2,000 rpm), for 2 h at 30 °C. In parallel, 2×10^6 cells were also centrifuged under same conditions but without lentivirus as a control for puromycin selection (Mock). Then, about 16 h later (day 1), the cells were collected, pooled and centrifuged again at 448*g* to remove the lentivirus and polybrene, and the cell pellet was resuspended in complete medium and plated into 15 cm tissue-culture-treated plates at 0.4×10^6 cells per ml or in 6-well plates at the same density for the control (mock) cells. The cells were then cultured for 72 h at which time (day 4) the cells were counted and plated at 0.4×10^6 cells per ml in 15 cm tissue-culture-treated plates with fresh medium containing puromycin (0.5 μg ml^{-1}) to select for puromycin-transduced cells. After 72 h (day 7), cells were counted using the Vi-Cell XR Cell Counter and the MOI was calculated using the following equation: (number of puromycin-resistant cells infected with the sgRNA library/total number of cells surviving without puromycin after infection with the sgRNA library) − (number of puromycin-resistant mock-infected cells/total number of mock-infected cells). These experiments demonstrated that 25 μl ml^{-1} of CP1985 virus was needed to achieve a MOI of about 0.3–0.6.

For the screen, adenosine or cytosine base editor Cas9-expressing NCI-H1048 cell lines were counted using the Vi-Cell counter on day 0. Two replicates of 2.4×10^7 cells (which would yield representation of at least 2,000 cells per sgRNA if MOI = 0.3) were pelleted and resuspended at 2×10^6 cells per ml in 1 ml of complete medium containing 25 μl ml^{-1} of the pooled sgRNA library (CP1985) lentivirus and 8 μg ml^{-1} polybrene. A parallel experiment was performed on day 4 to determine the actual MOI of the screen as described above, which showed that the MOI of the screen was about 0.6. On the same day (day 7), puromycin-containing medium was exchanged with fresh complete medium not containing puromycin for all cells in the screen.

On day 10, cells from each replicate were pooled, counted and then split into two additional replicates (four replicates in total). In total, 6×10^6 cells from each replicate were collected for an ETP for representation of 2,000 cells per sgRNA. This was done by washing cells in PBS and freezing cell pellets at −80 °C for genomic DNA isolation. The remaining cells from each replicate were then split into two treatment arms: (1) CIRc-004 (cyclin A/B RxL inhibitor, 200 nM) and (2) CIRc-005 as a negative control and comparator (inactive enantiomer of CIRc-004, 200 nM) with 4.5×10^6 cells in each treatment arm plated in 15 cm tissue culture plates at 0.2×10^6 cells per ml in complete medium containing the respective drugs listed above to maintain representation of 1,500 cells per sgRNA. Mock-infected cells were maintained at the same density for all drug conditions and carried in parallel for the entire screen described below.

The medium on the plates under drug selection was exchanged every 3 days with complete medium containing fresh drug at the concentrations described above. Treatment arms were counted and passaged when cells were about 80% confluent and split back to a representation of 4.5×10^6 cells at a density of 0.2×10^6 cells per ml onto 15 cm tissue culture plates. This occurred for the CIRc-005 inactive enantiomer every 3 days as CIRc-005 had no effect on cellular proliferation. As the CIRc-004 exhibited strong cytotoxicity, this treatment arm required medium exchange only every 3 days. When cells were passaged, the cells were pooled, counted and replated maintaining 1,500 cells per sgRNA. The remaining cells were divided into aliquots of 6×10^6 cells, washed in PBS and the cell pellets were frozen for genomic DNA isolation. The screen was terminated on day 26 when there was an obvious growth advantage in the CIRc-004 arm infected with the sgRNA library relative to the mock infected cells treated with the same compounds.

After completion of the screen, genomic DNA was isolated using the Qiagen Genomic DNA midi prep kit (51183) and mini prep kit (51106) according to the manufacturer's protocol. Raw Illumina reads were normalized between samples using $\log_2$[(sgRNA reads/total reads for sample) × 1 × 10^6) + 1]. LFC values in Supplementary Fig. 2a,b were calculated by subtracting the plasmid DNA (pDNA) log-normalized value from the CIRc-005 LTP (day 26) log-normalized value and this was used for replicate reproducibility and dropout of essential sgRNA versus negative-control sgRNAs. To calculate the *z*-scored LFC values in Fig. 3b and Supplementary Fig. 2c–e, we first subtracted the log-normalized value of the negative enantiomer control (CIRc-005) at the LTP (day 26) from the log-normalized value of the cyclin A/B RxL inhibitor (CIRc-004) at the LTP (day 26). This LFC value (CIRc-004 minus CIRc-005) for each sgRNA was *z*-scored, a transformation that factors in the performance of the control guides, using the following equation: z score = $(x - \mu)/\sigma$, where x, μ and σ correspond to the LFC of an individual guide, the mean LFC of all negative control guides and the s.d. of all control guides, respectively. These *z*-scored LFC values for each sgRNA were then matched to the annotated CP1985 library where Beagle (Broad Institute) was used to predict the expected nucleotide edit and plotted for each tiled gene as indicated in each figure panel listed above. The averaged data from the four replicates were used for all analyses shown in the manuscript. All raw data and outputs of each analysis listed above are provided in Supplementary Table 5.

CRISPR–Cas9 base editor screen with the cyclin A/B RxL inhibitor with focused *CCNB1* target validation

To validate the exact mutations enriched after CIRc-004 treatment in *CCNB1* corresponding to the amino acids 117–285, which contained several enriched *CCNB1* variants from our original base editor screen in Fig. 3b, we repeated the screen as in Fig. 3a at scale with a representation of 1,500 cells per sgRNA, and at the LTP (day 26), mRNA was isolated from the cyclin A/B RxL inhibitor (CIRc-004)-treated and enantiomer control (CIRc-005)-treated arms using the Quick-RNA Miniprep kit (Zymo Research) according to the manufacturer's instructions. The RNA concentration was determined using the Nanodrop 8000 (Thermo Fisher Scientific) system. A cDNA library was synthesized using iScript Reverse Transcription Supermix for RT-qPCR (BioRad, 1708841) according to the manufacturer's instructions with 3,000 ng of RNA. The target site on *CCNB1* was amplified by two-step PCR using KOD XTREME HOT START DNA POLYMERASE (Sigma-Aldrich, 71975-3) using 25% of the total cDNA reaction above. For the first PCR step, *CCNB1* 1F, 5′-GGAACGGCTGTTGGTTTCTG-3′; and *CCNB1* 1R, 5′-AAGTAAAAGGGGCCACAAGC-3′ primers were used to amplify a 1,514 bp region. Then, 0.2 μl of the first PCR reaction was used for a second round of PCR amplification using the following primers: 2F, 5′-CGCCTGAGCCTATTTTGGTTG-3′; and *CCNB1* 2R, 5′-CCATCTGTCTGATTTGGTGCTTAG-3′ to yield a 510 bp product. This final PCR product was column purified using the QIAquick Gel Extraction kit (Qiagen, 28704) and sent for amplicon sequencing using next-generation sequencing by the MGH DNA Core Facility and analysed using MGH DNA Core's complete amplicon sequencing pipeline for data analysis of >600 bp amplicons using the following *CCNB1* NM_031966.4 refseq amplicon: CG CCTGAGCCTATTTTGGTTGATACTGCCTCTCCAAGCCCAATGGAAACA

TCTGGATGTGCCCCTGCAGAAGAAGACCTGTGTCAGGCTTTCTCTGATG
TAATTCTTGCAGTAAATGATGTGGATGCAGAAGATGGAGCTGATCCAA
ACCTTTGTAGTGAATATGTGAAAGATATTTATGCTTATCTGAGACAACT
TGAGGAAGAGCAAGCAGTCAGACCAAAATACCTACTGGGTCGGGAAG
TCACTGGAAACATGAGAGCCATCCTAATTGACTGGCTAGTACAGGTTC
AAATGAAATTCAGGTTGTTGCAGGAGACCATGTACATGACTGTCTCCAT
TATTGATCGGTTCATGCAGAATAATTGTGTGCCCAAGAAGATGCTGCAG
CTGGTTGGTGTCACTGCCATGTTTATTGCAAGCAAATATGAAGAAATG
TACCCTCCAGAAATTGGTGACTTTGCTTTTGTGACTGACAACACTTAT
ACTAAGCACCAAATCAGACAGATG.

To analyse variants from the *CCNB1* refseq above, the percentage of mismatched reads at individual base positions were normalized to the percentage of sequencing reads to get the percentage of variants at each position and then averaged across two independent experiments. Then the enrichment of percentage of variants in the CIRc-004-treated arm was compared to the variants in the CIRc-005-treated arm to determine the fold change in CIRc-004 versus CIRc-005 at the LTP. All data outputs are in Supplementary Table 5.

AlphaFold protein co-folding prediction

Co-folding of proteins were done by AlphaFold 2 implemented in ColabFold[76]. The default parameters were used to predict their relative positions (parameters: msa_mode (MMseqs2_UniRef_Environmental), pair_mode (unpaired_paired), model_type (auto), number of cycles (3), recycle_early_stop_tolerance(auto), relax_max_iterations (200), and pairing_strategy (greedy)). The resulting co-folding structure along with the PAE files was analysed using ChimeraX software[77]. The command 'alphafold contacts /A to /B distance 3' was used to identify residues potentially interacting within a putative predicted distance of less than 3.0 Å.

Modelling the impact of cyclin B mutations on CIRc-004 binding

Schrodinger software suite (2024-3 version) was used to conduct modelling studies on cyclin B. Initially, the binding model of CIRc-004 to wild-type cyclin B1 was generated using the crystal structure of the cyclin B–p-CDK2 complex (PDB: 2JGZ). The crystal structure was superimposed onto the cyclin A–CIRc-004 model by performing backbone alignment using the Protein Structure Alignment tool in Maestro, and was prepared using the Protein Preparation Workflow with the default settings. Starting from the binding pose in the cyclin A model, CIRc-004 was minimized in the cyclin B's RxL site using Prime MM-GBSA with the VSGB solvent model, OPLS4 force field and a rigid protein, followed by docking using Glide SP with the 'refine-only' option. The resulting binding model was then used as the input structure for free-energy perturbation (FEP) calculations[78,79] to assess the binding of CIRc-004 to various single and double mutants of cyclin B. Using the protein FEP for ligand selectivity module, the relative binding free energies of CIRc-004 to various cyclin B mutants were computed with the wild-type cyclin B treated as the reference. The default settings were used for the FEP calculations with the SPC water model and OPLS4 force field.

Generation of endogenous *CCNB1* mutations using Cas9 base editing

sgRNA sequences targeting specific base edits in *CCNB1* were selected from the CP1985 sgRNA library based on *z*-scored LFC enrichment after CIRc-004 treatment in our primary screens, synthesized by IDT technologies and cloned using the same approach as for sgRNA oligo cloning described above. These sgRNAs were integrated into the GFP-expressing pMV_AA013 lentiviral vector (Broad Institute) using sgRNA Cloning method described above. NCI-H1048 cells, expressing either pRDA_867 (A>G base editor Cas9) or pRDB_092 (C>T base editor Cas9), were transduced with the pMV_AA013 plasmid carrying the sgRNA sequences and GFP and subsequently subjected to puromycin selection to establish stable edited cell lines.

The following sgRNA oligos were used for A>G edits: non-targeting sense (5′-CAACGTCGCGAACGTCGTAT-3′); non-targeting antisense (5′-ATACGACGTTCGCGACGTTG-3′); human *CCNB1* Tyr170His sense (5′-ACATATTCACTACAAAGGTT-3′); human *CCNB1* Tyr170His antisense (5′-AACCTTTGTAGTGAATATGT-3′); human *CCNB1* Tyr177Cys sense (5′-TATGCTTATCTGAGACAACT-3′); human *CCNB1* Tyr177Cys antisense (5′-AGTTGTCTCAGATAAGCATA-3′); human *CCNB1* Gln213Arg/Met241Val sense (5′-GGTTCAAATGAAATTCAGGT-3′); human *CCNB1* Gln213Arg/Met241Val antisense (5′-ACCTGAATTTCATTTGAACC-3′); human *CCNB1* Val227Ala/Ser228Pro sense (5′-ATGGAGACAGTC ATGTACAT-3′); human *CCNB1* Val227Ala/Ser228Pro antisense (5′-ATGTACATGACTGTCTCCAT-3′).

The following sgRNA oligos were used for C>T edits: non-targeting sense (5′-CAACGTCGCGAACGTCGTAT-3′); non-targeting antisense (5′-ATACGACGTTCGCGACGTTG-3′); human *CCNB1* Glu169Lys sense (5′-CATATTCACTACAAAGGTTT-3′); human *CCNB1* Glu169Lys antisense (5′-AAACCTTTGTAGTGAATATG-3′); human *CCNB1* Glu314Lys sense (5′-TGTACCTCTCCAATCTTAGA-3′); human *CCNB1* Glu314Lys antisense (5′-TCTAAGATTGGAGAGGTACA-3′); human *CCNB1* Ala346Thr/Gly347Arg sense (5′-CTCCTGCTGCAATTTGAGAA-3′); human *CCNB1* Ala346Thr/Gly347Arg antisense (5′-TTCTCAAATTGCAGCAGGAG-3′); human *CCNB1* Glu374Lys sense (5′-GAGATTCTTCAGTATATGAC-3′); human *CCNB1* Glu374Lys antisense (5′-GTCATATACTGAAGAATCTC-3′).

FACS-based competition assay

The GFP-expressing stable base-edited cells were combined with their parental base editor counterpart cells (without the sgRNA and GFP) at a ratio of 1:4 with the exact ratio confirmed by FACS analysis for GFP and seeded at a density of 0.1×10^6 cells per ml in 10 cm dishes. The cells were cultured in the presence of CIRc-004 (20 nM or 200 nM) or DMSO. Cells were collected for FACS analysis on days 6 and 13. After each timepoint, cells were replated and cultured in the presence of drug with fresh drug added every 3 days. On day 13, the remaining cells after FACS were collected, and genomic DNA was extracted. Data from the FACS-based competition assay at day 13 is shown in Fig. 3e.

To verify the exact mutations in *CCNB1* made by the base-editing sgRNAs and to determine whether CIRc-004 caused enrichment of these mutations, genomic DNA from the competition assay above at day 13 was collected and PCR amplification of the *CCNB1* target region (forward 3F, 5′-GCCCAATGGAAACATCTGGATG-3′; reverse 3R, 5′- GCGATCTCTTAAGAAATGCTGCCC-3′) was performed followed by next-generation sequencing using CRISPR amplicon sequencing conducted at the MGH DNA Core Facility as previously described[80]. Variant reads are listed in Supplementary Table 5.

MS cyclin B1 CIRc-004-dependent interactome sample preparation

To identify proteins that are modulated by CIRc-004, we performed cyclin B immunoprecipitation followed by mass spectrometry in NCI-H1048 cells treated with CIRc-004 (50 nM),CIRc-005 (50 nM) or DMSO for 2 h. The cyclin B1 immunoprecipitation was performed as described above with the following modifications: 10 mg cell extract was rotated overnight at 4 °C with 10 µg anti-cyclin B antibodies. After cyclin B1 immunoprecipitation, beads were washed with PBS before freezing at −80 °C. Dry beads were resuspended with 200 µl of Smart digest buffer (Thermo Fisher Scientific, 60113-101) before adding 3 µl of Smart trypsin. Beads were digested in a Thermo block (Thermo Fisher Scientific) for 1 h 30 min at 70 °C with 1,400 rpm (~250*g*) agitation. Trypsin digestion was then stopped by adding trifluoroacetic acid at 1% final concentration. The samples were then desalted using SOLA HRP SPE cartridges (Thermo Fisher Scientific, 60109-001) according to the manufacturer's instructions. Purified peptide eluates were dried by vacuum centrifugation and re-suspended in 0.1% formic acid and stored at −20 °C until analysis.

LC–MS/MS analysis

Liquid chromatography–tandem mass spectrometry (LC–MS/MS) analysis was performed using an Ultimate 3000 HPLC connected to an Orbitrap Ascend Tribrid instrument (Thermo Fisher Scientific) and interfaced with an EASY-spray source. Then, 0.5% of the tryptic peptides were loaded onto an AcclaimPepMap100 trap column (100 µm × 2 cm, PN164750; Thermo Fisher Scientific) and separated on a 50 cm EasySpray column (ES903, Thermo Fisher Scientific) using a 60 min linear gradient from 2 to 35% B (acetonitrile, 0.1% formic acid) and at a 250 nl min^{-1} flow rate. Both trap and column were kept at 50 °C. The Orbitrap Ascend was operated in data-independent mode (DIA) to automatically switch between MS1 and MS2, with minor changes from previously described method[81–83]. In brief, MS1 scans were collected in the Orbitrap at a resolving power of 45,000 at *m*/*z* 200 over an *m*/*z* range of 350–1,650 *m*/*z*. The MS1 normalized AGC was set at 125% (5×10^5 ions) with a maximum injection time of 91 ms and a RF lens at 30%. DIA MS2 scans were then acquired using the tMSn scan function at 30,000 orbitrap resolution over 40 scan windows with variable width, with a normalized AGC target of 1,000%, maximum injection time set to auto and a 30% collision energy.

Mass spectrometry data analysis

DIA-NN software (V8.1) was used to analyse the raw data in library-free mode and using the recommended default settings[83]. In brief, a library was created from human UniProt SwissProt database (downloaded 22 July 2022 containing 20,386 sequences) using deep learning. Trypsin was selected as the enzyme (1 missed cleavage), N-term M excision and methionine were enabled. The identification and quantification of raw data were performed against the in silico library applying 1% FDR at precursor level and match between runs (MBR). Perseus (v.1.6.2.2) was used to further analyse the DIA-NN protein group output. Protein intensities were log_2-transformed and normalized by median subtraction (by column) after applying a pre-processing filter based on valid numbers (3 out of 3 in at least one group). Subsequently, missing values were imputed following the normal distribution down shifted. A two-sample Student's *t*-test combined with multiple-testing correction using permutation-based FDR (5%) was applied. For ranking the proteins based on intensity, the average intensity was calculated for all values in the three treatment groups, log_{10}-transformed and ranked. CIRc-004-dependent interactome is included in Supplementary Table 6.

Animal studies

All mouse experiments complied with National Institutes of Health guidelines. The PDX studies were approved and performed at the Dana-Farber Cancer Institute Animal Care and Use Committee. The NCI-H69 and NCI-H1048 xenograft studies were approved and performed at Labcorp Early Development Laboratories and Pharmaron (Ningbo) Technology Development, respectively. Housing conditions for mice include a 12 h–12 h day–night cycle where the temperature is maintained at 72 °F.

SCLC cell line xenograft studies

For NCI-H69 studies, 5×10^6 NCI-H69 cells were suspended in serum-free RPMI1640 medium, combined with an equal volume of ECM gel (Sigma-Aldrich, E1270), and implanted subcutaneously into the flanks of 7–8-week-old female Nude mice (Envigo, Hsd:Athymic Nude-*Foxn1*^{nu}). After 13 days, when tumours were between 88–200 mm^3 in size, mice were randomized and put into treatment groups of CIRc-028 or vehicle (5% DMSO, 10% Solutol HS15, in 85% D5W). Mice were treated daily with i.v. injections of 100 mg per kg CIRc-028 or vehicle for 14 days. Tumours were measured with callipers 3 times per week for the duration of the study. Tumours were collected 18 h after the last dose, formalin fixed for 24 h and paraffin embedded for IHC analysis.

For NCI-H1048 studies, 3×10^6 NCI-H1048 cells were suspended in a 1:1 mixture of HITES medium and Matrigel (Corning, 354234) and implanted subcutaneously into the flanks of 6–8-week-old female BALB/c nude mice (GemPharmatech Biotech, D000521). After 16 days, when tumours were between 180–315 mm^3 in size, the mice were randomized and put into treatment groups. Treatment with CIRc-028 and vehicle was carried out as described above for NCI-H69 xenografts. Tumours were measured with callipers twice per week for the duration of the study. For NCI-H69 and NCI-H1048 xenograft studies, the investigator was not blinded but was agnostic to the outcome of the study. Animal use protocols specified that animals with tumour volumes larger than 2,000 and 2,500 mm^3, respectively, or experiencing greater than 20% body weight loss or other severe clinical signs of deteriorating condition would be euthanized and these end-point criteria were not exceeded for any mice on study without prompt euthanasia.

Bulk RNA-seq, PCA and differential gene expression analysis

RNA-seq was performed on untreated SCLC DFCI-393 and DFCI-402 PDX tumours that were used for the PDX studies. For RNA-seq analysis of experimental PDX, DFCI-393 tumours were treated with the orally bioavailable cyclin A/B RxL inhibitor CIRc-014 at 100 mg per kg orally three times per day or vehicle (30% PEG400, 20% Solutol HS15, 50% Phosal 53 MCT) three times a day for 4 days and tumours were collected 8 h after the morning dose on the last day of treatment and snap-frozen. Six independent tumours from six independent mice were used for CIRc-014 and five independent tumours from five independent mice were used for vehicle. For RNA-seq of NCI-H1048 cell line, cells were plated at 500,000 cells per ml in the presence of DMSO (vehicle), cyclin A/B RxL inhibitor (CIRc-004 or CIRc-014, 200 nM), inactive enantiomer (CIRc-005, 200 nM) or a CDK2i (PF-07104091, 500 nM). Then, 24 h after drug treatment, cells were collected for RNA. The NCI-H1048 cell line experiments were done in two biologically independent experiments. RNA was extracted using the RNeasy mini kit (Qiagen, 74106) including a DNase digestion step according to the manufacturer's instructions. Total RNA was submitted to Novogene. The libraries were prepared using the NEBNext Ultra II non-stranded kit. Paired-end 150 bp sequencing was performed on NovaSeq 6000 sequencer using S4 flow cell. Sequencing reads were mapped to the hg38 genome by STAR. Statistics for DEGs were calculated by DESeq2 (v.1.36.0) (Supplementary Tables 4 and 7).

Principal component analysis (PCA) in Extended Data Fig. 11g was performed using the top 500 genes with the largest s.d. of log-transformed FPKM (fragments per kilobase of transcript per million mapped fragments) values and these genes were subjected to PCA using the removeBatchEffect function in the limma package (v.3.58.1) and prcomp function of R software (v.4.3.3). The log-transformed sum of *ASCL1*, *NEUROD1*, *CHGA*, *CHGA*, *INSM1* and *SYP* FPKM values was calculated as the neuroendocrine score for each sample. FPKM values are included in Supplementary Table 7. Heat maps were generated by calculating the *z* score using log-transformed FPKM values. To calculate the *z* score, a log-transformed FPKM value was subtracted from the mean and then divided by the s.d. The genes were then sorted for the log_2-transformed fold change of treatment versus control samples. *z*-score values are provided in Supplementary Tables 4 and 7. For HALLMARK pathway enrichment analysis, differentially expressed genes were tested if over-represented against the HALLMARK pathways from the MSigDB using R packages msigdbr (v.7.5.1) and clusterProfiler (v.4.8.3). List of differentially expressed genes are included in Supplementary Tables 4 and 7.

PDX studies

PDXs were generated from either tumour biopsies or pleural effusions of patients with SCLC. All patient samples were collected after obtaining written informed consent. PDX tumour DFCI-393 originated from a surgical biopsy at resistance from a patient who received previous

chemotherapy and radiation. The surgical biopsy of DFCI-393 was directly implanted directly into the subrenal capsule of NSG mice for expansion. DFCI oncopanel genomic DNA sequencing of DFCI-393 showed an *RB1* E280* mutation with a single-copy deletion of *RB1* at 13q14.2, and a *TP53* K132N mutation with single-copy deletion of *TP53* at 17p13.1 together showing biallelic inactivation of *RB1* and *TP53*. DFCI-402 was derived from pleural effusion of a patient who was treated with first-line carboplatin/etoposide and then second-line nivolumab and the pleural effusion was removed as part of routine clinical care. The pleural fluid from the effusion was immune depleted and implanted subcutaneously to make DFCI-402. DFCI oncopanel genomic DNA sequencing of DFCI-402 showed an RB1 R358* mutation with copy loss of 13 probably contributing to biallelic loss of *RB1*. It also showed a *TP53* G154Afs*16 mutation. RNA-sequencing of DFCI-393 and DFCI-402 with confirmation by immunoblot analysis showed that both PDX models are neuroendocrine-high SCLCs and DFCI-393 dominantly expresses ASCL1 while DFCI-402 expresses both ASCL1 and NEUROD1. RNA-seq data are included in Supplementary Table 7.

PDX model generation

Studies and procedures were performed at Dana Farber Institute in accordance with Institutional Animal Care and Use Committee (IACUC) guidelines in an AAALAC accredited vivarium. PDX models were generated using 7- to 8-week-old female NSG (*NOD.Cg-Prkdcscid Il2rgtm1Wjl/SzJ*) mice purchased from Jackson Laboratories. After initial implantation of patient samples, all PDX tumours were expanded and passaged continuously in NSG mice as subcutaneous tumours.

In vivo efficacy and PD studies in SCLC PDX models with the orally dosed cyclin A/B RxL inhibitor CIRc-014

Female NSG mice (aged 7–8 weeks) were used for all in vivo studies. PDX tumour fragments were dipped in Matrigel and implanted subcutaneously in NSG mice. Tumour growth was measured twice weekly when palpable. Once tumour volumes reached approximately 200 ± 50 mm^3, mice were randomized using Studylog software into the treatment groups as: vehicle (30% PEG400, 20% Solutol HS15, 50% Phosal 53 MCT) or orally bioavailable cyclin A/B RxL inhibitor CIRc-014 (100 mg per kg, Circle Pharma). For the DFCI-393 model, CIRc-014 was administered orally three times a day for 28 days continuously and, for the DFCI-402 model, it was administered orally twice a day for 28 days continuously. For the DFCI-393 model, tumour samples were collected on day 28 after 8 h and for DFCI-402, tumours were monitored for regrowth after treatment withdrawal. Animals were euthanized if the tumour was necrotic/ulcerated or if the tumour volume exceeded 2,000 mm^3. For the PD study in DFCI-393, mice bearing PDX tumours were treated with either vehicle or CIRc-014 (100 mg per kg orally three times per day) for 4 days. All tumour samples were collected 8 h after the morning dose on the last day of treatment. Tumour samples were fixed and snap-frozen for further downstream IHC analysis (see below). For DFCI-393 and DFCI-402 PDX studies, the investigator was not blinded but was agnostic to the outcome of the study. Animal-use protocols specified that animals with tumour volumes larger than 2,000 or experiencing >15% body weight loss or other severe clinical signs of deterioration would be euthanized, and these endpoint criteria were not exceeded for any mice on study without prompt euthanasia.

Pharmacokinetic plasma analysis with the cyclin A/B RxL inhibitor CIRc-014 in the DFCI-393 SCLC PDX model

For the pharmacokinetic studies with the orally bioavailable cyclin A/B RxL inhibitor CIRc-014, DFCI-393 PDX-tumour-bearing NSG mice were used from the PD study above. After 4 days of CIRc-014 being dosed at 100 mg per kg orally three times per day, plasma timepoint sampling was conducted after the last dose in the CIRc-014 treatment group ($n = 6$). Animals 1–3 were bled at 0.5 and 2 h and animals 4–6 at 1 and 4 h followed by terminal bleed through cardiac puncture at 8 h. Blood was collected in K2EDTA tubes, centrifuged and plasma was collected, frozen and sent for analysis. The concentration of CIRc-014 was quantified in the mouse plasma samples using LC–MS/MS at Charles River Laboratories. CIRc-014 was used as a reference standard and glyburide (Sigma-Aldrich) was used as the internal standard. Blank matrix CD-1 mouse plasma, pooled/mixed gender with K_2EDTA anticoagulant (BioIVT) was used to prepare calibration standards and quality-control samples.

Sample extraction was performed on ice. A 10 µl aliquot of sample (calibration standards, quality control samples, blanks and study samples) was added to a 96-well plate. Then, 60 µl of internal standard solution (100 ng ml^{-1} glyburide in acetonitrile) was added to each well, except for wells designated for matrix blanks to which 60 µl of acetonitrile was added. The samples were covered, vortexed and centrifuged for 5 min. Then, 50 µl of supernatant was transferred to a new 96-well plate and the samples were diluted with 50 µl of MilliQ water before analysis. A Waters Acquity UPLC BEH C18, 50 × 2.1 mm (1.7 µm) column was used and maintained at 50 °C during analysis. 5% acetonitrile/water with 0.1% formic acid was used as mobile phase A and 5% acetonitrile/methanol with 0.1% formic acid was used as mobile phase B. The chromatography condition with flow rate at 0.8 ml min^{-1} was started with 60% B, ramped to 90% B in 1 min and further increased to 95% B in 0.05 min and held for 0.25 min and the column was re-equilibrated at the initial conditions for 0.4 min. Analyte and internal standard were detected using an Applied Biosystems Sciex API 6500 triple quadrupole mass spectrometer. The instrument was equipped with an electrospray ionization source (550 °C) operated in the positive-ion mode. The analyte and internal standard were monitored in the multiple-reaction-monitoring (MRM) scan mode. The selected $[M+H]^+$ precursor ions were m/z 962.4 for CIRc-014, and 494.1 for glyburide, and the product ions monitored were at m/z 423.4 and 169.0 for CIRc-014 and glyburide, respectively. Linear fitting with $1/x^2$ weighting for a calibration range from 1.00 to 10,000 ng ml^{-1} was used for data analysis. Analytical results for all samples met acceptance criteria.

Pharmacokinetic plasma analysis with the i.v. dosed cyclin A/B RxL inhibitor CIRc-028 in NCI-H69 and NCI-H1048 SCLC xenografts

For the pharmacokinetic studies with the i.v. dosed cyclin A/Bi CIRc-028, NCI-H69- and NCI-H1048-tumour bearing Nude mice were used from the cell line xenograft efficacy studies described above. After 14 days of dosing with CIRc-028 at 100 mg per kg i.v. once per day, plasma timepoint sampling was conducted after the last dose in the CIRc-028 groups. For the NCI-H69 study, animals 1–5 were bled at 5 min followed by terminal bleed by cardiac puncture at 4 h, and animals 6–10 were bled at 0.5 and 2 h followed by terminal bleed by cardiac puncture at 18 h. For the NCI-H1048 study, animals 1–8 were bled at 5 min and at 0.25, 0.5, 1, 2, 4 and 8 h followed by terminal bleed by cardiac puncture at 24 h. Blood was collected in K2EDTA tubes, centrifuged and plasma was collected, frozen and sent for analysis.

For the NCI-H69 study, the concentration of CIRc-028 was quantified in the mouse plasma samples by LC–MS/MS at Integrated Analytical Solutions. CIRc-028 was used as a reference standard and dextromethorphan (Sigma-Aldrich) was used as the internal standard. Blank matrix mouse plasma, with K2EDTA anticoagulant (Bioreclamation) was used to prepare the calibration standards and quality-control samples. Sample extraction was performed on ice. A 20 µl aliquot of sample (calibration standards, quality control samples, blanks and study samples) was added to 2 volumes of cold internal standard solution except samples designated for matrix blanks to which 40 µl of acetonitrile was added. The samples were covered, vortexed and centrifuged for 30 min at 6,100*g*. An aliquot of each supernatant was transferred to an autosampler plate and diluted with 2 volumes of 0.2% formic acid in water before analysis. A Waters Acquity UPLC BEH C18, 50 × 2.1 mm (1.7 µm) column or equivalent was used and maintained at room temperature

during analysis. Water with 0.2% formic acid was used as mobile phase A and acetonitrile with 0.2% formic acid was used as mobile phase B. The chromatography condition with a flow rate at 1.2 ml min^{-1} was started with 5% B, ramped to 95% B in 1.5 min and held for 0.2 min at 95% B with a flow rate of 0.8 ml min^{-1} and the column was re-equilibrated at initial conditions for 0.5 min. The analyte and internal standard were detected using an Applied Biosystems Sciex API 4000 triple quadrupole mass spectrometer. The instrument was equipped with an electrospray ionization source operated in the positive-ion mode. The analyte and internal standard were monitored in the MRM scan mode. The selected $[M+H]^+$ precursor ions were *m/z* 976.4 for CIRc-028, and 272.2 for dextromethorphan, and the product ions monitored were at *m/z* 596.0 and 215.2 for CIRc-028 and dextromethorphan, respectively. Power fit regression with no weighting for a calibration range from 25 to 50,000 ng ml^{-1} was used for data analysis. Analytical results for all samples met acceptance criteria.

For the NCI-H1048 study, the concentration of CIRc-028 was quantified in the mouse plasma samples by LC–MS/MS at Pharmaron Laboratories. CIRc-028 was used as a reference standard. Blank BALB/c nude mice matrix mouse plasma with K2EDTA anticoagulant was used to prepare calibration standards and quality-control samples. Sample extraction was performed on ice. A 10 µl aliquot of sample (calibration standards, quality control samples, blanks and study samples) was added to 200 volumes of cold internal standard solution in acetonitrile except samples designated for matrix blanks to which 200 µl of acetonitrile was added. The samples were covered, vortexed and centrifuged for 15 min at 4,000 rpm. An aliquot of each supernatant was transferred to an autosampler plate and diluted with 2 volumes of with water before analysis. A phenomenex Halo ES-CN 2.7 µ (30 × 3 mm) column or equivalent was used for analysis. 95:5 water:acetonitrile with 0.1% formic acid was used as mobile phase A and 95:5 acetonitrile:water with 0.1% formic acid was used as mobile phase B. The chromatography condition with flow rate at 0.6 ml min^{-1} was started with 10% B, ramped to 100% B in 1.7 min and held for 0.3 min at 95% B and the column was re-equilibrated at initial conditions for 0.4 min. The analyte and internal standard were detected using an Shimadzu LCMS-8050 quadrupole mass spectrometer. The instrument was equipped with an electrospray ionization source operated in the positive-ion mode. The analyte and internal standard were monitored in the MRM scan mode. The selected $[M+H]^+$ precursor ion was *m/z* 976.4 and the product ion monitored was *m/z* 596.35 for CIRc-028. An appropriate internal standard was used. An appropriate linear fit was used for calibration range from 0.5 to 2,000 ng ml^{-1} was used for data analysis. Analytical results for all samples met acceptance criteria.

IHC staining

IHC staining was performed with a Bond RX Autostainer (Leica Biosystems) using a Polymer Refine Detection kit (Leica Biosystems). Sections (thickness, 4 µm) were serially cut from formalin-fixed paraffin-embedded mouse tumour samples to perform single IHC studies using antibodies recognizing p-KNL1 (1:100, rabbit monoclonal antibody, Cell Signaling, 40758), and cleaved caspase-3 (1:400, rabbit monoclonal antibody, Cell Signaling, 9664). The immunostained slides were scanned at (×40) using the PhenoImager HT instrument (Akoya Biosciences). For each slide, tumour areas were identified by a pathologist (Y.N.L.) and manually annotated using the HALO system. The number of positive and negative tumour cells was then determined using the HALO platform multiplex-IHC v.3.2.5 algorithm (Indica laboratory) and the percentage of positive tumour cells was subsequently calculated.

Statistical analysis

For the CRISPR–Cas9 screen in Fig. 2, the data were analysed using the Apron, STARS and Hypergeometric analysis algorithms on the GPP portal (https://portals.broadinstitute.org/gpp/screener/). Genes were considered hits if $q < 0.25$, using the STARS analysis.

For all experiments with statistical data, the number of independent biological replicates is indicated in each figure legend. For immunoblots shown in Figs. 2i,k,n,o, 3i–k, 4b,e,g,j,k and 5d and Extended Data Figs. 2k, 5h,j, 6f–h,l, 7a, 8g,i, 9f,g and 10b–e,g,i,k, at least three biological replicates were performed and representative immunoblots are shown. For immunoblots shown in Figs. 3h and 4c and Extended Data Figs. 8h,u, 9d,e,h–k and 10f, at least two biological replicates were performed and representative immunoblots are shown. Raw immunoblots are included in Supplementary Fig. 1, and quantification of immunoblots is included in Supplementary Tables 8 and 9. For dose–response assays in Figs. 1f, 2d–g,l and 4f, h, i and Extended Data Figs. 2d,f, 4a–h, 5k and 8a,c,e, the mean of three independent biological replicates is shown unless otherwise specified. For dose–response assays shown in Fig. 2p and Extended Data Fig. 8j–t, the representative mean of two technical replicates is shown and each experiment was performed in three biological replicates. For dose–response assay shown in Extended Data Fig. 8v–x, the representative mean of two technical replicates is shown and each experiment was performed in two biological replicates. For the live-cell imaging experiment in Extended Data Fig. 6a, representative micrographs are shown from two biological replicates and, for Extended Data Fig. 2l, average data are shown of six technical replicate wells per treatment given, performed in two biological replicates. For the immunofluorescence experiment in Extended Data Figs. 6c and 10a, representative micrographs are shown from three biological replicates. For the IHC experiments in Fig. 5c,d,k,l, representative micrographs are shown from at least five independent tumours per treatment group and the data are quantified in Fig. 5e,f,m,n.

For in vivo xenograft experiments in Fig. 5a,b,i,j, two-way ANOVA was used to compare drug treatment versus vehicle. For all other experiments, statistical significance was calculated using unpaired two-tailed Students *t*-tests. *P* values were considered to be statistically significant if $P < 0.05$. Error bars represent s.d. unless otherwise indicated. No statistical methods were used to pre-determine sample sizes, but sample sizes are similar to those used previously for in vivo experiments.

Reporting summary

Further information on research design is available in the Nature Portfolio Reporting Summary linked to this article.

Data availability

Data from the genome-wide CRISPR–Cas9 resistance screen with the cyclin A/B RxL inhibitor, the cyclin A/B/E RxL Inhibitor or the CDK2 Inhibitor are included in Supplementary Table 3. The RNA-seq experiments of NCI-H1048 cells treated with cyclin A/B RxL inhibitors or the CDK2i are included in Supplementary Table 4. Data from the CRISPR–Cas9 base-editor screens with the cyclin A/B RxL inhibitor in Fig. 3 are included in Supplementary Table 5. Data from the mass spectrometry analysis of the cyclin B1 CIRc-004-dependent interactome in Fig. 3 are included in Supplementary Table 6. FPKM values from the bulk RNA-seq experiments of SCLC PDX models DFCI-393 and DFCI-402 are included in Supplementary Table 7. The RNA-seq experiments of DFCI-393 PDXs treated with cyclin A/B RxL inhibitors are included in Supplementary Table 7. The raw RNA-seq data have been deposited at the Gene Expression Omnibus (GEO) under accession GSE291451. The mass spectrometry proteomics data have been deposited to the ProteomeXchange Consortium via the PRIDE partner repository[84] under dataset identifier PXD055112. Any other data and materials can be requested from the corresponding author on reasonable request. Source data are provided with this paper.

Code availability

Custom code was not used in this study.

67. Bockus, A. T. et al. Going out on a limb: delineating the effects of beta-branching, *N*-methylation, and side chain size on the passive permeability, solubility, and flexibility of sanguinamide A analogues. *J. Med. Chem.* **58**, 7409–7418 (2015).
68. Leung, S. S., Mijalkovic, J., Borrelli, K. & Jacobson, M. P. Testing physical models of passive membrane permeation. *J. Chem. Inf. Model.* **52**, 1621–1636 (2012).
69. Rezai, T. et al. Conformational flexibility, internal hydrogen bonding, and passive membrane permeability: successful in silico prediction of the relative permeabilities of cyclic peptides. *J. Am. Chem. Soc.* **128**, 14073–14080 (2006).
70. Rezai, T., Yu, B., Millhauser, G. L., Jacobson, M. P. & Lokey, R. S. Testing the conformational hypothesis of passive membrane permeability using synthetic cyclic peptide diastereomers. *J. Am. Chem. Soc.* **128**, 2510–2511 (2006).
71. Nielsen, D. S. et al. Orally absorbed cyclic peptides. *Chem. Rev.* **117**, 8094–8128 (2017).
72. White, T. R. et al. On-resin *N*-methylation of cyclic peptides for discovery of orally bioavailable scaffolds. *Nat. Chem. Biol.* **7**, 810–817 (2011).
73. Bockus, A. T. et al. Probing the physicochemical boundaries of cell permeability and oral bioavailability in lipophilic macrocycles inspired by natural products. *J. Med. Chem.* **58**, 4581–4589 (2015).
74. Leung, S. S., Sindhikara, D. & Jacobson, M. P. Simple predictive models of passive membrane permeability incorporating size-dependent membrane-water partition. *J. Chem. Inf. Model.* **56**, 924–929 (2016).
75. Andrews, M. J. et al. Design, synthesis, biological activity and structural analysis of cyclic peptide inhibitors targeting the substrate recruitment site of cyclin-dependent kinase complexes. *Org. Biomol. Chem.* **2**, 2735–2741 (2004).
76. Mirdita, M. et al. ColabFold: making protein folding accessible to all. *Nat. Methods* **19**, 679–682 (2022).
77. Meng, E. C. et al. UCSF ChimeraX: tools for structure building and analysis. *Protein Sci.* **32**, e4792 (2023).
78. Ross, G. A. et al. The maximal and current accuracy of rigorous protein-ligand binding free energy calculations. *Commun. Chem.* **6**, 222 (2023).
79. Abel, R., Wang, L., Harder, E. D., Berne, B. J. & Friesner, R. A. Advancing drug discovery through enhanced free energy calculations. *Acc. Chem. Res.* **50**, 1625–1632 (2017).
80. Hong, D. et al. Plasticity in the absence of NOTCH uncovers a RUNX2-dependent pathway in small cell lung cancer. *Cancer Res.* **82**, 248–263 (2021).
81. Muntel, J. et al. Comparison of protein quantification in a complex background by DIA and TMT workflows with fixed instrument time. *J. Proteome Res.* **18**, 1340–1351 (2019).
82. O'Brien, D. P. et al. Structural premise of selective deubiquitinase USP30 inhibition by small-molecule benzosulfonamides. *Mol. Cell. Proteom.* **22**, 100609 (2023).
83. Demichev, V., Messner, C. B., Vernardis, S. I., Lilley, K. S. & Ralser, M. DIA-NN: neural networks and interference correction enable deep proteome coverage in high throughput. *Nat. Methods* **17**, 41–44 (2020).
84. Perez-Riverol, Y. et al. The PRIDE database and related tools and resources in 2019: improving support for quantification data. *Nucleic Acids Res.* **47**, D442–D450 (2019).

Acknowledgements We thank W. G. Kaelin Jr for discussions and feedback; N. Barrows for technical assistance; and A. Ashworth, B. Stillman and J. Pines for their advice. This work was supported by an SRA from Circle Pharma (M.G.O. and D.N.), a William Raveis Charitable Fund Damon Runyon Clinical Investigator Award (CI-101-19; M.G.O.), the Kaplan Family Fund (M.G.O.) and the Deborah A. Connolly Small Cell Lung Cancer Research Fund (M.G.O.). D.N. is a UT Presidential Scholar and holds the Joseph F. Sambrook, PhD, Distinguished Chair in Biomedical Science. D.N. is supported by the Welch Foundation I-1879 and V-I-0002-20230731, and the Program in Molecular Medicine supported by an anonymous donor.

Author contributions S. Singh and C.E.G. contributed to conceptualization, methodology, validation, formal analysis, investigation, data curation and writing of manuscript. Y.T.D. conducted the CRISPR knockout screen, and S. Singh carried out all associated experiments. S. Singh. also performed the CRISPR base-editor screen and all related experiments, including live-cell imaging, dose–response assays, cloning, flow cytometry, immunoprecipitations, immunofluorescence, RNA-seq and analysis of tumour samples. L.-F.L. performed the Cancer Hallmark Pathway analysis. Y.N.L., V.S. and S. Signoretti. performed the immunohistochemistry analysis of the tumour sections. A. Sarkar and A. Spektor assisted with the live-cell imaging experiment. M.F., V.K., S.X. and D.N. conceptualized and performed the forward genetic screen in iHCT-116 cells. C.E.G., R.O., I.V., R.F. and B.K. supervised, performed and analysed the immunoprecipitation–mass spectrometry experiment. S.S.F.L. performed the modelling studies. F.H.-I., D. He, M.W.M., M.N., N.N.G., B.F.-W., L.H., M.P.B., B.M.L., J.F.L., D. Hoang, Y.G., M.C., M.K.D., S.M., C.B., J.A.S., K.Y. and N.J.D. assisted with development and characterization of the macrocycles. J.F., R.B. and P.C. performed the pharmacokinetic development/characterization of the macrocycles. B.L. supervised the SCLC cell line xenograft studies. K.N., B.T. and P.C.G. performed and supervised the in vivo efficacy and pharmacokinetic/pharmacodynamic studies in SCLC PDX models. Y.L. assisted with analysis of bulk RNA-seq. M.-A.L. assisted with the live-cell imaging using FUCCI reporter system. M.A.-R. generated the DOX-on inducible E2F1 cell lines. X.L. performed the AlphaFold analysis. J.G.D. provided methodological support for the CRISPR screens. D.S., A.T.B., P.C., J.B.A., E.W.W., M.E., C.K., R.S. and D.J.E. contributed to resources, visualization, supervision and project administration. D.N. and P.D.G. contributed to conceptualization, methodology, investigation, resources, supervision, project administration, writing and funding acquisition. M.G.O. contributed to conceptualization, methodology, investigation, formal analysis, validation, resources, data curation, visualization, supervision, overall project administration, writing the original and revised manuscript, and funding acquisition.

Competing interests M.G.O. reports grants from Eli Lilly, Takeda, Novartis, BMS, Auron Therapeutics and Circle Pharma. M.G.O. and D.N. received an SRA from Circle Pharma to fund this work. C.E.G., R.O., F.H.-I., D. He, M.W.M., M.N., N.N.G., S.S.F.L., B.F.-W., L.H., M.P.B., B.M.L., D.S., J.F.L., D. Hoang, Y.G., M.C., M.K.D., S.M., C.B., J.A.S., K.Y., N.J.D., A.T.B., J.F., R.B., P.C., J.B.A., L.-F.L., B.L., E.W.W., C.K., M.E., R.S., D.J.E. and P.D.G. are employees of Circle Pharma. The other authors declare no competing interests.

Additional information

Supplementary information The online version contains supplementary material available at https://doi.org/10.1038/s41586-025-09433-w.

Correspondence and requests for materials should be addressed to Matthew G. Oser.

Peer review information *Nature* thanks Christian Heinis and the other, anonymous, reviewer(s) for their contribution to the peer review of this work.

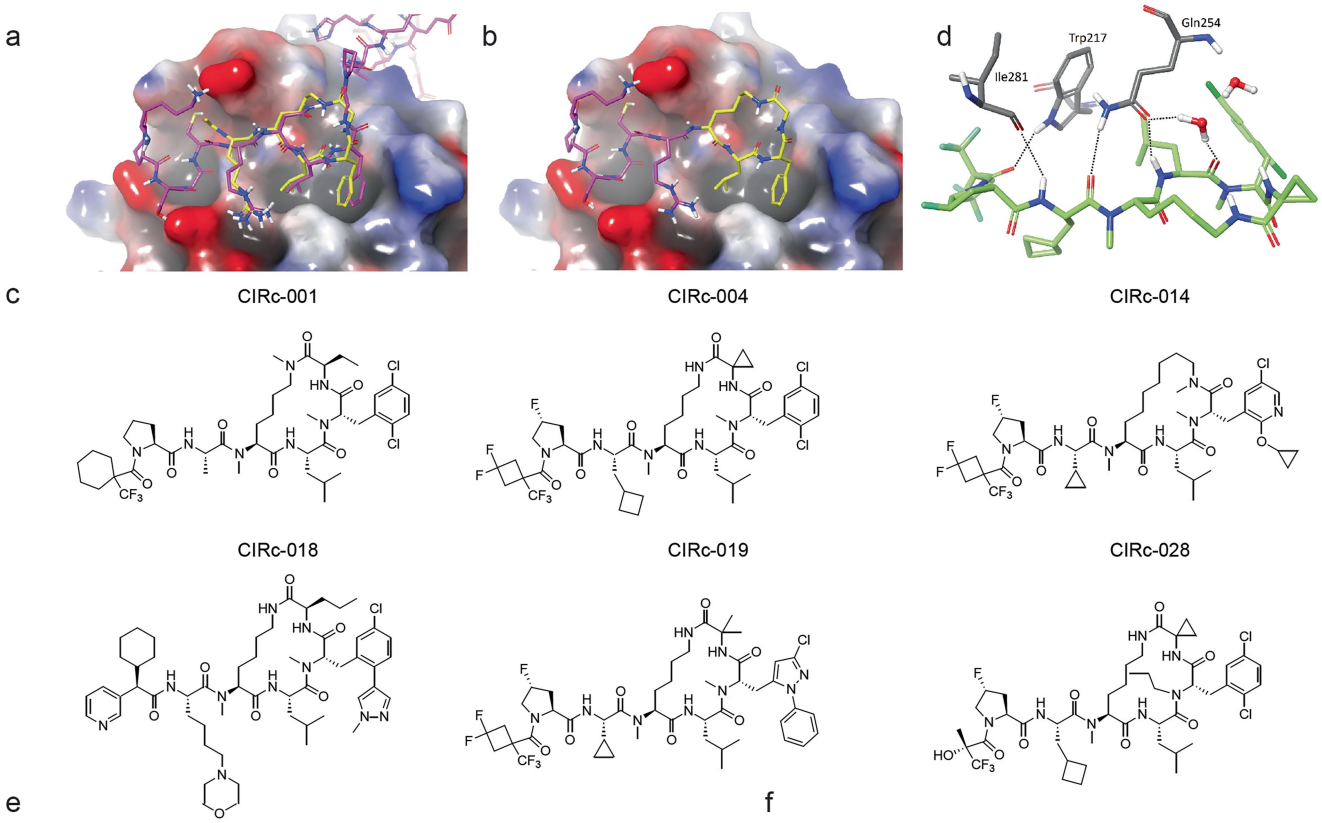

e

Compound	N	Cyclin A / Cdk2			Cyclin B / Cdk1			Cyclin E / Cdk2		
		K_D	k_a	k_d	K_D	k_a	k_d	K_D	k_a	k_d
CIRc-001	n=2	3.3	2.1×10^{5}	6.9×10^{-4}	3.8	3.7×10^{5}	1.3×10^{-3}	35	1.1×10^{5}	3.8×10^{-3}
CIRc-004	n=5	13	1.6×10^{5}	2.1×10^{-3}	2	5.5×10^{5}	1.1×10^{-3}	260	1.7×10^{5}	4.2×10^{-2}
CIRc-014	n=2	2.8	3.4×10^{5}	9.7×10^{-4}	0.97	7.1×10^{5}	6.7×10^{-4}	40	1.7×10^{5}	6.6×10^{-3}
CIRc-018	n=2	3.1	4.6×10^{5}	1.4×10^{-3}	137	4.4×10^{5}	6.0×10^{-2}	96	2.7×10^{5}	2.6×10^{-2}
CIRc-019	n=2	55	2.4×10^{5}	1.3×10^{-2}	8.8	6.3×10^{5}	5.5×10^{-3}	590	2.1×10^{5}	0.12
CIRc-028	n=3	11	1.6×10^{5}	1.7×10^{-3}	1	5.3×10^{5}	5.3×10^{-4}	110	1.3×10^{5}	1.5×10^{-2}

Dissociation constant (KD; in nM), association rate (ka; in M-1sec-1) and dissociation rate (kd; in sec-1)

f

Compound	MW	CLogP	KSOL	LogD	MDCK Papp (A-B)
CIRc-001	930.93	8.72	27.7	3.76	16.2
CIRc-004	994.90	7.19	NA	4.21	0.52
CIRc-014	962.47	7.60	27.3	3.86	13.2
CIRc-018	1029.77	8.14	NA	NA	0.30
CIRc-019	1000.48	5.20	NA	NA	NA
CIRc-028	976.93	9.37	18.6	3.63	0.40

Molecular Weight (MW), calculated water/oil partition (cLogP), kinetic solubility(KSOL), measured distribution coefficient (LogD) and MDCK cell apical to basolateral permeability (MDCK Papp; x10-6 cm/sec).

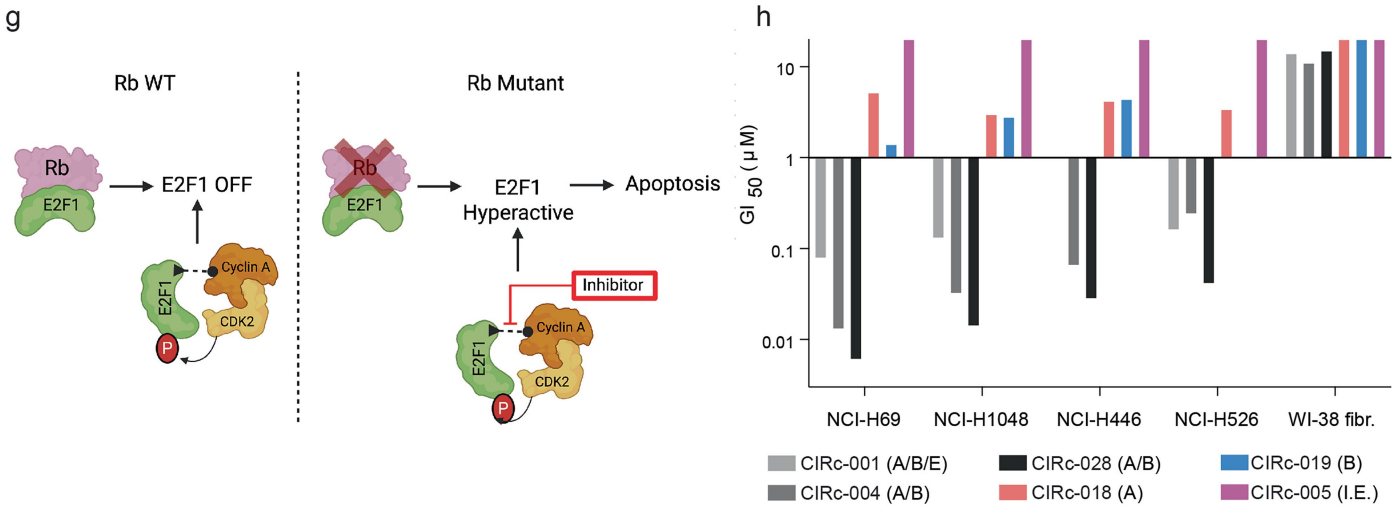

Extended Data Fig. 1 | See next page for caption.

Extended Data Fig. 1 | Discovery of Cyclin RxL Inhibitors. a, Overlay of cyclin A/Cdk2 complexes shown in surface representation with bound ligands at the RxL binding site, including a macrocycle (yellow, PDB: 1URC) and p27Kip1 (purple, PDB: 1JSU). **b**, Computational model of a lariat decapeptide macrocycle bound at the RxL binding site, based on the bound structures of p27Kip1 (purple) and lariat macrocycle (yellow), as a ligand alignment template for binding prediction. **c**, Structures of CIRc-001, CIRc-004, CIRc-014, CIRc-018, CIRc-019 and CIRc-028. Two published cyclin A2 co-crystal structures with ligand bound at the RxL binding site, including the macrocycle, Ace-Arg-Lys-Leu-Phe-Gly (PDB code: 1URC) and the p27Kip1 peptide (PDB code: 1JSU), were used to generate a reference binding mode for our lariat macrocycles (Extended Data Fig. 1a **above**). All modelling studies were performed using the Schrodinger software suite (version 2023-3). The crystal structures were first prepared using the Protein Preparation Workflow with default settings, and the cyclin A/Cdk2 complexes were subsequently aligned by using the protein structure alignment module. The bound ligands, aligned at the RxL binding motif, were combined to produce a template for novel ligand alignment. Specifically, the template model (Extended Data Fig. 1b **above**) is a lariat decapeptide (Lys-Pro-Ser-Ala-Cys-Arg-Lys-Leu-Phe-Gly) that contains the N-terminal hexapeptide segment of p27Kip1 (Lys25-Pro26-Ser27-Ala28-Cys29-Arg30, PDB: 1JSU) and the lariat cyclic pentapeptide (Lys502-Leu503-Phe504-Gly505, PDB: 1URC). To generate binding models of novel peptidic macrocycles, the 3D coordinates were generated by LigPrep and projected onto the template model by performing the maximum common substructure alignment for macrocycles in the ligand alignment module in Maestro (version 13.7.125) with cyclin A crystal structure (PDB: 1URC) specified as the receptor. The aligned ligand was further refined in the binding site by running Glide (ver. 10.0) SP docking with the "refine only" option in a docking grid based on the lariat-bound cyclin A crystal structure (PDB: 1URC). The docking grid was generated using the template model with default parameters. **d**, Detailed representation of modelled hydrogen bonds of CIRc-004 to Ile281, Trp217 and Gln 254 on cyclin A. **e**, Binding kinetic parameters determined in a WaveDelta instrument (Malvern Pananalytical) to Cyclin/Cdk complexes immobilized by amine coupling on a 4PCP chip (Malvern Pananalytical). Dissociation constant (K_D; in nM), association rate (k_a; in $M^{-1}sec^{-1}$) and dissociation rate (k_d; in sec^{-1}). **f**, Compounds physicochemical properties including Molecular Weight (MW), calculated water/oil partition (cLogP), kinetic solubility measured in 5% DMSO at pH 7.4 (mM), measured distribution coefficient between water and octanol (LogD) and MDCK cell apical to basolateral permeability (MDCK Papp; x10-6 cm/sec). **g**, Hypothesized model: In *RB1*-deficient cancers (e.g. SCLC) where E2F1 activity is dysregulated, targeting the cyclin A-E2F1 interaction hyperactivates E2F1, which could selectively impair tumour growth. Figure was created with BioRender. **h**. Waterfall plot of GI50s for four SCLC and the non-transformed WI-38 fibroblast cell lines for compounds listed in Fig. 1b.

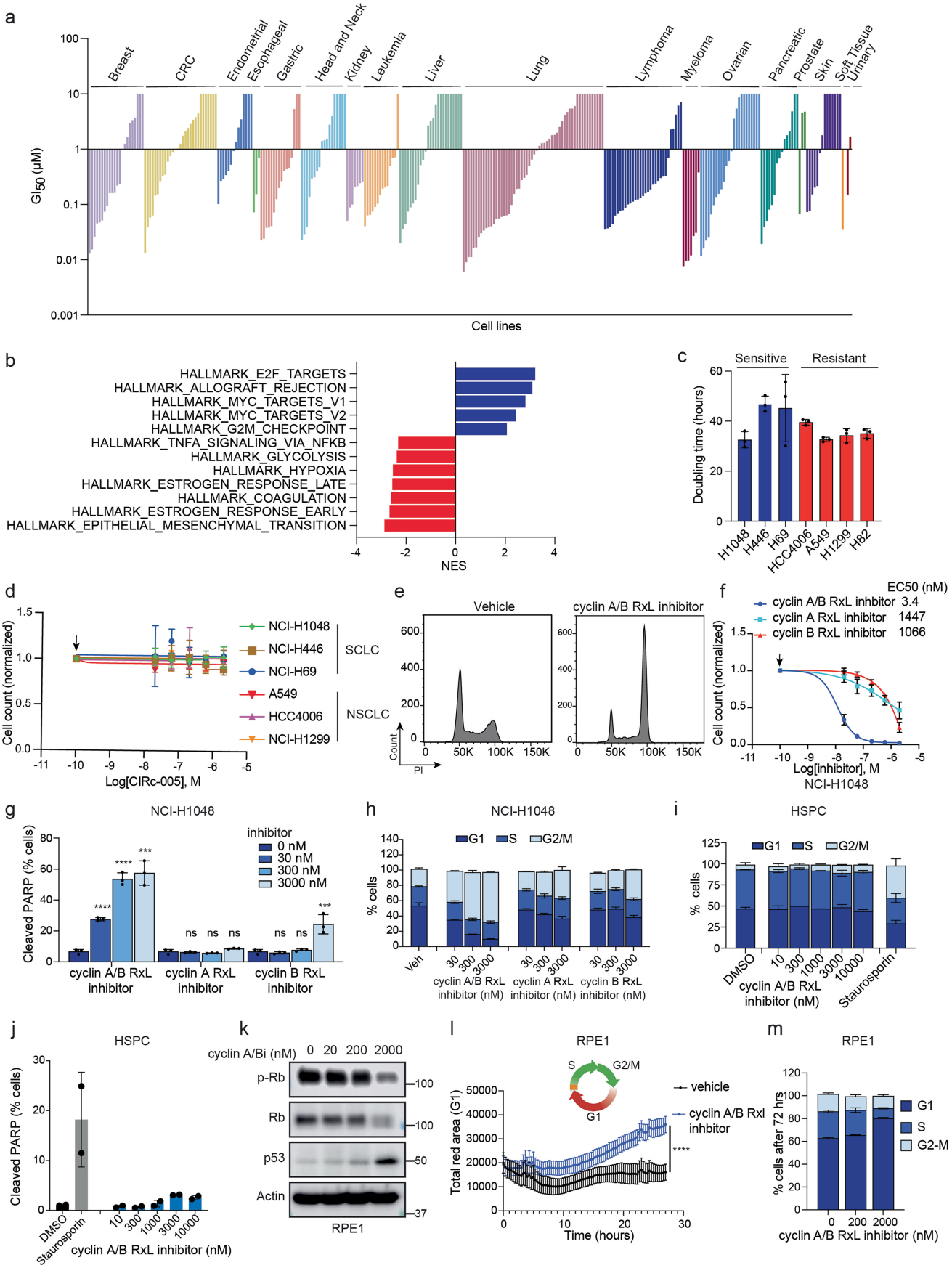

Extended Data Fig. 2 | See next page for caption.

Extended Data Fig. 2 | Cyclin A/B RxL Inhibitors Induce Apoptosis in Cancer Cells with High E2F Activity. a, Anti-proliferation GI_{50} waterfall plot of cyclin RxL A/B/E inhibitor (CIRc-001) tested against Horizon Discovery cancer cell line panel. n = 302 cell lines. **b**, Pathway enrichment scores for the top upregulated and down regulated MSigDb Hallmark gene sets within the differentially expressed genes identified between sensitive and resistant cell lines (n = 288 cell lines) to CIRc-001 using the data in A. Top pathways with FDR corrected <0.05 and Normalized Enrichment Score (NES) >= −/+ 2 are represented as blue (upregulated) or red (downregulated)). **c**, Average doubling time (hours) of sensitive (blue) and insensitive (red) cell lines using the data the DMSO control from Fig. 1f comparing cell counts at the endpoint (Day 6) compared to start (Day 0) of the dose-response assay. **d**, Dose response assays of the indicated human SCLC cell lines and insensitive human NSCLC cell lines treated for 6 days with increasing doses of the inactivate enantiomer of the cyclin A/B RxL inhibitor (CIRc-005). **e**, Representative histograms of flow cytometric analysis of propidium iodide (PI) stained NCI-H1048 cells treated with CIRc-004 (200 nM) or DMSO (vehicle) for 24 h. **f**, Dose response assays of NCI-H1048 cells treated for 6 days with increasing doses of the selective cyclin A RxL inhibitor (CIRc-018), the selective cyclin B RxL inhibitor (CIRc-019), or the cyclin A/B RxL inhibitor (CIRc-004). **g**, Quantitation of cleaved PARP positive cells analysed by flow cytometric analysis in NCI-H1048 cells treated for 3 days with the indicated doses of CIRc-018, CIRc-019, CIRc-004 or DMSO. Statistical significance was calculated using unpaired, two-tailed students t-test. **h**, Representative histograms of cell cycle distribution of NCI-H1048 cells treated with CIRc-018, CIRc-019, CIRc-004 or DMSO and then stained with PI. **i**) Representative histograms of cell cycle distribution of human hematopoietic stem and progenitor cells (HSPC) treated with CIRc-004, staurosporine (100 nM) or DMSO for 24 h. **j**) Quantitation of cleaved PARP positive cells analysed by flow cytometric analysis in HSPCs treated with CIRc-004, staurosporine (100 nM) or DMSO for 24 h. For **i**-**j**, n = 2 biological replicates. **k**, Immunoblot analysis of RPE1 cells treated with indicated concentrations of CIRc-004 for 72 h. **l**, Cell cycle phase progression measured over 27 h by time lapse imaging of RPE1 cells expressing FUCCI cell cycle reporter, treated with a higher concentration of CIRc-004 (2000 nM) which is required to promote cell cycle arrest in RPE1 cells (see Fig. 1f), or DMSO. Graph measures quantification of G1 (red FUCCI signal) cell cycle phase per image at progressive time points. Statistical significance calculated using 2-way ANOVA. n = 6 wells per treatment condition per replicate from 2 biological replicates, 1 representative experiment is shown. **m**, Representative histograms of cell cycle distribution of RPE1 cells treated with CIRc-004 (2000 nM) or DMSO for 72 h and then stained with PI. Data are mean +/− SD of 6 technical replicate wells. For **c**-**h**, **k, m**, n = 3 biological replicates. For **c**, **f**-**g** and **j**, data are mean +/- SD. Arrows in **d, f** indicates DMSO-treated sample which was used for normalization. Where indicated, ***=p < 0.001, ****=p < 0.0001.

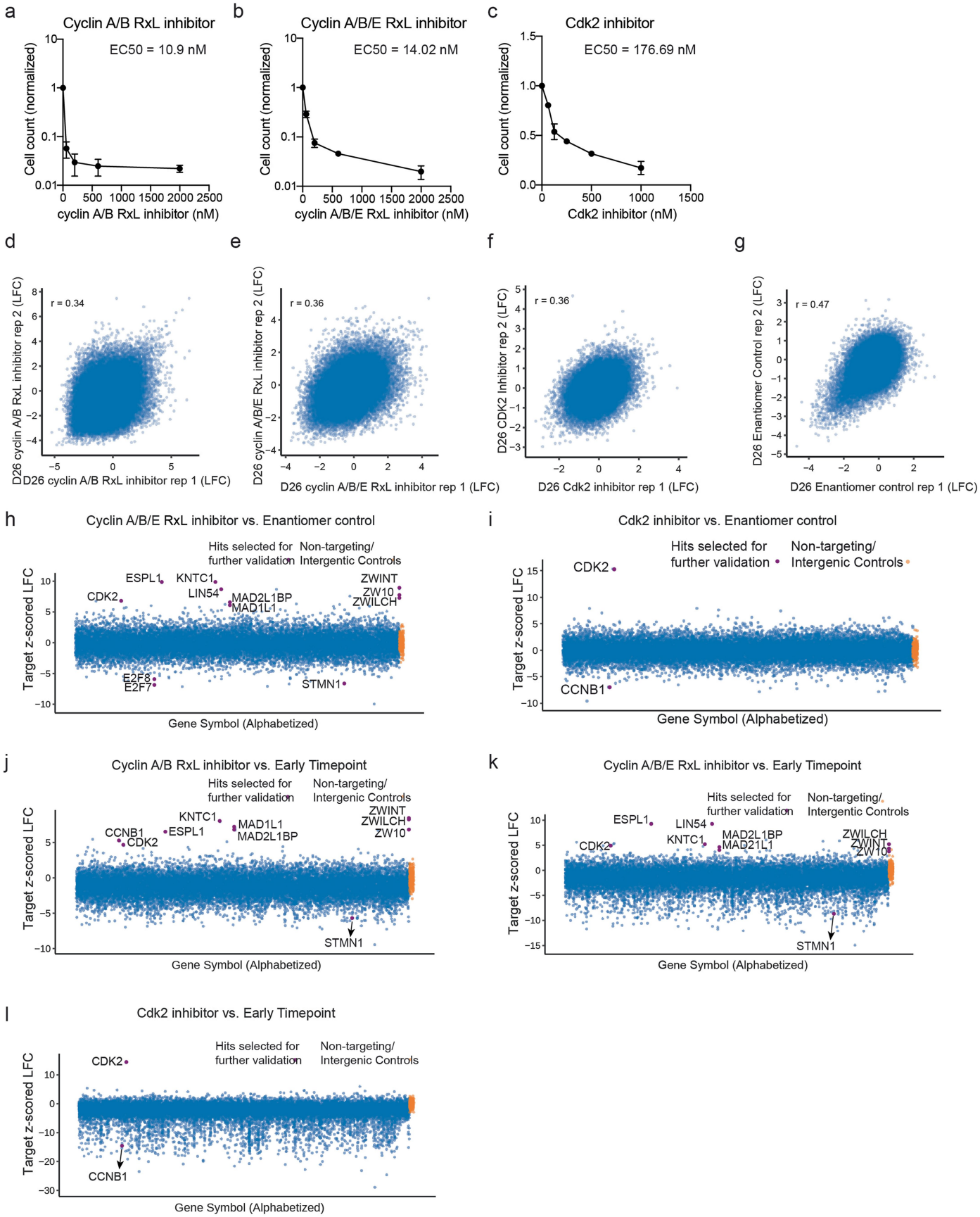

Extended Data Fig. 3 | See next page for caption.

Extended Data Fig. 3 | Genome-wide CRISPR/Cas9 Knockout Screens Identify Genes Necessary for Cyclin A/B RxL Inhibitors to Induce Apoptosis in SCLC Cell Lines. a-c, Dose response assays of NCI-H1048 cells treated with the indicated concentrations of the cyclin A/B RxL inhibitor (CIRc-004) (**a**), the cyclin A/B/E RxL inhibitor (CIRc-001) (**b**), or the orthosteric Cdk2 inhibitor (PF-07104091) (**c**) for 6 days. EC50's are indicated. For **a-b**, $n = 2$. For **c**, $n = 3$ biological replicates. **d-g**, Scatter plot of sgRNA abundance represented as Log Fold Change (LFC) comparing the 2 biological replicates of the CRISPR/Cas9 knockout screen for CIRc-004 (**d**), CIRc-001 (**e**), PF-07104091 (**f**), and CIRc-005 (inactive enantiomer of CIRc-004) (**g**). **h-l**, Top enriched and depleted hits from Apron analysis of CIRc-001 at the late timepoint (LTP) (day 26) relative to CIRc-005 enantiomer negative control at the LTP (day 26) (**h**), PF-07104091 LTP vs. CIRc-005 LTP (**i**), or CIRc-004 LTP vs. early timepoint (ETP) prior to drug treatment (day 10) (**j**), CIRc-001 vs. ETP (**k**), PF-07104091 vs. ETP (**l**). For **d-l**, $n = 2$ biological replicates.

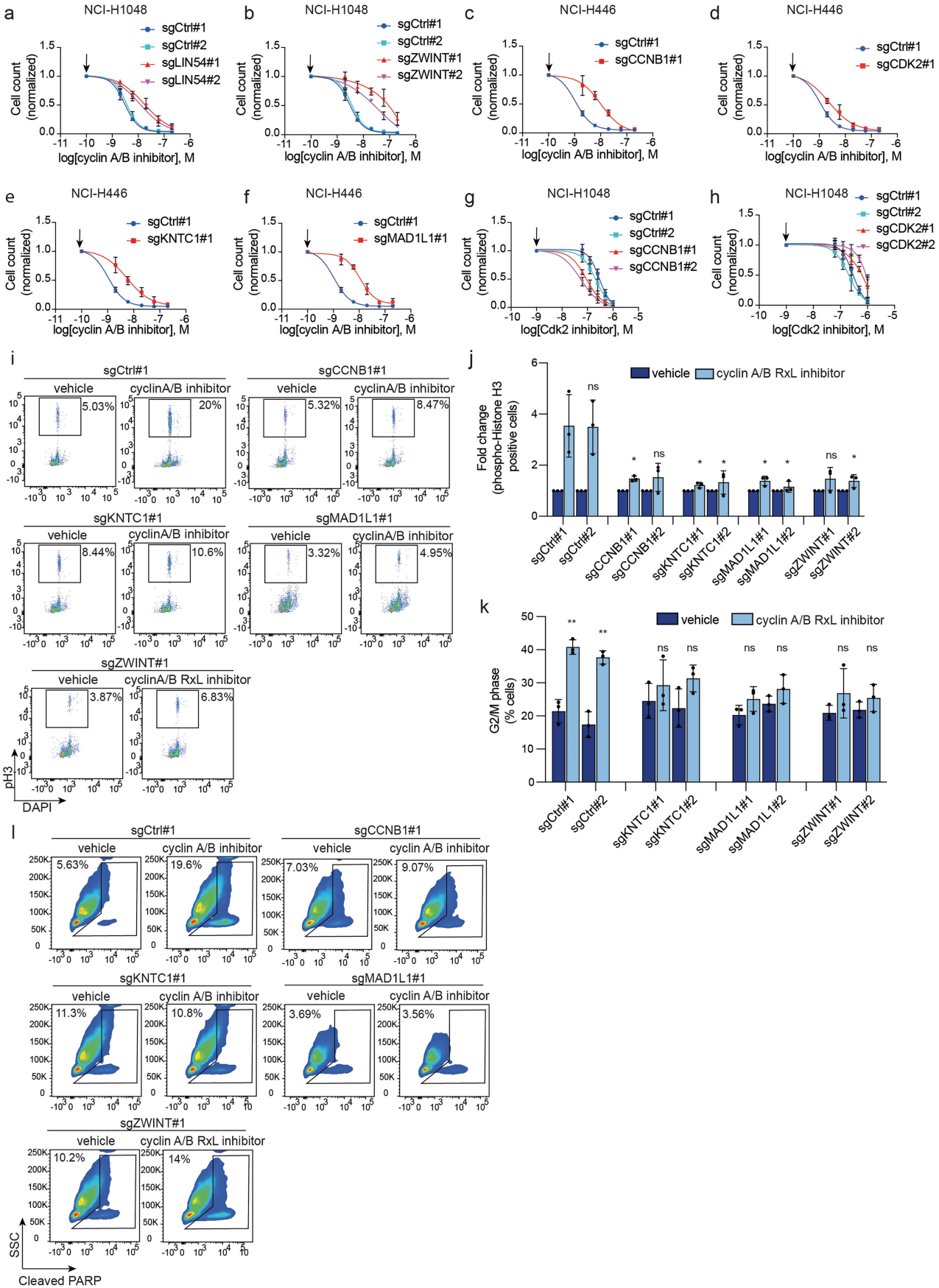

Extended Data Fig. 4 | See next page for caption.

Extended Data Fig. 4 | Validation of Genes that Modulate Response to Cyclin A/B RxL Inhibitors or CDK2 Inhibitors. a-b, Dose response assays of NCI-H1048 cells infected with two independent non-targeting sgRNAs (sgCtrl) or two independent sgRNAs against *LIN54* (**a**) or *ZWINT* (**b**), and treated for 6 days with increasing doses of the cyclin A/B RxL inhibitor (CIRc-004). **c-f**, Dose response assays of NCI-H446 cells infected with sgCtrl or sgRNAs against **C**) *CCNB1* (**c**), *CDK2* (**d**), *KNTC1* (**e**), *MAD1L1* (**f**), treated for 6 days with increasing doses of CIRc-004. **g-h**, Dose response assays of NCI-H1048 cells infected with two non-targeting sgRNAs (sgCtrl) or two independent sgRNAs against *CCNB1* (**g**) or *CDK2* (**h**), and treated for 6 days with increasing doses of the Cdk2 inhibitor (PF-07104091). **i**) Representative flow cytometric analysis of phospho-histone H3 in NCI-H1048 cells infected with the indicated sgRNAs and treated with CIRc-004 at 20 nM or DMSO for 24 h. **j-k**, Quantitation of cells in mitosis by flow cytometry analysis using phospho-histone H3 from **i** (**j**) or PI (**k**) of NCI-H1048 cells transduced with the indicated sgRNAs and then treated with CIRc-004 at 20 nM or DMSO for 24 h. **l**) Representative flow cytometric analysis from Fig. 2h of cleaved PARP in NCI-H1048 cells infected with the indicated sgRNAs and treated with CIRc-004 at 20 nM or DMSO for 3 days. For **i**, data are shown as fold change relative to vehicle. For **a-h, j, k**, $n = 3$ biological replicates and data are mean +/− SD. Arrows in **a-h** indicates DMSO-treated sample used for normalization. Statistical significance in **j, k** was calculated using unpaired, two-tailed students *t*-test. Where indicated, *=$p < 0,05$, **=$p < 0.01$.

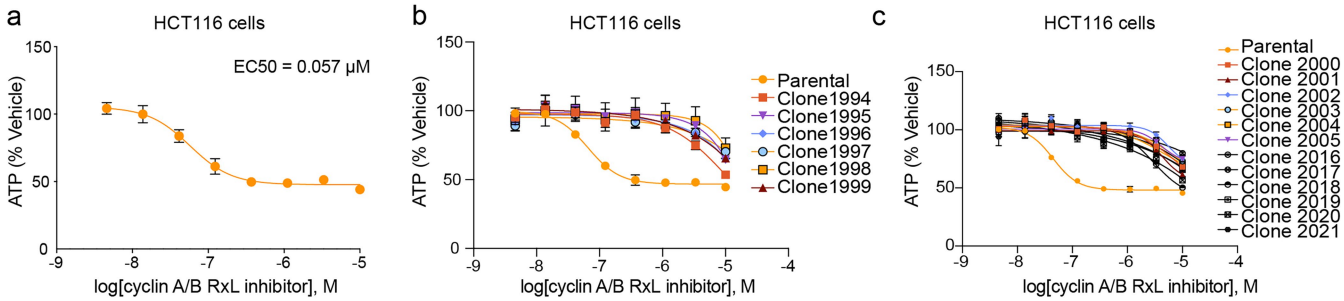

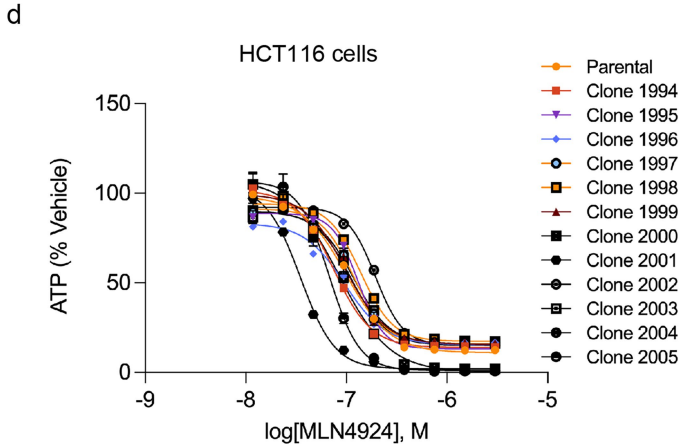

e

Clone #	IAA	Barcode sequence
1994	-	GTGTCTGTCTGAGAGAGTGACACA
1995	-	GAGAGTGTGTGTGTGAGTCTCAGT
1996	-	CAGTCAGTCTCTGTCACAGAGACA
1997	-	CAGTCAGTCTCTGTCACAGAGACA
1998	-	GTGTGTGAGAGTGAGTGTCTGAGT
1999	-	GACACTGACACTCAGTGAGTCAGA
2000	+	CTGACAGTGACTCAGACTGTGAGT
2001	+	GTCTGTGAGTGAGTGTGAGTCACT
2002	+	CTGACAGAGTCTGTGAGACACACT
2003	+	GTGAGTGTGACTGTGAGTCAGTCA
2004	+	GTGTCTGTCTCTCAGTCTCACTCA
2005	+	GACAGTCAGTCAGAGTCTCAGTCT
2016	+	GTGTCTGACACTCAGTCTGAGAGT
2017	+	GTGTGTCTGTCTCTGTGAGTCACT
2018	+	GAGACAGTCACTGAGTGACTGACT
2019	+	CAGTCAGAGACAGACAGTCAGTCT
2020	+	CTGTCACTGAGTCTGTGTGACTGT
2021	+	CAGAGTCAGAGAGTCAGAGAGACA

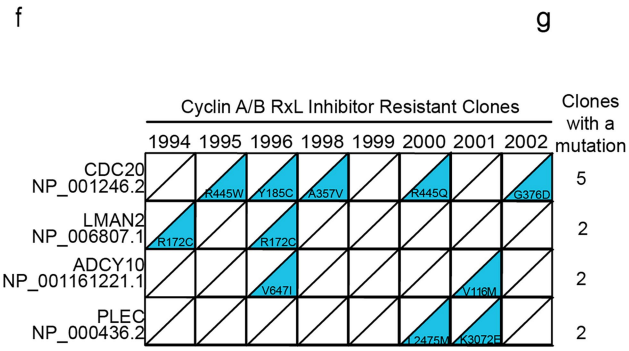

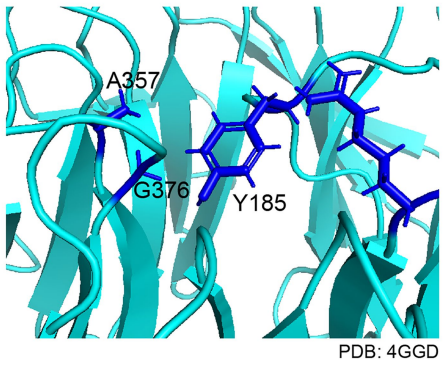

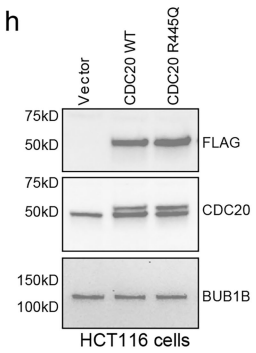

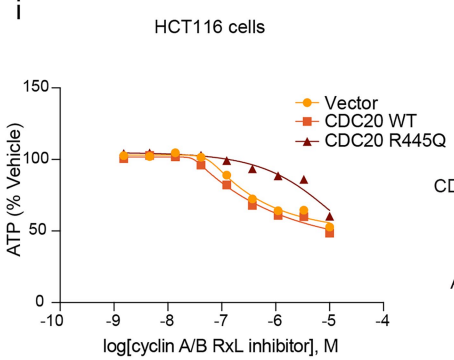

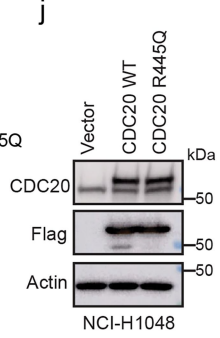

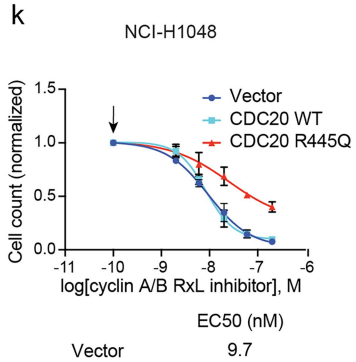

EC50 (nM)

Vector	9.7
CDC20 WT	10.01
CDC20 R445Q	72.6

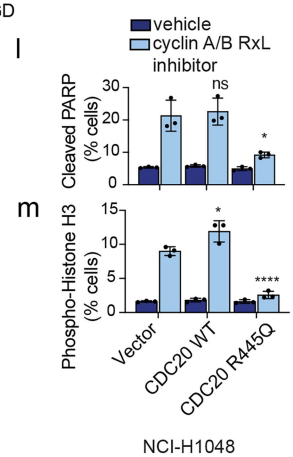

Extended Data Fig. 5 | See next page for caption.

Extended Data Fig. 5 | Forward Genetic Screen Identifies CDC20 Mutants that Cause Resistance to a Cyclin A/B RxL Inhibitor. a, Dose response curve of iHCT116 cells treated with increasing doses of cyclin A/B RxL inhibitor (CIRc-004). **b-c**, Dose-response curves for six clones isolated from Mut-low iHCT116 cells (**b**) and 12 clones from Mut-high iHCT116 cells treated with increasing doses of CIRc-004 for 3 days (**c**). **d**, Dose response curve to MLN4924 of different CIRc-004 resistant iHCT116 clones. For **a-d** *n* = 2 technical replicates. Data are mean +/− SEM. **e**, Barcode sequences identified in 18 different CIRc-004 resistant clones, common sequences are marked in blue. **f**, Genes recurrently mutated (≥2 clones) among eight CIRc-004-resistant iHCT-116 clones from the forward genetic screen. **g**, Mutated residues (blue) in CDC20 (PDB 4GGD) present in CIRc-004 resistant clones. **h**, Immunoblot analysis of iHCT116 cells stably expressing vector, Flag-CDC20 WT, or Flag-CDC20 R445Q mutant. **i**, Dose response assay of iHCT-116 cells from **h** treated with increasing doses of CIRc-004. For **i**, *n* = 3 technical replicates. Data are mean +/− SEM. **j**, Immunoblot analysis of NCI-H1048 cells stably expressing empty vector, Flag-CDC20 WT, or Flag-CDC20 R445Q; Actin run on separate gel as a sample processing control. **k-m**, NCI-H1048 cells from **j** assessed for CIRc-004 dose response (**k**), cleaved PARP (**l**), and phospho-histone H3 (**m**) by flow cytometry following CIRc-004 treatment (20 nM). For **k-m**, *n* = 3 biological replicates; data represent mean ± SD. Statistical significance determined by unpaired, two-tailed Student's t-test. Where indicated, *=p < 0,05, ****=p < 0.0001.

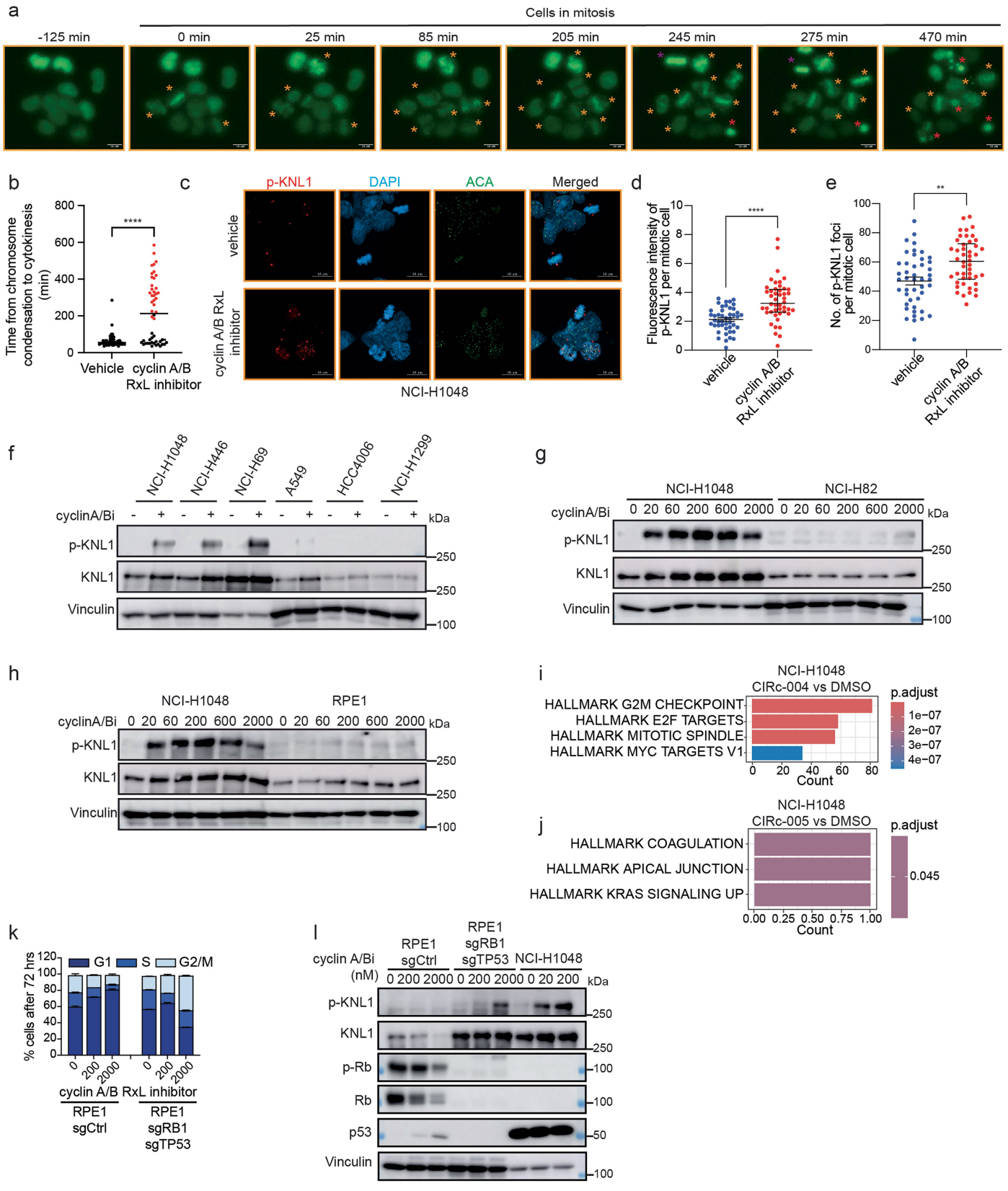

Extended Data Fig. 6 | See next page for caption.

Extended Data Fig. 6 | Cyclin A/B RxL Inhibitors Promote SAC Activation in Sensitive SCLC Cell Lines which Requires Loss of RB1 and TP53.
a, Representative images from time-lapse fluorescent microscopy of NCI-H1048 cells expressing H2B-GFP treated with 20 nM cyclin A/B RxL inhibitor (CIRc-004) over 10 h (yellow star: arrested mitotic nuclei, purple star: normal mitotic nuclei, red star: apoptotic nuclei). Magnification = 20x, scale bar 10 μm. **b**, Dot plot showing time (mins) from chromosome condensation to cytokinesis completion in CIRc-004 vs vehicle treated cells. Cells that failed to complete cytokinesis by experimental end point are shown in red. n = 50 total mitotic nuclei per condition were counted from 2 independent experiments. Statistical significance was calculated using unpaired, two-tailed students *t*-test. **c**, Representative phospho-KNL1, DAPI and anti-centromere antibody (ACA) confocal microscopy images of NCI-H1048 cells treated with cyclin A/B RxL inhibitor (CIRc-004) at 20 nM or DMSO for 24 h. Magnification = 63x, scale bar = 10 μm. **d-e**, Dot plot measuring fluorescence intensity of phospho-KNL1 per mitotic cell (**d**) or number of phospho-KNL1 foci per mitotic cell (**e**) of NCI-H1048 cells from **c** n = 45 mitotic cells from 3 biological replicates. **f**, Immunoblot analysis of the indicated human SCLC cell lines (NCI-H1048, NCI-H446, and NCI-H69) and insensitive human NSCLC cell lines (A549, HCC4006, and NCI-H1299) treated for 24 h with CIRc-004 at 200 nM or DMSO. Note, this immunoblot contains the same lysates from Fig. 2i and is included to ensure that the differences in phospho-KNL1 levels after CIRc-004 treatment between cell lines are not a consequence of being loaded on independent immunoblots. **g-h**, Immunoblot analysis comparing p-KNL1 levels of insensitive NCI-H82 (**g**) and RPE1 (**h**) cell lines after treatment with CIRc-004 for 24 h. NCI-H1048 cells (a sensitive model) are included as a benchmark control. **i-j**, Bar graphs of significantly enriched Hallmark pathways (Padj <0.05) from RNA-seq comparing CIRc-004 vs. DMSO (**i**) and CIRc-005 vs. DMSO (**j**). For**, i, j**, *n* = 2 biological replicates. **k**, Representative histograms of flow cytometric analysis of PI stained RPE1 cells transduced with indicated sgRNAs targeting *RB1 and TP53* (sgRB1, sgTP53) or a non-targeting control (sgCtrl) and then treated with CIRc-004 or DMSO for 72 h. *n* = 3 biological independent experiments. **l**, Immunoblot analysis of indicated RPE1 cells and NCI-H1048 treated with CIRc-004 or DMSO for 72 h. Representative immunoblot from 3 independent experiments is shown. Where indicated, *=p < 0,05, **=p < 0.01, ***=p < 0.001, ****=p < 0.0001.

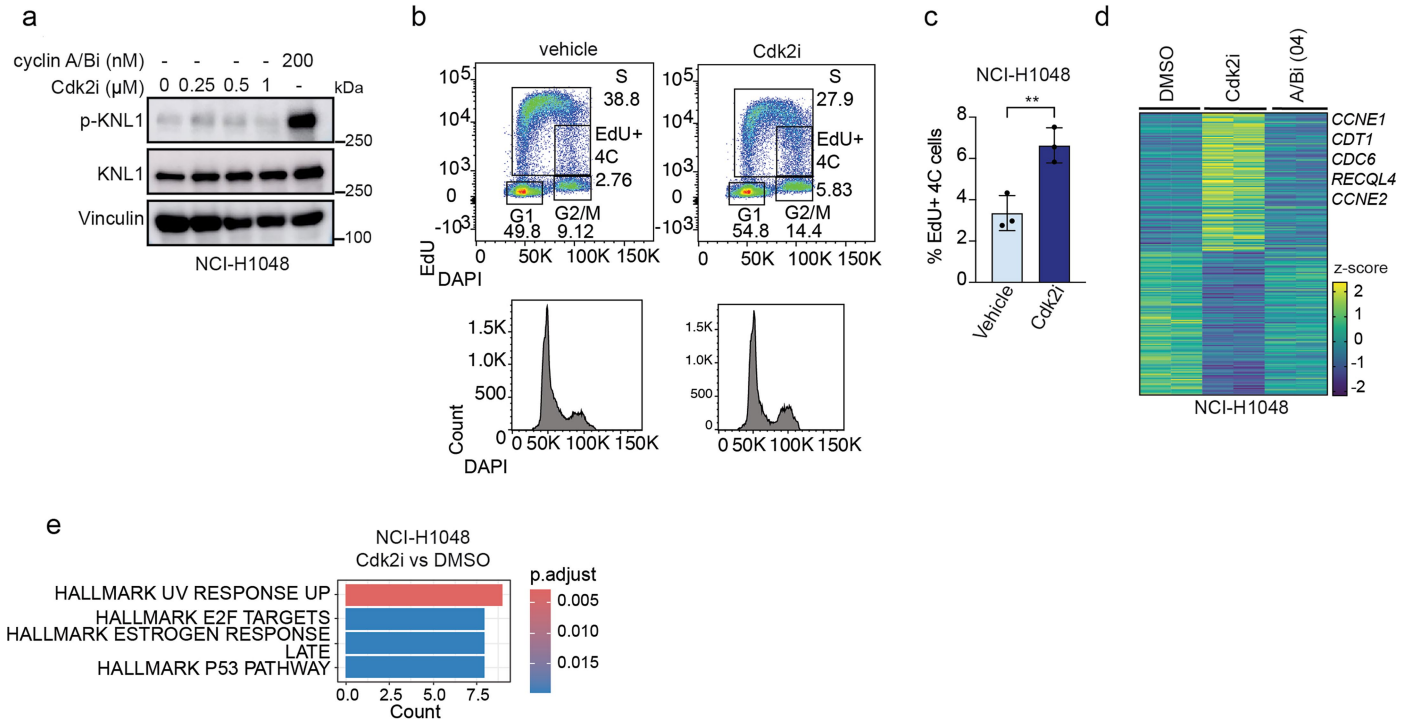

Extended Data Fig. 7 | Cyclin A/B RxL and CDK2 Inhibitors Act via Distinct Mechanisms. a, Immunoblot analysis of NCI-H1048 cells treated with indicated doses of Cdk2 inhibitor (PF-07104091) for 24 h. CIRc-004 (200 nM) is included as a benchmark control. **b**, Representative flow cytometric analysis of EdU and DAPI in NCI-H1048 cells treated with PF-07104091 at 500 nM or DMSO (vehicle) for 24 h. **c**, Quantification of the EdU positive 4c population after drug treatment shown in **b**. Data are mean +/− SD. $n = 3$ biological replicates. Statistical significance calculated using unpaired, two-tailed students *t*-test. **=$p < 0.01$. **d**, Heat map of *z*-scores from RNA-seq data of NCI-H1048 cells treated with the Cdk2 inhibitor (PF-07104091 at 500 nM), cyclin A/B RxL inhibitor (CIRc-004 at 200 nM), or DMSO for 24 h. Data is sorted for Log2FoldChange of Cdk2 inhibitor (replicate 1 and 2) vs. DMSO (replicate 1 and 2) showing genes with padj<0.05 which was 110 top up-regulated and 113 down-regulated genes. $n = 2$ biological replicates. Relevant up-regulated genes are labelled on right. **e**, Bar graphs showing top significantly enriched Hallmark pathways (padj<0.05) calculated using differentially expressed genes from bulk RNA-seq experiment in **d** comparing Cdk2 inhibitor vs. DMSO in NCI-H1048 cells.

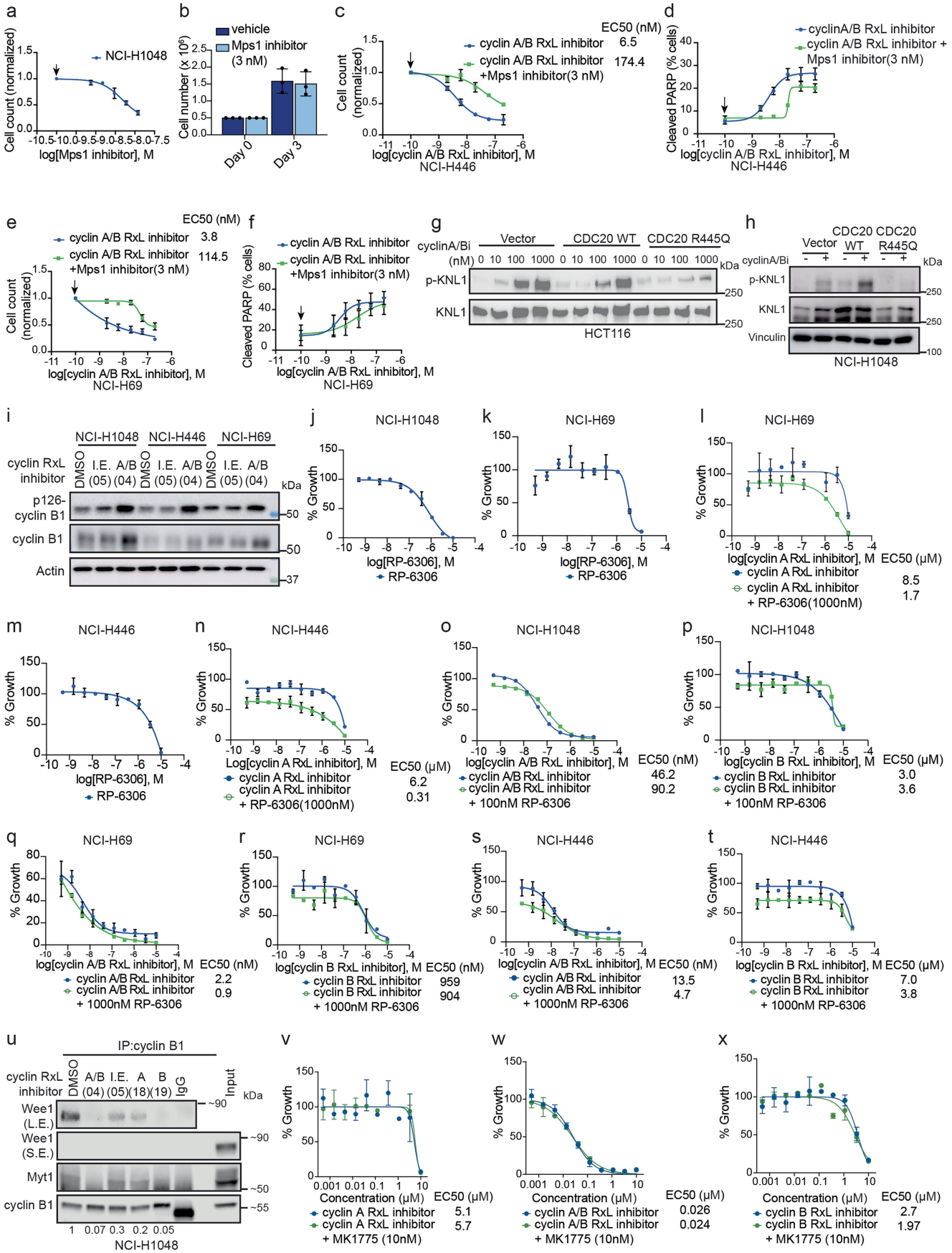

Extended Data Fig. 8 | See next page for caption.

Extended Data Fig. 8 | Mechanisms by which Cyclin A/B RxL Macrocycles Promote SAC Activation. a, Dose response assay of NCI-H1048 cells treated with increasing concentrations (0 nM, 1.5 nM, 3 nM, 6 nM, 12 nM) of the Mps1 inhibitor (BAY-1217389). *n* = 2 biological replicates. Note that 3 nM of BAY-1217389 effectively blocked phosphorylation of the MPS substrate KNL1 (see Fig. 2k) without blocking cellular proliferation and hence 3 nM of BAY-1217389 was used for all rescue experiments. **b**, The raw cell counts of the dose response with BAY-1217389 from **a** showing that NCI-H1048 cells treated with BAY-1217389 at 3 nM proliferated over the 3-day dose response assay similar to the DMSO untreated control. **c**-**f**, Dose response assays of NCI-H446 (**c**) or NCI-H69 (**e**) cells, and non-linear regression curves of cleaved PARP FACS analysis of NCI-H446 (**d**) or NCI-H69 (**f**) cells treated with increasing concentrations of CIRc-004 in presence or absence of the Mps1 inhibitor (BAY-1217389) at 3 nM for 3 days. Data are mean +/− SD. Arrows in **a**, **c**-**f** indicates DMSO-treated sample used for normalization. **g, h**, Immunoblot analysis of HCT116 (**g**) or NCI-H1048 (**h**) cells stably expressing empty vector, Flag-CDC20 WT, or Flag-CDC20 R445Q mutant treated with CIRc-004 with indicated concentrations for 24 h. For **a**-**b, d**-**f**, *n* = 3 biological replicates. For **c**, **h**, *n* = 2 biological replicates. **i**, Immunoblot analysis for cyclin B pS126 in indicated SCLC lines treated with CIRc-004 (300 nM), CIRc-005 (inactive enantiomer, 300 nM), or DMSO for 4 h. n = 3 biological replicates. **j**-**t**, NCI-H1048 (**j,o,p**), NCI-H69 (**k,l,q,r**), or NCI-H446 (**m,n,s,t**) cells treated with RP-6306 (Myt1 inhibitor) alone (**j,k,m**) or in combination with the cyclin A RxL inhibitor (CIRc-018) (**l**, **n**), cyclin A/B RxL inhibitor (CIRc-004) (**o,q,s**), or the cyclin B RxL inhibitor (CIRc-019) (**p,r,t)** for 5 days. For **j**-**t**, data are mean +/− SD of two technical replicates. n = 3 biological replicates. **u**, Immunoblot analysis of Wee1 after cyclin B1 IP in NCI-H1048 cells treated with CIRc-004, inactive enantiomer (I.E., CIRc-005), CIRc-018, CIRc-019, or DMSO. All inhibitors were used at 300 nM for 2 h. *n* = 2 biological independent experiments. **v**-**x**, Dose response assay of NCI-H1048 cells treated with Wee1 inhibitor (MK 1775, 10 nM) in combination with CIRc-018 (**v**), CIRc-004 (**w**), or CIRc-019 (**x**) for 5 days. Data are mean +/− SD of two technical replicates. *n* = 2 biological replicates.

a

Mutation	Pred. Affinity of CIRc-004 (kcal/mol)			Predicted effect on ligand binding
WT	0.0	±	0.40	
Met201Val	0.4	±	0.48	Low
Ala203Thr	-0.6	±	0.52	Low
Ile204Thr	1.0	±	0.48	High
Ile206Val	0.4	±	0.41	Low
Asp207Gly	0.2	±	0.47	Low
Trp208Arg*	9.3	±	0.52	High
Trp208Ala	3.0	±	0.43	High
Gln213Arg	0.0	±	0.46	Low
Met214Val	0.6	±	0.41	Medium
Gln213Arg/Met214Val	0.2	±	0.45	Low
Val227Ala	0.2	±	0.41	Low
Ser228Pro	0.2	±	0.42	Low
Val227Ala/Ser228Pro	0.5	±	0.42	Medium

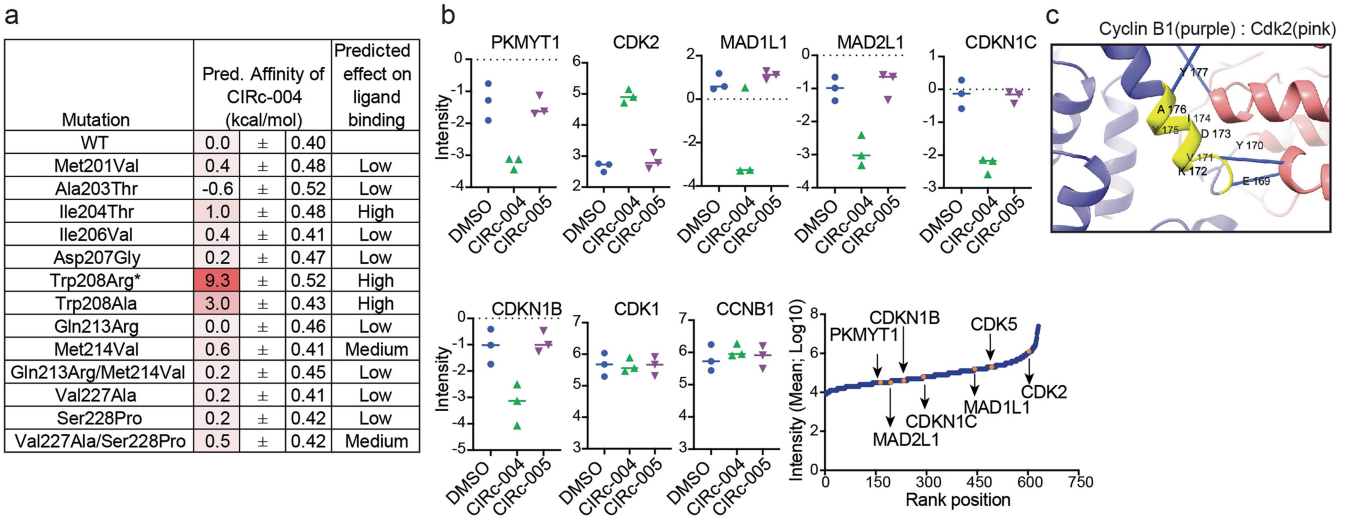

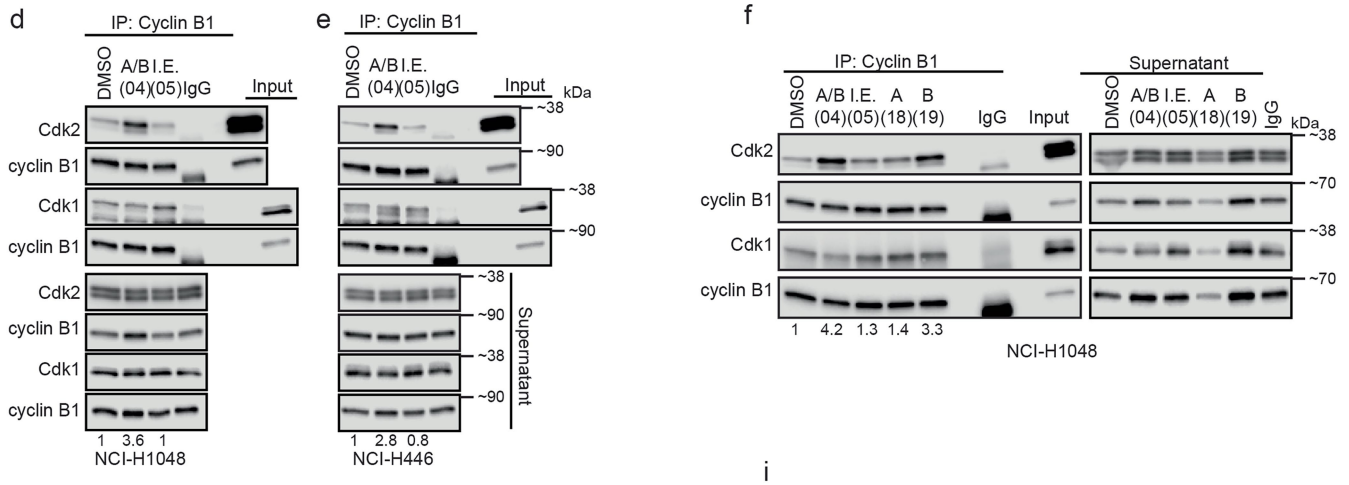

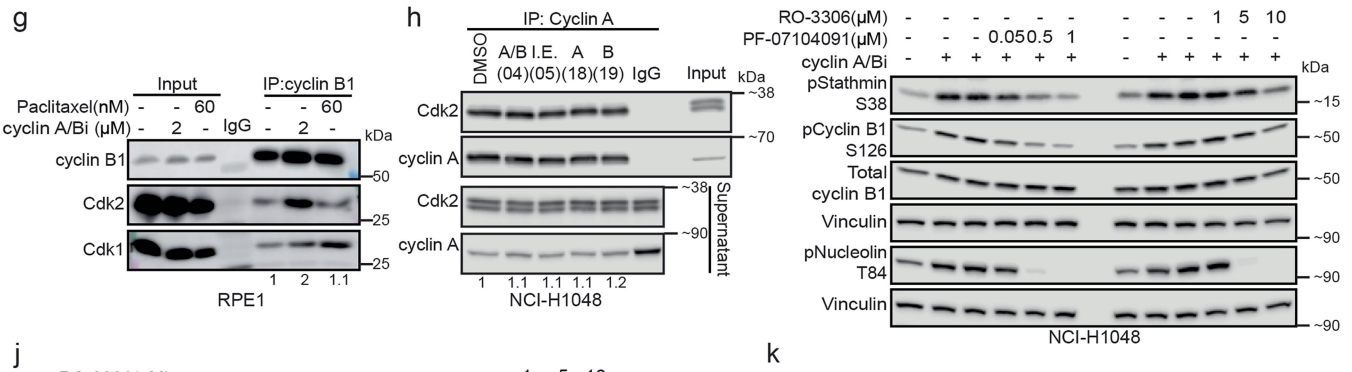

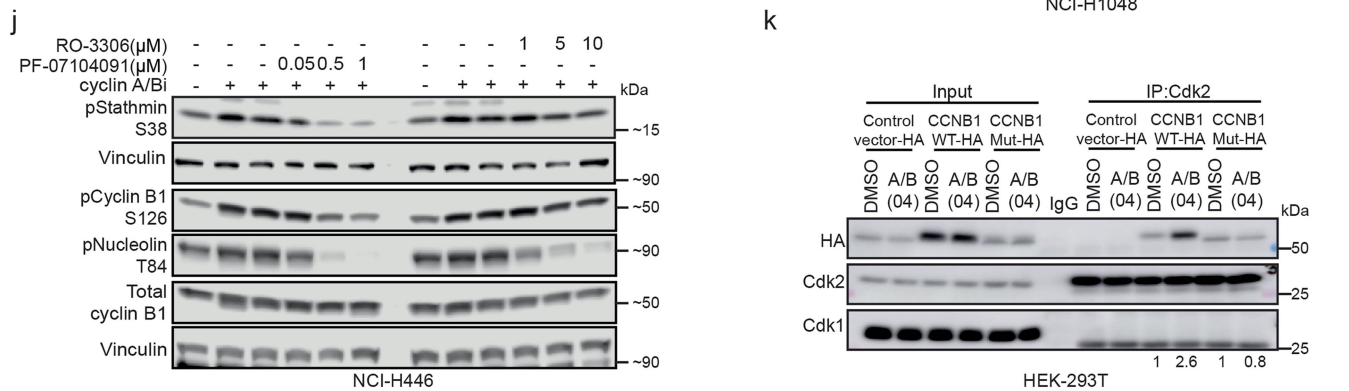

Extended Data Fig. 9 | See next page for caption.

Extended Data Fig. 9 | Cyclin A/B RxL Inhibitors Induce a Neomorphic Cyclin B-Cdk2 Interaction. a, Predicted effects of cyclin B mutations identified from the base editor screen on CIRc-004 ligand binding determined by free energy perturbation (FEP) calculations (see Methods). Mutating residues at the RxL binding site, including Ile204 and Trp208 were predicted to have the most significant effect, reducing binding affinity by 1 to 3 kcal/mol relative to cyclin B WT. Mutations of Met214Val and Val227Ala/Ser228Pro mutations showed medium impact on ligand binding 0.5-0.6 kcal/mol. *The energy convergence for the Trp208Arg mutations was poor possibly due to a conformational change from the Arg where Arg's side chain became solvent-exposed instead of being buried under the ligand. To supplement this, the Trp208Ala mutation was examined. Consistently, both Trp208Ala and Trp208Arg mutations were predicted to have a high effect on ligand binding. **b**, Mass spectrometry analysis after IP of endogenous Cyclin B1 in NCI-H1048 cells treated with CIRc-004 (50 nM), CIRc-005 (50 nM) (inactive enantiomer of CIRc-004, I.E) or DMSO for 2 h. Plots show the relative abundance of the indicated proteins as Intensity (MaxLFQ, 3VN1 group, log 2 Median centred, missing values imputed). Data points indicate values obtained from $n = 3$ biological replicates. Bottom right panel: Ranking plot of the log10 average of the 3 groups (CIRc-004, CIRc-005, DMSO) of raw protein abundance where proteins of interest (POI) are indicated within the total dataset. **c**, AlphaFold2 model of cyclin B1:Cdk2 complex is shown. Amino acids 169-177 of cyclin B are highlighted in yellow showing Cdk interacting region (pink). Solid lines indicate hydrogen bonds between the two proteins with interacting amino acid residues of cyclin B indicated. **d**, Immunoblot analysis after IP of endogenous cyclin B1 in NCI-H1048 cells treated with CIRc-004 (300 nM), CIRc-005 (I.E), or DMSO for 2 h. Note that this is the same immunoblot from Fig. 3h but now includes the supernatant. **e**, Immunoblot analysis after IP of endogenous cyclin B1 in NCI-H446 cells treated with CIRc-004 (300 nM), CIRc-005 (I.E), or DMSO for 2 h. **f**, Immunoblot analysis after IP of endogenous cyclin B1 in NCI-H1048 cells treated with CIRc-004 (300 nM), CIRc-005 (I.E), cyclin A RxL inhibitor (CIRc-018, 300 nM), cyclin B RxL inhibitor (CIRc-019, 300 nM) or DMSO for 2 h. **g**, Immunoblot analysis after IP of endogenous cyclin B1 in RPE1 cells treated with CIRc-004 (2000 nM), paclitaxel (60 nM) or DMSO for 2 h. For **d**-**h**, Cdk2 band intensity is normalized to cyclin B1 shown at the bottom. **h**, Immunoblot analysis after IP of endogenous cyclin A in NCI-H1048 cells treated with CIRc-004 (300 nM), CIRc-005 (I.E), cyclin A RxL inhibitor (CIRc-018, 300 nM), cyclin B RxL inhibitor (CIRc-019, 300 nM) or DMSO for 2 h. Cdk2 band intensity is normalized to cyclin A shown at the bottom. **i**-**j**, Immunoblot analysis of NCI-H1048 (**i**) or NCI-H446 (**j**) cells treated cyclin A/B RxL inhibitor (CIRc-004) at 200 nM, Cdk1 inhibitor (RO-3306), Cdk2 inhibitor (PF-07104091) at the concentrations indicated or DMSO for 4 h. **k**, Immunoblot analysis after IP of endogenous Cdk2 in HEK-293T cells expressing CCNB1 WT-HA, CCNB1 triple mutant-(E169K/Y170H/Y177C)-HA, or a negative control vector, and treated with CIRc-004 (300 nM) or DMSO for 2 h. HA band intensity is normalized to Cdk2 shown at the bottom. For **f**, **g**, **i**, representative immunoblots from $n = 3$ biological independent experiments are shown. For **d**, **e**, **h**, **j**, **k**, representative immunoblots from $n = 2$ biological independent experiments are shown.

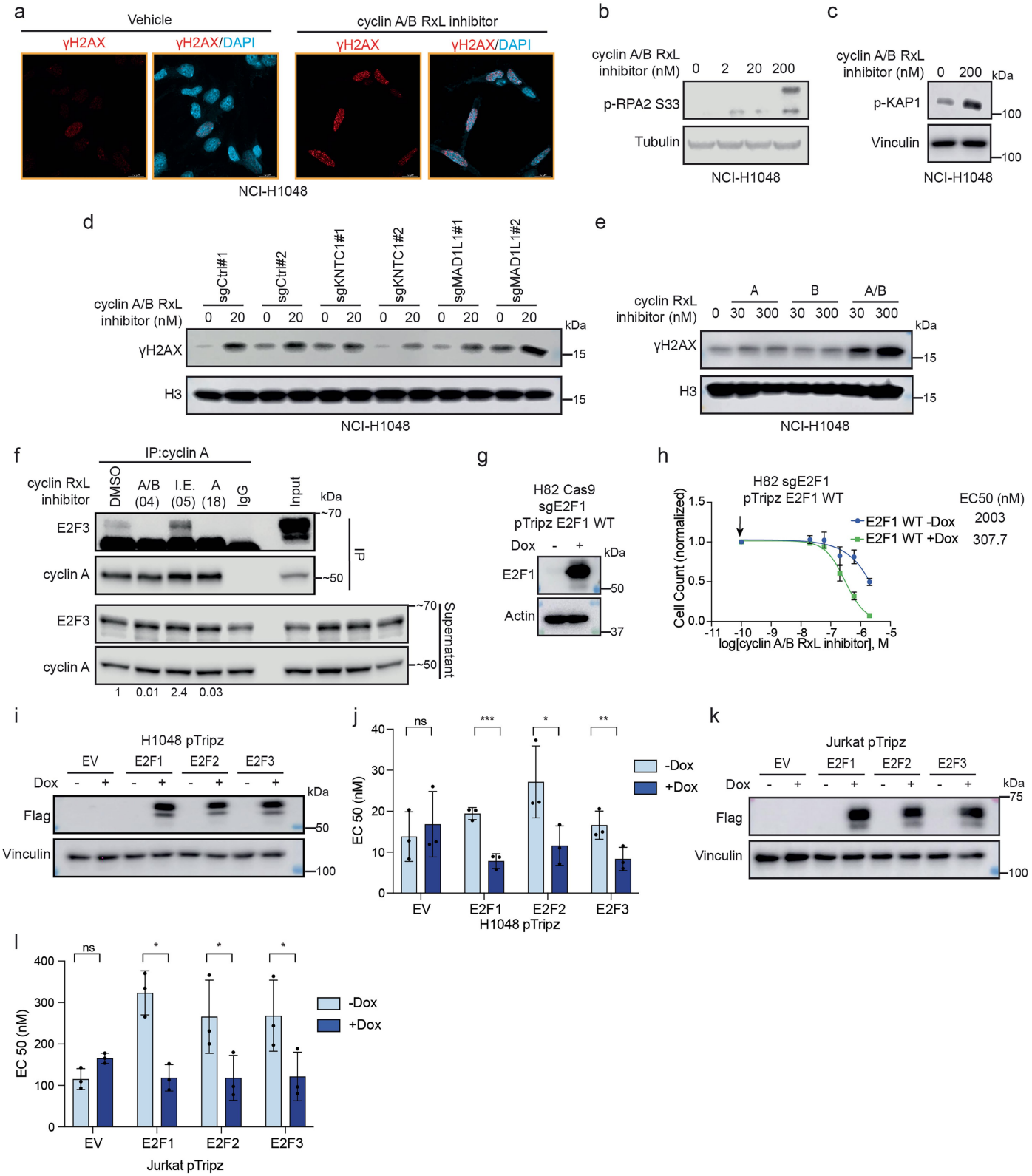

Extended Data Fig. 10 | See next page for caption.

Extended Data Fig. 10 | Cyclin A RxL Inhibition Leads to E2F Hyperactivation to Promote Sensitivity to Cyclin A/B RxL Inhibitors. a, Representative γH2AX and DAPI confocal microscopic images of NCI-H1048 cells treated with the cyclin A/B RxL inhibitor (CIRc-004) at 20 nM or DMSO for 72 h. Magnification = 63x, scale bar = 10 µm. **b, c**, Immunoblot analysis for phospho-RPA2 S33 (**b**) and phospho-KAP1 (**c**) of NCI-H1048 treated with CIRc-004 at indicated concentrations for 24 h. **d**, Immunoblot analysis of NCI-H1048 cells infected with indicated sgRNAs and then treated CIRc-004 at 20 nM or DMSO for 72 h. **e**, Immunoblot analysis of histone lysates from NCI-H1048 cells treated with the selective cyclin A RxL inhibitor (CIRc-018), the selective cyclin B RxL inhibitor (CIRc-019), the cyclin A/B RxL inhibitor (CIRc-004), or DMSO (vehicle) for 72 h. **f**, E2F3 Immunoblot analysis after IP of endogenous cyclin A in NCI-H1048 cells treated with CIRc-004 (300 nM), CIRc-005 (inactive enantiomer of CIRc-004, I.E), cyclin A RxL inhibitor (CIRc-018) or DMSO for 2 h. E2F3 band intensity is normalized to cyclin A shown at the bottom. *n* = 2 biological independent experiments. **g**, Immunoblot analysis of NCI-H82 cells infected with a doxycycline (DOX) inducible E2F1 sgRNA-resistant cDNA and then superinfected with an sgRNA targeted endogenous E2F1 grown in the presence or absence of DOX for 24 h. **h**, Dose response assays of NCI-H82 cells from **g** grown in the presence or absence of DOX for 24 h and then treated with increasing concentrations of CIRc-004 for 6 days. Data are mean +/− SD and arrows indicates DMSO-treated sample which was used for normalization. **i,k**, Immunoblot analysis of NCI-H1048 (**i**) and Jurkat (**k**) cells infected with a doxycycline (DOX) inducible E2F1, E2F2 or E2F3 cDNA grown in the presence or absence of DOX for 24 h. **j**, **l**, Quantitation of average half-maximal effective concentration (EC50) without (light blue) or with (dark blue) DOX of NCI-H1048 (**j**) or Jurkat cells (**l**) from **i, k** expressing DOX inducible E2F1, E2F2, E2F3 treated with CIRc-004 at increasing concentrations for 3 days (**j**) or 6 days (**l**). For **a-e**, **h,j, l**, representative immunoblots from 3 independent experiments are shown. For histone blots in **d**, **e**, total histone H3 run as sample processing control on separate gel.

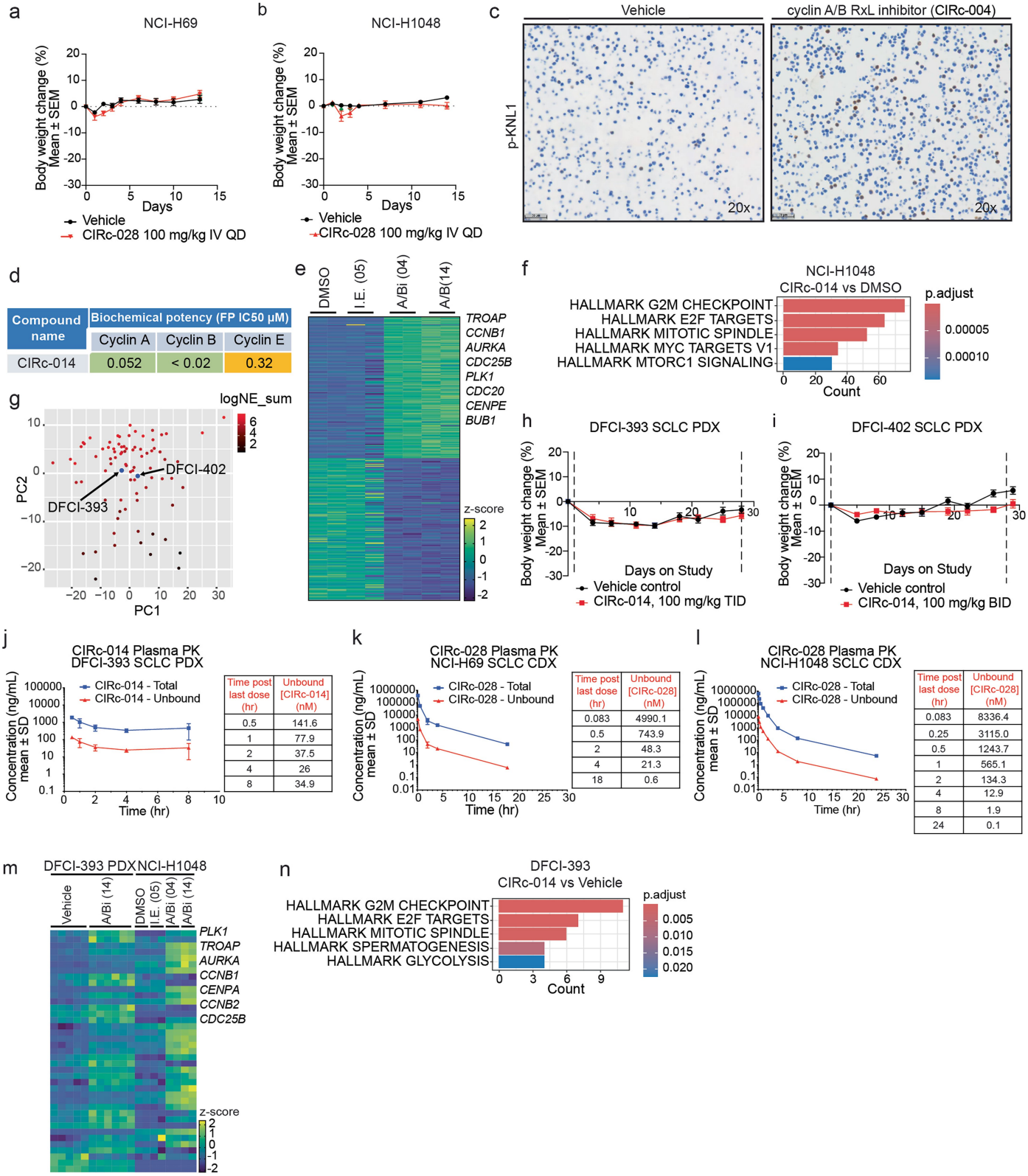

Extended Data Fig. 11 | See next page for caption.

Extended Data Fig. 11 | Pharmacokinetic and Pharmacodynamic Studies of Cyclin A/B RxL Inhibitors in SCLC Cell-Line Xenograft and Patient-Derived Xenograft Models. a, b, Body weights of mice enrolled in the NCI-H69 (**a**) or NCI-H1048 (**b**) xenografts efficacy treatment studies treated for 14 days with vehicle, cyclin A/B RxL inhibitor (CIRc-028, 100 mg/kg IV QD). For **a**, *n* = 10 independent mice per arm. For **b**, *n* = 10 independent mice for vehicle and n = 8 independent mice for CIRc-028 arm. QD=Every day. **c**, Representative IHC micrographs of cell pellets from NCI-H1048 cells treated with CIRc-004 at 200 nM or DMSO (vehicle) overnight and then stained for phospho-KNL1 to validate the phospho-KNL1 antibody for IHC. Magnification=20x, scale bar = 50 µm. **d**, Biochemical activity of the orally bioavailable cyclin A/B RxL macrocyclic inhibitor (CIRc-014) for cyclin A1/Cdk2, cyclin E1/Cdk2 and cyclin B/CDK1 complexes measured by Fluorescence Polarization. CIRc-014 was used for in vivo efficacy studies in SCLC PDX models in Fig. 5g–n. **e**, Heat map of z-scores from RNA-seq data of NCI-H1048 cells treated with cyclin A/B RxL inhibitor (CIRc-004 or CIRc-014 at 200 nM), inactive enantiomer (CIRc-005 at 200 nM) or DMSO for 24 h. Data is sorted for Log2FoldChange of CIRc-004 (replicate 1 and 2) vs. DMSO (replicate 1 and 2) showing genes with Padj<0.05 which was 150 top up-regulated and down-regulated genes. Relevant up-regulated genes shown on the right. **f**, Bar graphs showing top significantly enriched Hallmark pathways (padj<0.05) calculated using differentially expressed genes from bulk RNA-seq experiment in **e** comparing CIRc-014 vs. DMSO in NCI-H1048 cell line. For **e, f**, *n* = 2 biological replicates. **g**, Principal component analysis (PCA) from RNA-seq data integrating RNA-seq data from DFCI-393 and DFCI-402 PDX models with 81 primary SCLC human samples from George et al. Nature 2015[1]. Bar scale shows neuroendocrine score (see Methods). **h,i**, Body weights of mice enrolled in the DFCI-393 SCLC PDX (**h**) or DFCI-402 SCLC PDX (**i**) efficacy studies treated for 28 days with CIRc-014 (100 mg/kg PO TID for DFCI-393 and 100 mg/kg PO BID for DFCI-402) or vehicle. For DFCI-393 PDX in **h**, n = 10 independent mice for vehicle and *n* = 9 independent mice for CIRc-014. For DFCI-402 PDX in **i**, *n* = 10 independent mice per arm for both vehicle and CIRc-014. TID=three times a day; BID=two times a day. **j**, Plasma concentration of CIRc-014 from NSG mice bearing DFCI-393 PDX tumours treated with CIRc-014 100 mg/kg PO TID in the pharmacodynamic study in Fig. 5k–n. Mice were dosed for 4 days and plasma was collected at the times indicated after the last dose. Unbound concentrations (nM) at indicated time points shown on the right. Data are mean +/− SEM. *n* = 2 for 1-hour time point; *n* = 3 independent mice for 30-min, 2 and 4-hour timepoints; and *n* = 6 mice for 8-hour timepoint. **k, l**, Plasma concentration of CIRc-028 at the end of the efficacy studies where CIRc-028 was dosed 100 mg/kg IV QD for 14 days in CDX models of NCI-H69 model (**k**) shown in Fig. 5a or NCI-H1048 model (**l**) shown in Fig. 5b. Unbound concentrations (nM) at indicated time points shown on the right. Data are mean +/− SEM. For **k**, *n* = 5 mice for each time point. For **l**, *n* = 8 mice for each time point. For **j**, study run in NSG mice and NOD SCID % plasma protein binding (PPB) used to estimate unbound fraction. For **k-l**, studies run in Athymic Nude and BALB/c Nude mice, respectively, and % PPB from each strain was used to estimate unbound fraction. Plasma was collected from mice after the last dose and CIRc-014 or CIRc-028 concentrations were determined by LC-MS/MS. **m**, Heat map of z-scores from RNA-seq data of DFCI-393 human SCLC PDX from Fig. 5k–n treated with CIRc-014 (100 mg PO TID) or vehicle for 4 days. Values are sorted for Log2FoldChange of CIRc-014 treated tumours (*n* = 6 tumours from independent mice) vs. vehicle treated tumours values (*n* = 5 tumours from independent mice) showing genes with Padj<0.05 which was 39 differentially expressed genes. Relevant up-regulated genes shown on the right. The NCI-H1048 cell line treated with cyclin A/B RxL inhibitors (CIRc-004, CIRc-014 at 200 nM), inactive enantiomer (CIRc-005 at 200 nM), or DMSO (vehicle) as shown in Extended Data Fig. 11e is included as a benchmark control showing overlap of genes upregulated in DFCI-393 PDX tumours after CIRc-014 and NCI-H1048 cell lines treated with cyclin A/B RxL inhibitors (CIRc-004 and CIRc-014). **n**, Bar graphs showing top significantly enriched Hallmark pathways (padj<0.05) calculated using differentially expressed genes from bulk RNA-seq experiment in **m** comparing CIRc-014 treated DFCI-393 PDX tumours (*n* = 6 tumours from independent mice) to vehicle treated DFCI-393 PDX tumours (*n* = 5 tumours from independent mice).

nature portfolio

Corresponding author(s): Matthew G. Oser

Last updated by author(s): May 29, 2025

Reporting Summary

Nature Portfolio wishes to improve the reproducibility of the work that we publish. This form provides structure for consistency and transparency in reporting. For further information on Nature Portfolio policies, see our Editorial Policies and the Editorial Policy Checklist.

Statistics

For all statistical analyses, confirm that the following items are present in the figure legend, table legend, main text, or Methods section.

n/a	Confirmed	
☐	☒	The exact sample size (*n*) for each experimental group/condition, given as a discrete number and unit of measurement
☐	☒	A statement on whether measurements were taken from distinct samples or whether the same sample was measured repeatedly
☐	☒	The statistical test(s) used AND whether they are one- or two-sided *Only common tests should be described solely by name; describe more complex techniques in the Methods section.*
☒	☐	A description of all covariates tested
☐	☒	A description of any assumptions or corrections, such as tests of normality and adjustment for multiple comparisons
☐	☒	A full description of the statistical parameters including central tendency (e.g. means) or other basic estimates (e.g. regression coefficient) AND variation (e.g. standard deviation) or associated estimates of uncertainty (e.g. confidence intervals)
☐	☒	For null hypothesis testing, the test statistic (e.g. *F*, *t*, *r*) with confidence intervals, effect sizes, degrees of freedom and *P* value noted *Give P values as exact values whenever suitable.*
☒	☐	For Bayesian analysis, information on the choice of priors and Markov chain Monte Carlo settings
☒	☐	For hierarchical and complex designs, identification of the appropriate level for tests and full reporting of outcomes
☐	☒	Estimates of effect sizes (e.g. Cohen's *d*, Pearson's *r*), indicating how they were calculated

Our web collection on statistics for biologists contains articles on many of the points above.

Software and code

Policy information about availability of computer code

Data collection

For IP-MS purified peptide eluates were run through an Ultimate 3000 HPLC connected to an Orbitrap Ascend Tribrid instrument.
For Bulk-RNA seq on untreated SCLC DFCI 393 and DFCI 402 PDX tumors that were used for the PDX studies, RNA-seq of experimental PDX, DFCI 393 tumors were treated with the orally bioavailable cyclin A/B RxL inhibitor CIRc-014 at 100 mg/kg PO TID or vehicle (30% PEG400, 20% Solutol HS15, 50% Phosal 53 MCT) and the NCI-H1048 cell line experiments done in 2 biological independent experiments, RNA was extracted using RNeasy mini kit (Qiagen #74106) including a DNase digestion step according to the manufacturer's instructions. Total RNA was submitted to Novogene Inc. The libraries were prepared using NEBNext Ultra II non-stranded kit. Paired end 150bp sequencing was performed on Novaseq6000 sequencer using S4 flow cell. Sequencing reads were mapped to the hg38 genome by STAR.

Data analysis

For CRISPR KO screen, raw Illumina reads were normalized between samples using: Log2[(sgRNA reads/total reads for sample) × 1e6) + 1]. Apron analysis, hypergeometric analysis, and STARS analysis were performed using the GPP web portal, https://portals.broadinstitute.org/gpp/screener/.
For CRISPR Base Editor screen, raw Illumina reads were normalized between samples using: Log2[(sgRNA reads/total reads for sample) × 1e6) + 1]. The Log Fold Change value was calculated between treatment arms and LFC value for each sgRNA was z-scored, using the following equation: z-score = (x - μ)/σ, where x, μ, and σ correspond to LFC of an individual guide, the mean LFC of all negative control guides, and standard deviation of all control guides, respectively.
Principal component analysis (PCA) on RNA-seq data was performed using the removeBatchEffect function in the limma package (version 3.58.1) and prcomp function of R software (version 4.3.3).
Statistics for DEGs from bulk-RNA seq were calculated by DESeq2 (1.36.0).
For HALLMARK pathway enrichment analysis, differentially expressed genes were tested if over-represented against the HALLMARK pathways from the MSigDB using R packages msigdbr (7.5.1) and clusterProfiler (4.8.3).
Heatmaps were generated by calculating z score using log transformed FPKM values. To calculate z score, a log transformed FPKM value was

subtracted from the mean and then divided by the standard deviation.
DIA-NN software (V8.1) was used to analyse the IP-MS data in library-free mode and using the recommended default settings.
Co-folding of proteins were done by AlphaFold 2 implemented in ColabFold. Default parameters were used to predict their relative positions. Specifically, those parameters are: msa_mode (MMseqs2_UniRef_Environmental), pair_mode (unpaired_paired), model_type (auto), number of cycles (3), recycle_early_stop_tolerance(auto), relax_max_iterations (200), and pairing_strategy (greedy). The resulting co-folding structure along with the PAE files were analyzed using ChimeraX software.
The Gene Set Variation Analysis (GSVA) method, utilizing the MSigDb Hallmark collection50 of RNA-seq data, was employed to calculate GSVA scores for E2F targets and G2/M checkpoint pathway using the GSVA Bioconductor package (version 1.50.5). The heatmap was constructed using the ComplexHeatmaps package (version 2.18.0) in R (version 4.3.2).
FACS analysis was performed on FlowJo 10.8.1. and FlowJo 10.9.0.
IF images were acquired using ZEN 2.3 SP1 software. Image analysis was performed Image J2 v2.9.0 software.
IHC images were analyzed using the HALO platform multiplex-IHC v3.2.5 algorithm (Indica lab).
Live cell images were analyzed using NIS Elements Viewer 4.2 (Nikon) and Incucyte Zoom / S3 live cell imagers (Essen Biosciences).
Schrodinger software suite (2024-3 version) was used to conduct modeling studies on cyclin B.
Immunoblots were quantified using Fiji (Image J2 v2.9.0) or LICOR Odyssey built-in Image Studio Software (v5.2).

For manuscripts utilizing custom algorithms or software that are central to the research but not yet described in published literature, software must be made available to editors and reviewers. We strongly encourage code deposition in a community repository (e.g. GitHub). See the Nature Portfolio guidelines for submitting code & software for further information.

Data

Policy information about availability of data

All manuscripts must include a data availability statement. This statement should provide the following information, where applicable:

- Accession codes, unique identifiers, or web links for publicly available datasets
- A description of any restrictions on data availability
- For clinical datasets or third party data, please ensure that the statement adheres to our policy

Data from the genome-wide CRISPR/Cas9 Resistance Screen with the Cyclin A/B RxL Inhibitor, the Cyclin A/B/E RxL Inhibitor, or the Cdk2 Inhibitor are included in Supplementary Table 3. The RNA-seq experiments of NCI-H1048 cells treated with cyclin A/B RxL inhibitors or the CDK2 inhibitor are included in Supplementary Table 4. Data from the CRISPR/Cas9 Base Editor Screens with the Cyclin A/B RxL Inhibitor in Figure 3 are included in Supplementary Table 5. Data from the Mass Spectrometry of the Cyclin B1 CIRc-004-Dependent Interactome in Figure 3 are included in Supplementary Table 6. FPKM values from the bulk RNA-sequencing experiments of SCLC PDX models DFCI-393 and DFCI-402 are included in Supplementary Table 7. The RNA-seq experiments of DFCI-393 PDXs treated with cyclin A/B RxL inhibitors are included in Supplementary Table 7. The raw proteomics data are available via ProteomeXchange with identifier PXD055112 via the PRIDE (PRoteomics IDEntifications - https://www.ebi.ac.uk/pride/) partner repository. The raw RNA-seq data are available on Gene Expression Omnibus (GEO) accession number GSE291451. Any other data and materials can be requested from the corresponding author upon reasonable request.

Research involving human participants, their data, or biological material

Policy information about studies with human participants or human data. See also policy information about sex, gender (identity/presentation), and sexual orientation and race, ethnicity and racism.

Reporting on sex and gender	N/A
Reporting on race, ethnicity, or other socially relevant groupings	N/A
Population characteristics	N/A
Recruitment	N/A
Ethics oversight	N/A

Note that full information on the approval of the study protocol must also be provided in the manuscript.

Field-specific reporting

Please select the one below that is the best fit for your research. If you are not sure, read the appropriate sections before making your selection.

☒ Life sciences ☐ Behavioural & social sciences ☐ Ecological, evolutionary & environmental sciences

For a reference copy of the document with all sections, see nature.com/documents/nr-reporting-summary-flat.pdf

Life sciences study design

All studies must disclose on these points even when the disclosure is negative.

Sample size	For NCI-H1048 xenograft study, n=10 independent mice for vehicle and n=8 independent mice for CIRc-028 arm. For NCI-H69 xenograft, n=10 independent mice for vehicle and CIRc-028 arm. For DFCI 393 PDX in n=10 independent mice for vehicle and n=9 independent mice for CIRc-014 arm. For DFCI 402 PDX n=10 independent mice per arm.

For immunofluorescence experiment, 15 blind images were taken per experiment and repeated in 3 biological independent experiments.
For IP-MS data, samples from 3 independent biological experiments were collected and analyzed.
For live-cell imaging experiment in Extended Data Fig. 6a-b, 2 biological experiments were performed and 50 blind cells total were analyzed.
For live-cell imaging experiment in Extended Data Fig. 2l, n=6 wells per treatment condition per replicate from 2 independent experiments, 1 representative experiment is shown.
For all other experiments, sample size was not predetermined and multiple biological replicates were performed (mostly 3, but exact numbers specified in figure legends) and repeated n times based on reproducibility and statistical significance. For all experiments, no statistical methods were used to predetermine sample sizes but our sample sizes are similar to those reported in previous publications.

Data exclusions

There were no data excluded in our study.

Replication

To ensure reproducibility, multiple independent biological replicates were performed as described above in sample size with specific numbers of biological independent experiments specified with exact numbers in each figure legend. All attempts at replication were successful for all experiments in this manuscript and there were no data excluded.

Randomization

Samples were randomly allocated to experimental groups. For in vivo studies in Figure 5 and Extended Data Fig. 11, all mice used were randomly assigned to receive either vehicle or treatment. For in vitro experiments, this means that the same cell lines from the same maintenance culture were infected with the indicated sgRNAs at the same time for each biological independent experiment and each biological independent experiment was performed independently on a different day.

Blinding

For the Bulk RNA-sequencing studies, the experiments were performed and analyzed by Novogene (RNA-seq) who were blinded to the purpose of the study and the study group.
For imaging experiments, blind images were taken using counter-stained nuclei and cells were chosen randomly to analyze.
Forward genetic screen by its virtue is an unbiased screen and did not require blinding. Blinding was not possible for the analysis portions of the CRISPR Knock-out screen, base editor screen, IP-MS but no data were excluded and therefore blinding was not relevant for analysis. For low throughput experiments, blinding was not possible as the scientist performing the experiments needed to know the conditions to perform the experiment, but the experiments were performed with the appropriate controls in multiple independent biological experiments, all data are included in this manuscript, and no data were excluded.

Reporting for specific materials, systems and methods

We require information from authors about some types of materials, experimental systems and methods used in many studies. Here, indicate whether each material, system or method listed is relevant to your study. If you are not sure if a list item applies to your research, read the appropriate section before selecting a response.

Materials & experimental systems

n/a	Involved in the study
☐	☒ Antibodies
☐	☒ Eukaryotic cell lines
☒	☐ Palaeontology and archaeology
☐	☒ Animals and other organisms
☒	☐ Clinical data
☒	☐ Dual use research of concern
☒	☐ Plants

Methods

n/a	Involved in the study
☒	☐ ChIP-seq
☐	☒ Flow cytometry
☒	☐ MRI-based neuroimaging

Antibodies

Antibodies used

The primary antibodies and dilutions used were: Mouse Anti-β-actin AC-15 (Sigma #A3854, 1:25,000), mouse anti-Vinculin hVIN-1 (Sigma# V9131, 1:10000), rabbit anti-phospho CASC5/KNL1 Thr943/Thr1155 D8D4N (Cell Signaling #40758, 1:1000), rabbit anti-CASC5/KNL1 E4A5L (Cell Signaling #26687, 1:1000), rabbit anti-cyclin B1 D5C10 (Cell Signaling #12231, 1:1000), rabbit anti-E2F1 (Cell Signaling #3742, 1:1000), CDC20 (Cell Signaling #4823S, 1:1000), FLAG (Sigma-Aldrich #A8592), rabbit-anti-phospho-stathmin (S38) (Cell Signaling #3426S, 1:1000), rabbit-anti-total stathmin (Abcam #ab52630), rabbit-anti-phospho-Cyclin B (S126) (Abcam #ab3488, 1:1000), rabbit-anti-phospho-nucleolin (T84) (Abcam #ab155977, 1:1000), rabbit-anti-phospho-FOXM1(T600) (Cell Signaling #14655S, 1:500), rabbit-anti-phospho-RPA2(S33) (Fortis Life Sciences #A300-246A, 1:2000), rabbit-anti-tubulin-HRP (Cell Signaling #9099S 1:5000), rabbit anti-Histone 3 DH12 (Cell Signaling #4499, 1:5000), rabbit anti-phospho Histone H2A.X Ser 139 (Cell signaling #2577, 1:1000) and anti-phospho KAP1 antibody (Cell Signaling #4127, 1:1000) . The secondary antibodies used and dilutions were: goat-anti-rabbit-IgG-HRP (Cell Signaling #7074S, 1:5000), Goat Anti-Mouse (Jackson ImmunoResearch #115-035-003, 1:5000) and Goat anti-Rabbit (Jackson ImmunoResearch #111-035-003, 1:5000).
For immunoprecipitation the primary antibodies and dilutions used were: anti-Myt1 (Fortis Life Sciences A302-424A 1:1000), mouse-anti-cyclin B (Cell Signaling #4135 1:1000), mouse-anti-E2F1 (SCBT #sc-251, 1:1000), mouse-anti-cyclin A (Cell Signaling #4656, 1:1000), mouse anti-CDK2 (Origene TA502935), rabbit anti-Cdc2 (Cell Signaling 28439). The secondary antibodies used and dilutions were: mouse-anti-rabbit (confirmation specific)-IgG HRP (Cell Signaling #5127, 1:2000), goat-anti-rabbit IgG-HRP (Cell Signaling #7074S, 1:5000), horse-anti-mouse IgG-HRP (Cell Signaling #7076S, 1:5000), goat-anti-mouse-IgE-HRP (Southern Biotech #1110-05, 1:5000), rabbit anti-Cyclin B1 D5C10 (Cell Signaling #12231, 1:1000), rabbit anti-Cdk2 E8J9T (Cell Signaling #18048, 1:1000) and mouse anti-HA. 11 epitope tag (BioLegend #901501, 1:1000). Anti-Wee1 antibody was used at 1:1000 (CST, Cat #4936). Anti-E2F3 antibody was used at 1:1000 (SCBT, cat #sc-56665).
For immunofluorescence , the primary antibodies used were rabbit anti-phospho Histone H2A.X Ser 139 (Cell Signaling #2577, 1:400); rabbit anti-phospho CASC5/KNL1 Thr943/Thr1155 D8D4N (Cell Signaling #40758, 1:400); ACA (Antibodies inc. #15-235, 1:500) and secondary antibodies used included Alexa Fluor 568 Goat anti-rabbit (Thermo Fisher Scientific #A11011, 1:300) and Alexa Fluor 647

Goat anti-human (Thermo Fisher Scientific #A21445, 1:300).
For FACS antibodies used included Pacific blue conjugated cleaved PARP antibody (Cell Signaling, Asp214, D64E10, #60068) and Alexa-647 conjugated phospho-histone H3 (Ser10) antibody (Cell Signaling, #3458)

Validation

All antibodies used for immunoblot analysis and IP experiments described above have been validated. This was done using different approaches. For cyclin B and Cdk2 antibodies, CRISPR inactivation of the target was performed followed by immunoblot analysis showing loss of target protein expression. CDC20, E2F1 and Flag were validated in cell lines engineered to overexpress Flag tagged CDC20 and E2F1. p-KNL1 antibody was validated by treating the cells with MPS1 inhibitor which has been validated previously to inhibit KNL1 phosphorylation. Gamma-H2AX antibody was validated by showing increase in DNA damage after chemotherapy treatment and H3 antibody is used as a loading control. P-cyclin B1, p-Stathmin and p-nucleolin were validated using selective Cdk1 and Cdk2 inhibitor treatments. Vinculin and b-actin are used in the lab as standard loading controls. Antibodies used for IF and IHC (p-KNL1) were validated in cell blocks after treatment with a cyclin A/B RxL inhibitor which was shown to increase phospho-KNL1 by immunoblot as described above. Antibodies used in FACS (p-H3, cleaved PARP) have been validated in a previously published paper where Aurora B Kinase inhibition induced mitotic arrest and apoptosis(PMID: 30373918). Anti-cdc2 and anti-CDK2 antibodies for WB were validated by co-IP western blot. Briefly, anti-cdc-2 or anti-CDK2 antibodies (cdc2 SCBT #SC-54; CDK2 SCBT #SC-6248) were used to immunoprecipitate CDK1 or CDK2 from cell lysates followed by western blot for CDK1 (CST #28439S) or CDK2 (Origene TA502935). The anti-cdc2 antibody detected a band of the appropriate molecular weight in the CDK1 pulldown but no band was detected in the CDK2 pull-down or IgG control and vice versa for the anti-CDK2 antibody. For anti-cyclin A and Cyclin B (CST # 4135) immunoblots, shRNA knockdown of the target was performed followed by immunoblot analysis showing >75% reduction in target protein expression. The anti-Myt1 antibody was validated in a previously published paper where stable PKMYT1 knock-out cell lines were generated by CRISPR inactivation and immunoblot analysis demonstrated loss of target protein expression (PMID: 35444283). Anti-Wee1 antibody (CST, Cat #4936) was validated in a previously published paper where Wee1 was knocked-down by siRNA. (PMID: 33257507). Anti-E2F3 antibody was (SCBT cat #sc-56665) validated in a previously published paper where exogenous tagged-E2F3 was inducibly expressed by doxycycline treatment (PMID: 33264622). Anti-phospho KAP1 antibody has been validated in a previously published paper showing induction after treating cells with DNA damage causing agents like Etoposide or exposing to irradiation (PMID: 37541219).

Eukaryotic cell lines

Policy information about cell lines and Sex and Gender in Research

Cell line source(s)

NCI-H446, NCI-H69 cells, NCI-H1048, NCI-H526, WI-38, NCI-H82, RPE-1 and 293T cells were originally obtained from American Type Culture Collection (ATCC). A549, HCC4006, and NCI-H1299 cells were a kind gift from Dr. Pasi Janne's laboratory at DFCI. NCI-H1048, Jurkat, NCI-H82 and MDA-MB-231 cells were originally obtained from ATCC and early passage cell lines were genetically modified to stably express a DOX-ON inducible E2F1 expression and were a kind gift from Dr. William G. Kaelin's lab. G-CSF mobilized human PB CD34+ cells were obtained from Stemcell Technologies (#700060.1 Lot:230472503C).

Authentication

Human cell lines as described above were originally obtained from ATCC where they were authenticated and then early passage cell lines were frozen and used for all experiments within 4 months of thawing.

Mycoplasma contamination

Early passage cells of all the cell lines listed above were tested for mycoplasma (Lonza #LT07-218) and then were frozen using Bambanker's freezing medium (Bulldog Bio) and maintained in culture no more than 4 months where early passage vials were thawed.

Commonly misidentified lines
(See ICLAC register)

There were no commonly misidentified cell lines used.

Animals and other research organisms

Policy information about studies involving animals; ARRIVE guidelines recommended for reporting animal research, and Sex and Gender in Research

Laboratory animals

SCLC xenograft studies were performed in 7-8 week old female Nude mice (Envigo, Hsd:Athymic Nude-Foxn1nu).
SCLC PDX studies were performed in 7-8 week-old female NSG (Jackson Laboratories, NOD.Cg-Prkdcscid Il2rgtm1Wjl/SzJ) mice.

Wild animals

There are no wild animals used in this study.

Reporting on sex

All mice used in the animal studies were 7-8 week old females.

Field-collected samples

This study does not include field-collected samples.

Ethics oversight

All experiments herein comply with all ethical regulations. Specifically, all mouse experiments complied with National Institutes of Health guidelines and were approved by Dana-Farber Cancer Institute Animal Care and Use Committee.

Note that full information on the approval of the study protocol must also be provided in the manuscript.

Plants

Seed stocks: N/A

Novel plant genotypes: N/A

Authentication: N/A

Flow Cytometry

Plots

Confirm that:

☒ The axis labels state the marker and fluorochrome used (e.g. CD4-FITC).

☒ The axis scales are clearly visible. Include numbers along axes only for bottom left plot of group (a 'group' is an analysis of identical markers).

☒ All plots are contour plots with outliers or pseudocolor plots.

☒ A numerical value for number of cells or percentage (with statistics) is provided.

Methodology

Sample preparation

For PI cell cycle analysis, early passage cells were washed once in ice-cold PBS and then fixed in ice-cold 80% ethanol (added dropwise) for at least 2 hours at -20 degrees celsius. The cells were then centrifuged at 206 x g (Eppendorf centrifuge 5804 R, A-4-44 rotor, 2000 rpm) for 5 mins, washed once in PBS, centrifuged again at 206 x g, and then washed again in PBS containing 0.5% BSA. Finally, cells were stained with Propidium Iodide (PI) (BD # 550825) for 15 minutes at room temperature.
For p-H3 and cleaved PARP FACS analysis early passage cells were treated with the drug for appropriate time and then washed once in room temperature PBS and then fixed in 4% paraformaldehyde for 15 minutes at room temperature. The cells were then centrifuged at 206 x g (Eppendorf centrifuge 5804 R, A-4-44 rotor, 2000 rpm) for 5 mins at room temperature, washed once in PBS, centrifuged again at 206 x g, and then permeabilized with ice cold methanol at 4 degrees celsius for 30 minutes. The cells were then washed again in PBS and then incubated with Alexa-647 conjugated phospho-histone H3 (Ser10) antibody (Cell Signaling, #3458) or Pacific blue conjugated cleaved PARP antibody (Cell Signaling, Asp214, D64E10, #60068) for 1 hour at room temperature, then washed once in PBS containing 0.5% BSA, centrifuged at 400 x g. FACS analysis was then performed to determine the % positive stained cells.
For FACS base EDU incorporation assay, early passage cells were pulsed for 1h with 10 micromolar EdU (Click-It Plus EdU Flow Cytometry Assay kit, Invitrogen #C10632) prior to collection. Following incubation, cells were washed once with ice-cold PBS and fixed by incubation in ice-cold 80% ethanol for at least 2 hours at -20 degrees celsius. EdU was fluorescently tagged with Alexa FluorTM 488 by click reaction (Click-it Plus EdU flow cytometry assay kit, Invitrogen, #C10632). DNA content was monitored by FxCycle Violet stain (Invitrogen, #F10347) or DAPI (Cell Signlaing, #4083).
For HSPC cell cycle and apoptosis analysis, Cell cycle profile and apoptosis detection: For FACS based EDU incorporation assay and apoptosis detection, HSPCs were pulsed for 1h with 10 micromolar EdU (Click-It Plus EdU Flow Cytometry Assay kit, Invitrogen #C10634) prior to collection. Following incubation, cells were washed once with PBS-BSA and then stained with an anti-CD34-Per-CP antibody. Next cells were fixed by incubation in 4% PFA. EdU was fluorescently tagged with Alexa FluorTM 647 by click reaction (Click-it Plus EdU flow cytometry assay kit, Invitrogen, #C10634). After EdU labeling, cells were stained with FITC-mouse anti-cleaved PARP (Asp214). DNA content was monitored by FxCycle Violet stain (Invitrogen, #F10347).

Instrument

All independent biological replicates of PI, p-H3 and cleaved PARP FACS experiments were analyzed on a LSR Fortessa flow cytometer (Becton Dickinson, Franklin Lakes, NJ) using the same Fortessa at the Dana-Farber Hematology Neoplasia flow cytometry core.
For EDU incorporation FACS, the cytometry analysis for EdU and DNA content was performed by full spectral flow cytometry on a Northern Lights cytometer (Cytek Biosciences)

Software

For all FACS experiments data was analyzed on FlowJo 10.8.1. and FlowJo 10.9.0.

Cell population abundance

Given these were healthy cell lines, the majority of cells (>80%) were live and all live cells were used for analysis of PI, p-H3 and EDU.
For cleaved PARP FACS all cell population was considered including dead cells to analyze apoptosis.

Gating strategy

Live cells were first gated on by forward scatter/side scatter, doublets were excluded, and then percent positive Alexa-647 conjugated phospho-histone H3 (Ser10) antibody (Cell Signaling, #3458), Propidium Iodide (BD # 550825) and Alexa Fluor 488 by click reaction (Click-it Plus EdU flow cytometry assay kit, Invitrogen, #C10632) was compared to a matched negative control.
For cleaved PARP analysis, all populations were gated on side scatter versus Pacific blue conjugated cleaved PARP (Cell

Signaling, Asp214, D64E10, #60068) to identify apoptotic cells.
To detect cells with EdU+ 4C DNA content, initial gating was performed to exclude cell debris by plotting SSC-H vs FSC-H. From this population, single cells were then selected by plotting FxCycle-Violet-H vs Fx-Cycle Violet-A and a gate was drawn to exclude doublets (cells with 2:1 Fx-Cycle-Violet area). Within the single cell population gate, EdU+ cells were identified by plotting EdU-AlexaFluor488 vs FxCycle-Violet. The EdU+ 4C DNA content population was identified as cells with AF488 signal above background (DMSO, no EdU control) with 4C DNA content.
HSPC cells were first gated by FSC-H vs SSC-H. From this population, single cells were then selected by plotting FxCycle-Violet-H vs Fx-Cycle Violet-A and a gate was drawn to exclude doublets (cells with 2:1 Fx-Cycle-Violet area). Within the single cell population gate, CD34+ cells were identified as cells with Per-CP signal above background (DMSO, no Per-CP antibody control). From the CD34+ population, EdU+ (S phase population) cells were identified as cells with AF647 signal above background (DMSO, no EdU control). G0-G1 population cells were identified as cells with background level EdU and 2N DNA content. G2-M phase cells were identified as cells with background level EdU and 4N DNA content. Cells with cleaved PARP were identified within the single cell gate as cells with FITC signal above background (DMSO, no anti-cPARP-FITC antibody control). Staurosporine was used as a positive control to identify cells with cleaved-PARP signal.
A gating strategy figure for all FACS analysis is included in supplementary figure 3 of the supplementary Information section.

☒ Tick this box to confirm that a figure exemplifying the gating strategy is provided in the Supplementary Information.